Chapter 3

Discovery of Mitochondriotropic Antioxidant based on Gallic Acid Attenuates LPS Induced Neuroinflammation via TLR-4, Nrf-2 / Keap-1 Signaling Pathway: Proof of Concept on Cellular and *In Vivo* Oxidative Stress Model

3.1 ABSTRACT

Mitochondria are complex organelle that plays a pivotal role in energy metabolism and regulation of stress responses and also serve as a major hub for biosynthetic processes. In addition to their well-established function in cellular energetics, it also serves as the primary site for the origin of intracellular reactive oxygen species (ROS), which function as signaling molecules and can lead to oxidative stress when generated in excess. Moreover, mitochondrial dysfunction is one of the leading cause of neuroinflammation. In this regard, we have rationally designed a triazine-derived mitochondriotropic antioxidants (Mito-TBA), based on gallic acid and triphenylphosphonium (TPP) cation to specifically target mitochondria to mitigate neuroinflammation. *In vitro* Mito-TBA-3 inhibits mitoautophagy and offers neuroprotection by inhibiting the LPS-induced TLR-4 activation and activating the Nrf-2/ ARE pathway in PC-12-derived neurons. *In vivo,* Mito-TBA-3 rescued memory deficit, reversed depression-like behaviour, inhibited neuroinflammation, and decreased proinflammatory cytokines in an LPS-induced neuroinflammation rat model. Overall, based on biophysical, *in vitro* and *in vivo* analysis, Mito-TBA-3 offers valuable insights as a potent therapeutic lead molecule to combat neurodegeneration, even outperforming a well-known non-steroidal anti-inflammatory drug (Aspirin), it also has the potential to use as a promising therapeutic candidate for other mitochondrial oxidative stress-related disorders.

3.2 INTRODUCTION

Neurodegenerative disease (NDD), intracranial tumours, craniocerebral trauma, cerebrovascular disease, spinal cord disease, and other neurological disorders are among the leading causes of disability, death, and morbidity worldwide.[1,2] In the past few years population expansion, ageing, urbanization, and longer life expectancy had a significant impact on the epidemiological patterns, which has led to concerns about a surge in neurological disorder and its associated burden.[3,4] Neurological disorders itself caused around 10 million fatalities in the year 2019 alone.[5] Pathological disorders, including Alzheimer's disease (AD), Parkinson's disease (PD) and stroke, are the most common forms of neurodegeneration, which progressively damages the structural or functional activity of neuronal cells.[6,7] Synaptic dysfunction, cell death in the nervous system, and the acceleration of neurodegenerative disease progression are all results of an excessive consumption and release of ROS and proinflammatory

cytokines induced by various pathological factors in neuroinflammation. [8–11] In response to excessive ROS, cells have developed antioxidant defense systems to mitigate the detrimental impact of excessive ROS generation.[12,13] These methods involve enzymes like superoxide dismutase (SOD) and catalase (CAT), which aid in the neutralization of ROS and hinder their buildup. If the formation of ROS surpasses the capacity of the antioxidant defense system, it results in oxidative stress, which can cause cellular malfunction and contribute to the development of many disorders ranging from cardiovascular to neurological.[14,15] Hence, it is important to uphold an equilibrium between the generation of ROS and the protection provided by antioxidant defense mechanisms in order to preserve cellular well-being and avert oxidative damage.

Despite comprising only 2% of the body weight, the brain receives 15% of the cardiac output and 20% of the total oxygen consumed by the body.[16,17] A major portion of this energy demand comes from neurons, as they need to maintain a homeostasis condition across the plasma membrane to generate an action potential. Neurons are heavily dependent on mitochondria for their energy demands due to their low glycolytic capability, which makes them rely heavily on aerobic oxidative phosphorylation (OXPHOS) for the energy requirements.[18] However, OXPHOS is a significant contributor to the production of harmful endogenous free radicals, such as hydroxyl (OH), hydrogen peroxide (H_2O_2), and superoxide (O_2^-) radicals, which are byproducts of normal cellular respiration.[19] Increasing evidence suggests that reactive free radicals released by mitochondrial malfunction are one of the major contributors to the oxidative stress seen in NDD.[20] Therefore, any disturbance in the mitochondrial structure and function can have significant implications for normal neuron functioning. Hence, comprehending the influence of oxidative stress on mitochondria is of the utmost importance in formulating strategies that protect against cellular damage and uphold general welfare.

Phytochemical antioxidants are one of the most common naturally occurring substances found in the human diet, which act as a natural antioxidant against ROS, and approximately 30% of the phytochemicals consumed in the human diet are hydroxybenzoic acids (HBAs) and hydroxycinnamic acids (HCAs).[21] HCAs and HBAs, like gallic and caffeic acid, respectively, have various well-known methods for interacting with biological systems, one of which is their antioxidant activity through (i) scavenging free radicals, (ii) chelating pro-oxidant transition metals, (iii) modulating gene expression relevant to antioxidants; and (iv) inhibiting systems that generate radicals.[22] These antioxidants have been shown to have positive impacts on health, possibly via activating pathways that respond to oxidative stress. Multiple studies have shown that HCAs are useful in preventing and treating various diseases associated to oxidative stress, including atherosclerosis, inflammatory damage, cancer, and cardiovascular diseases.[23]

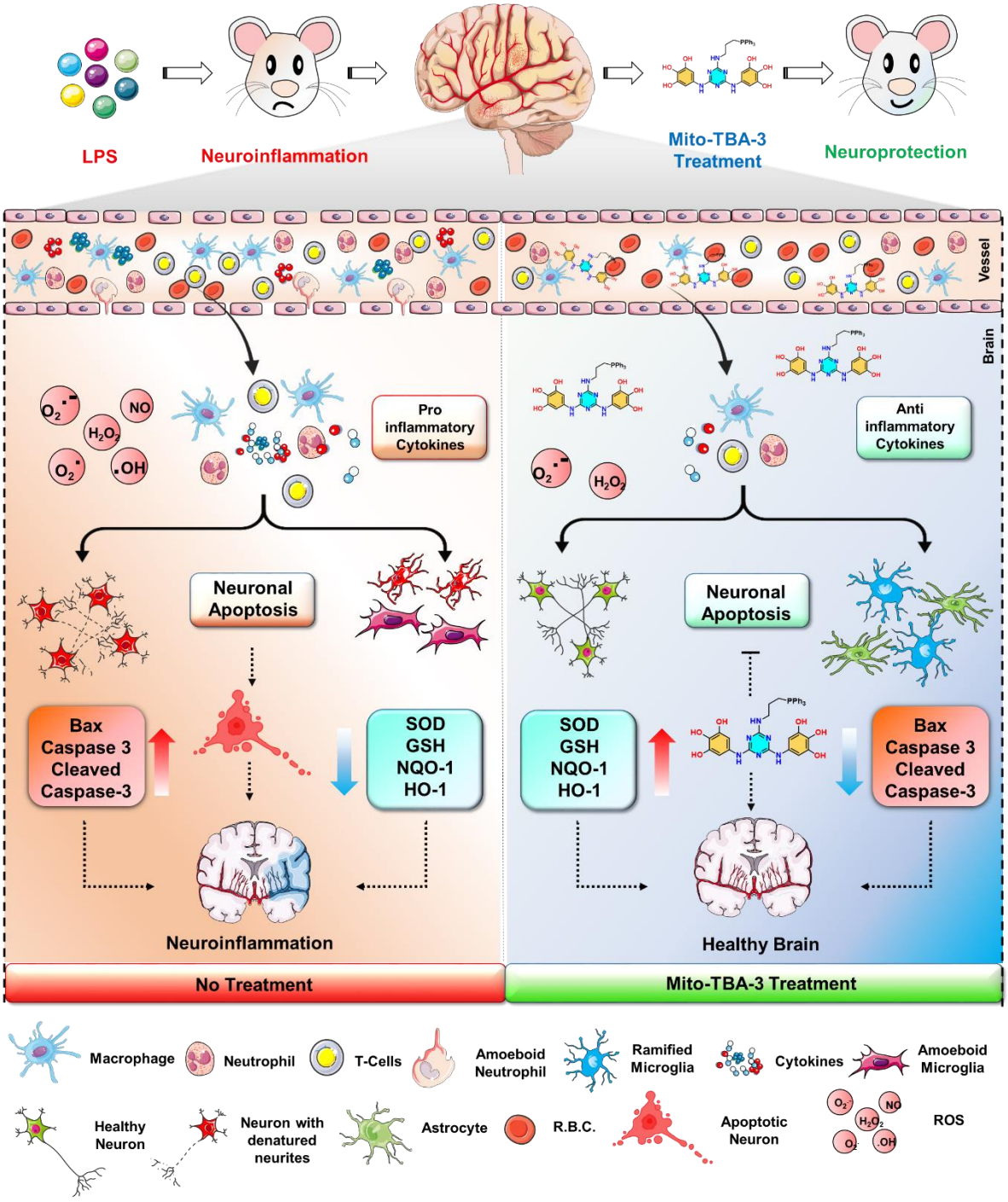


Figure 3.1 Schematic illustration of the mechanism of action of Mito-TBA-3 in LPS induced neuroinflammation.

Hence, keeping the above factors in mind, we have designed a mitochondrion targeting traizine base antioxidant (Mito-TBA) for increasing the cellular resistance against the LPS-induced oxidative stress by activating the Nrf-2 / Keap-1 pathway, which ultimately boosts the expression of local antioxidant defense genes (SOD, CAT, HO-1) and contributed to the enhanced capacity of neuronal cells to counteract oxidative stress. Collectively, Mito-TBA showed an excellent therapeutic effect on LPS-induced neuroinflammation rats by alleviating memory impairment, anxiety, depression-like behaviour and locomotor dysfunction. Moreover, our results showed

that our lead molecule, Mito-TBA-3, showed exceptionally good neuroprotection in both *in vitro* and *in vivo* studies (**Figure 3.1**). Moreover, it also significantly surpassed Aspirin in alleviating neuroinflammation, which is the widely accepted and most effective treatment for neuroinflammation.

3.3 MATERIALS AND METHODS

3.3.1 Materials and Reagents: The 1H NMR and 13C NMR spectra were obtained using a Bruker Advance 500 MHz spectrometer at a temperature of 300 K, with tetramethylsilane (TMS) used as the internal standard. The mass spectra were obtained using an Agilent Technologies electrospray ionisation (ESI) Q-TOF mass spectrometer equipment (G6530C). The analysis using high-performance liquid chromatography (HPLC) involved the use of a Shimadzu C18 column with dimensions of 150 mm × 4.6 mm × 5 µm. Rink amide AM resin and Fmoc-protected amino acids were purchased from Novabiochem (Germany).

ABTS, DPPH were purchased from Sigma, H_2O_2, DCFH-DA were purchased from Merck 3-(4,5-dimethylthiazol-2-yl)-2,5-diphenyl tetrazolium bromide (MTT) (M2128, Sigma), Fetal Bovine Serum (Invitrogen 2023-01-30), Antimycotic antibiotic solution (Himedia A002), Penicillin Streptomycin solution (Invitrogen 15140-122), Trypsin EDTA Solution (Sigma T4174), Bovin Serum Albumin (BSA) (83803, SRL), PVDF Membrane (Millipore), Immobilon Western HRP Substrate (Millipore WBLU F0500), Anti-Rabbit IgG HRP linked, (CST-7074, Dilution 1: 10k), HRP conjugated secondary Antibody (Anti-Mouse IgG HRP linked, CST 7076, Dilution 1: 5k), Mouse mAb IL-6 (Abcam, ab9324), Rabbit mAb Anti-BCl-xl (Abcam, 32370) Rabbit Anti-Bax (CST, 2772), Rabbit mAb to Anti-Bad (Abcam, 32445) Rabbit mAb to GAPDH (CST, 2118), Goat Anti-Rabbit IgG HandL (Cy3.5) preadsorbed (Abcam, ab6941), Goat anti-mouse IgG H and L Alexa Fluor 488, (Thermo, A11029, Dilution 1:400), Hoecsht 33258 (ab228550, Abcam).

3.3.2 General Procedure of Synthesis: Nuclear magnetic resonance (NMR) spectra were acquired using Bruker Avance spectrometers operating at 500 MHz at a temperature of 300 K, with tetramethylsilane (TMS) used as an internal standard. Mass spectrometry (MS) data were obtained employing an Agilent Technologies LC/MSD TOF instrument. Before analysis, all compounds underwent routine verification via thin-layer chromatography (TLC) and 1H NMR. TLC and preparative TLC were conducted on silica gel GF/UV 254 plates, while chromatograms were developed on silica gel (200−300 mesh, Merck) and visualized under UV light at 254 nm and 365 nm. Solvents were of reagent grade and, when necessary, subjected to purification and drying using standard methods. cyanuric chloride and various substituted anilines were procured commercially from TCI and Alfa aesar. Organic solutions were subsequently dried over anhydrous sodium sulfate. Following reactions and extractions, solvents were concentrated using a rotary evaporator under reduced pressure. High-performance liquid chromatography (HPLC) analyses were performed under the following conditions: employing a Shimadzu C18 column (150

mm × 4.6 mm × 5 µm), with a mobile phase consisting of 30-70% acetonitrile in an aqueous solution, detection wavelength set at 254 nm, flow rate maintained at 1 mL/min, temperature set to 30 °C. All synthesized compounds exhibited purity exceeding 95% as determined by HPLC analysis.

3.3.2.1 General Procedure for the Preparation of 1: Sodium Carbonate (6.52 mM, 2.0 eq.) and substituted aniline (6.52 mM, 2.0 eq.) were added to a solution containing cyanuric chloride (3.26 mM, 1.0 eq.) in acetone (8 mL) at 0 °C. The resulting mixture was stirred at 0 °C for 2 hours followed by an additional 6 hours at room temperature. After solvent removal under reduced pressure, ice water (10 mL) was added to the reaction mixture, and the resulting solid was collected via vacuum filtration. The solid was washed with water (2 × 20 mL) and dried under vacuum. Purification of the solid was achieved through flash chromatography on silica gel using a mixture of ethyl acetate and petroleum ether as eluent to afford purified product 1 as a yellowish-white solid in 60-75% yield.[24]

3.3.2.2 Procedure for the Preparation of 2: 3-bromopropylamine hydrobromide (1.81 mM, 1.0 eq.) was dissolved in 5 mL of acetonitrile (MeCN) followed by the addition of Triphenylphosphine (1.81 mM, 1.0 eq.) to the solution. The resulting mixture was refluxed for 15 hours. After the completion of reflux, the reaction mixture was cooled to room temperature, and the white precipitate was separated by filtration. The filtrate was washed three times with ethyl acetate (EtOAc, 20 mL). Finally, the obtained residue was dried under a vacuum to obtain (3-aminopropyl) triphenylphosphonium bromide (**2**) in 90% yield.[25]

3.3.2.3 General Procedure for the Preparation of 3a-c: Under an argon atmosphere, a mixture comprising compound **(1)** (0.47 mM, 1.0 eq.), (3-aminopropyl) triphenylphosphonium bromide **(2)** (0.71 mM, 1.5 eq.), and Triethylamine (0.95 mM, 2.0 eq.) in 5 mL of ethanol was refluxed for 18 hours. The reaction mixture was then concentrated under a vacuum followed by purification of the product via chromatography on silica gel using a mixture of dichloromethane and methanol as a solvent system.[26] The purified compound (0.28 mM, 1.0 eq.) was dissolved in anhydrous dichloromethane (2 mL) under an argon atmosphere and stirred at a temperature of −70 °C. Boron tribromide (1.42 mM, 1 M solution in dichloromethane) was added to the solution, and the reaction mixture was maintained at −70 °C for 10 minutes. Then reaction was allowed to warm to room temperature with continuous stirring for 12 hours. After quenching the reaction with water to destroy BBr_3, purification was conducted by preparative TLC. The resulting product was dissolved in methanol, dried over anhydrous Na_2SO_4, filtered, and the solvent was evaporated.[27]

3.3.2.4 Characterization of (3a): Pale yellow solid, 57% yield, 1H NMR (500 MHz, MeOD) δH 7.91-7.69 (m, 15H), 7.36-7.26 (m, 4H), 6.89-6.71 (m, 4H),3.39-3.32 (m, 4H), 2.08-1.98 (m, 2H); 13C NMR (500 MHz, MeOD) δc: 134.95, 134.93, 133.4, 133.3, 130.2, 130.1, 127.1, 124.0, 118.4, 117.7, 115.7, 114.9, 21.7, 19.3, 19.2; ESI-MS calculated for $C_{36}H_{34}N_6O_2P$ $[M]^+$ 613.2481, found 613.2553; HPLC purity observed was 96.12%.

3.3.2.5 Characterization of (3b): Yellowish brown solid, 55% yield, 1H NMR (500 MHz, MeOD) δH 7.85-7.81 (m, 3H), 7.73-7.65 (m, 12H), 6.73-6.68 (m, 4H), 6.00-5.95 (m, 2H), 3.60 (t, J = 6.0 Hz, 2H), 3.48-3.42 (m, 2H), 2.08-2.03 (m, 2H); 13C NMR (500 MHz, MeOD) δc: 164.5, 158.0, 134.7, 133.3, 133.2, 130.0, 129.9, 118.6, 117.9, 99.9, 22.2, 19.3, 18.4; ESI-MS calculated for $C_{36}H_{34}N_6O_4P$ $[M]^+$ 645.2379, found 645.2396; HPLC purity observed was 98.99%.

3.3.2.6 Characterization of (3c): Brown solid, 51% yield, 1H NMR (500 MHz, MeOD) δH 7.85 (s, 4H), 7.71-7.69(m,11H), 6.64 (s, 2H), 6.47 (s, 2H), 3.69 (t, J = 7.0 Hz, 2H), 3.42-3.36 (m, 2H), 2.02-2.01 (m, 2H); 13C NMR (500 MHz, MeOD) δc: 146.2, 145.5, 134.8, 133.4, 133.3, 130.2, 130.1, 118.3, 116.2, 21.8, 19.9, 19.5; ESI-MS calculated for $C_{36}H_{34}N_6O_6P$ $[M+H]^+$ 678.2356, found 678.2300; HPLC purity observed was 99.1%.

3.3.3 Determination of Cytotoxicity: The cytotoxicity of the Mito-TBAs on both dPC12 and SH-SY5Y cells was assessed using the MTT test, as previously described.[28] dPC12 and SH-SY5Y cells were cultured in a 96-well plate at a density of 3 x 10^5 cells and 3 x 10^4 cells per well, respectively, for a duration of 24 hours. Subsequent cells were exposed to increasing concentrations (ranging from 1.56 μM to 200 μM) of Mito-TBA 1, Mito -TBA 2, and Mito -TBA 3, and were then cultured for an additional 24 hours. Subsequently, MTT was introduced and the absorbance of the formazon salt was measured at 570 nm using a thermal variolux scan microplate reader (VL0L00D0).

3.3.4 DPPH Free Radical Scavenging Test: DPPH is a widely recognised free radical cation used to assess the antioxidative capacity of any antioxidative substance.[29,30] To assess the scavenging ability of Mito -TBA 1, Mito -TBA 2 & Mito -TBA 3, a solution of DPPH reagent with a concentration of 80 μg/mL was prepared. Then, 100 μL of this solution was mixed with an equal volume of the sample (Mito-TBAs) at various concentrations ranging from 5 μM to 200 μM. The mixture was incubated in darkness for 30 minutes. Gallic acid served as the positive control. Subsequently, the absorbance of the mixture was measured at a wavelength of 516 nm, and the rate of scavenging of free radicals was determined using the following formula:

$$Radical\ Scavenging\ (\%) = \{(A)control - (A)sample\ /\ (A)control\}\ x\ 100$$

3.3.5 ABTS Free Radical Scavenging Test: The ABTS assay was conducted with several modifications from the previous literature.[30] In summary, a 5 mL solution of ABTS reagent with a concentration of 7 mM was created by combining it with 88 μL of potassium persulfate with a concentration of 140 mM. This mixture was then left to generate free radicals for a duration of 12 hours in a dark environment. The solution was diluted at a ratio of 1: 40 parts solvents (volume/volume) before to use. In order to assess the scavenging capacity of MITO-TBAs, a mixture was prepared by combining 100 μL of ABTS reagent with 100 μL of the sample at various concentrations ranging from 5 μM to 200 μM. The mixture was then incubated in darkness for a duration of 30 minutes. Subsequently, the absorbance was recorded at a wavelength of 734 nm, and the rate of scavenging of free radicals was determined using the following formula:

$$Radical\ Scavenging\ (\%) = \{(A)control - (A)sample\ /\ (A)control\}\ x\ 100$$

***3.3.6 In Vitro* CCA Assay:** In order to assess the effectiveness of Mito-TBA in suppressing redox activity, we conducted a CCA experiment using the procedure that we have previously described.[31] In summary, the process involves incubating a non-fluorescent compound called coumarin-3-carboxylic acid (CCA, 150 μM), along with Cu^{2+} (10 μM), and either Mito-TBAs or ascorbic acid (10 μM), separately in PBS (0.1 mM, pH = 7.4) at a temperature of 37 °C. Subsequently, the intensity of fluorescent excitation and emission is measured using a thermo varioluxscan microplate reader, with an excitation wavelength of 385 nm and an emission wavelength of 452 nm.[32]

3.3.7 Calcein-AM/PI Live Dead Assay: The oxidative rescuing ability of Mito-TBA was assessed using the Calcein-AM and Propidium Iodide (PI) assay.[33] Calcein-AM is a non-fluorescent compound that can enter cells, and once inside, it is quickly broken down by cellular esterase enzymes. This breakdown process converts Calcein-AM into a highly fluorescent green compound. On the other hand, Propidium Iodide (PI) is a red fluorescent stain that can only enter dead cells and is used to stain the cell nucleus and chromosomes. Initially, dPC12 cells were cultivated in a 35 mm culture dish with a density of 3 x 10^5 cells/mL. Subsequently, the cells were exposed to a concentration of 50 μg / mL LPS for approximately 4 h to induce the production of reactive oxygen species (ROS) in a serum-free environment, thus creating a ROS-enriched state. Additional cells were subjected to treatment with only Mito-TBA. Following treatment, cells were simultaneously stained with calcein-AM (3 μM) and PI (3 μM) in phenol red-free colourless DMEM medium for 15 minutes at 37 °C in a dark environment within the CO_2 incubator. Subsequently, the medium was extracted and the cells were rinsed with filtered PBS. The fluorescence images were promptly acquired using a fluorescent microscope (OLYMPUS IX83), with red fluorescence indicating deceased cells and green fluorescence indicating viable cells. In addition, the photos were quantified using Image J software.

3.3.8 Determination of Intracellular Basal ROS Level: The basal level of cellular reactive oxygen species (ROS) was measured using a DCFH-DA probe.[34] The nonfluorescent probe DCFH-DA is employed to measure the quantity of reactive oxygen species (ROS) present within cells. This probe has the capability to traverse the cell membrane and enter the cytoplasm. Once inside, it undergoes conversion into DCFH by the intracellular esterase. In addition, DCFH reacted with intracellular free radicals to produce the fluorescent compound DCF, which exhibited an excitation wavelength of 488 nm and an emission wavelength of 520 nm. The dPC12 cells were initially cultivated on a 35 mm ibidi culture dish with a density of 3 x 10^5 cells/mL and were given 24 hours to develop. Subsequently, cells were exposed to a concentration of 50 μg / mL of LPS under serum-free conditions for a duration of 4 hours in order to induce the production of reactive oxygen species (ROS). The cells were treated with Mito-TBA 3 for a duration of 24 hours after a 4-hour completion period. Afterwards, the cells were treated with a concentration of 10 μM of DCFH-DA in medium without phenol red for a duration of 30 minutes. In order to assess the impact of Mito-TBA 3 on cellular ROS production, an extra group of cells was subjected to staining with DCFHDA, but without being exposed to an environment enriched with LPS. The images were obtained using an Olympus IX83 microscope. In order to measure the level of ROS the cells were rinsed with PBS, treated with an alkaline solution to break

them apart, and then subjected to centrifugation at a force of 2500g for a duration of 10 minutes. [35] Additionally, the liquid portion was moved to a 96 well plate and the intensity of fluorescence was quantified at 485 nm excitation and 525 nm emission using a thermal varioluxscan microplate scanner. The fluorescence intensity values obtained from the different experimental wells were quantified as a percentage relative to the fluorescence intensity recorded in the control wells.

3.3.9 Measurement of Cellular Oxidative Stress in Live Cells: In order to assess the capacity of Mito-TBA 3 to remove ROS in living cells, we employed the CellROX deep red reagent.[36] This reagent is initially non-fluorescent when in its reduced form but becomes fluorescent when oxidised by ROS, with a peak emission at about 650 nm. To generate ROS, we utilised LPS as a source. dPC12 cells were initially exposed to a concentration of LPS for a duration of 4 hours in the absence of serum, resulting in a state with an increased level of ROS. Cells that were cultivated without LPS served as the control group. The cells, both treated and untreated with LPS, were then cultured in a medium containing Mito-TBA 3. Following a 24-hour incubation period, the cells were rinsed with PBS and treated with a 5 μM concentration of Cell ROX deep red dye at 37 °C for 30 minutes in a colourless DMEM medium. After 30 minutes, the cells were rinsed with PBS and imaged using a fluorescent microscope (Olympus IX83) at 60x magnification. The photos were subjected to quantitative analysis by determining the mean fluorescence intensity using the NIH Image J programme.

3.3.10 Measurement of Mitochondrial Superoxide ROS: The measurement of mitochondrial superoxide was conducted using the mitochondria-specific fluorescent probe MitoSOX Red.[37] Additionally, Mito Tracker Green was employed to verify the location of the mitochondria, and DAPI stain was used to establish the localization of the nucleus. The mitosox red dye emits red fluorescence when it undergoes oxidation by superoxide anions. The initial step involved cultivating cells in LPS to induce the creation of ROS. Subsequently, the cells were subjected to treatment with Mito-TBA 3 for an additional 24 hours to scavenge the ROS. The cells were stained with 5 μM of MitoSOX red and 200 nM mitotracker green for 15 minutes in the absence of light, using colourless DMEM at a temperature of 37 °C. Following incubation, the cells were stained with DAPI (1 μM) and seen using an Olympus IX83 fluorescent microscope. The MitoSOX intensity in each panel was quantified using Image J software.

3.3.11 Measurement of Mitochondria Membrane Potential ($\Delta\Psi_M$): The assessment of mitochondrial membrane potential (ΔΨM) was conducted using JC-1 dye through double fluorescence labelling of mitochondria.[38] Initially, cells were cultured on a 35 mm culture dish, following the previously mentioned procedure. In summary, cells were exposed to LPS to induce the production of ROS in the absence of serum. Subsequently, the cells were cultured under treatment conditions for an additional 24 hours to promote growth. Following a wash with PBS, the cells were treated with a 5 μM concentration of JC-1 dye for 30 minutes at a temperature of 37 °C. After the staining process, the cells were washed again and seen using a fluorescence microscope. Mitochondrial depolarization in each group was quantified by determining the ratio of red to green fluorescence intensity per cell using NIH Image J analysis software.

3.3.12 Determination of Cellular Morphology by F-actin Staining: The measurement of F-actin cytoskeleton was done using a phalloidin stain. Initially dPC12 cells were cultured on a 35 mm culture dish, following the previously mentioned procedure. In summary, cells were exposed to LPS to induce the production of ROS in the absence of serum. Subsequently, the cells were cultured under treatment conditions for an additional 24 hours to promote growth. Following a wash with PBS, the cells were stained with phalloidin dye for 30 minutes at a temperature of 37 °C. After the staining process, the cells were washed again and seen using a fluorescence microscope.

3.3.13 RNA extraction and quantitative reverse transcriptase- PCR (RT-qPCR): Total RNA from dPC12 cells was isolated before and after LPS stimulation and treatment with Mito-TBA-3 using the PureLink RNA Mini Kit (Cat. No. 12183018A, Invitrogen), in accordance with the manufacturer's instructions. Each sample's RNA content and purity (A260/A280 > 1.8) were assessed using a Thermo Fisher Scientific NanoDrop 1000 spectrophotometer. cDNA was synthesised from total RNA (300 ng) with RevertAid First Strand cDNA Synthesis Kit (Cat. No. K1621, Thermo Scientific) following the manufacturer's instructions. The synthesized cDNA was diluted 10x times before proceeding with RT-qPCR along with iTaqTM universal SYBR Green supermix (2x) to analyse the gene of interest in BioRad CFX-96. GAPDH was employed as an endogenous control to normalise the expression levels of mRNA. Primers for all the genes with accession id are listed in Table and the relative mRNA expression was determined using the $2^{-\Delta\Delta Ct}$ method.[39]

3.3.14 Immunocytochemistry (ICC) of NFκB Nuclear Translocation: The dPC12 cells were cultured on 35 mm confocal dishes with glass bottoms and allowed to grow for 24 h, followed by LPS induction, as indicated in the previous section. Following treatment, the cells were fixed using a 4% solution of formaldehyde for 2 h at 37 °C. Subsequently, they were rinsed three times with PBS and made permeable with 0.3% Triton X-100 and 2% BSA in PBS for a duration of 30 minutes. Following a single wash with PBS, the cells were exposed to primary antibodies, specifically P65-NFκB and Phalloidin in PBS. The cells were further rinsed three times with PBS, exposed to FITC/TRITC conjugated secondary antibodies for 2 hours at a temperature of 37 °C, and then treated with Hoechst 33258 for 10 minutes to stain the nuclei. Afterwards, the cells were seen using a fluorescent microscope (Olympus IX83).

3.3.15 Primary Neuronal Culture: Our previously reported procedure was followed to culture primary cortical neurons from pregnant female rats of the E14-E16 age range. In summary, cortical neurons were grown in a culture dish coated with Poly-D-lysine. The neurons were cultured at a density of 1×10^5 cells / mL in Neurobasal media. The media was supplemented with 2% B27, 200 mM GlutaMax, 1% penicillin-streptomycin, and 1% foetal bovine serum. In addition, the cortical neurons were exposed to $A\beta_{42}$ for the generation of oxidative stress and neuronal loss. Further, cortical neurons were treated with Mito-TBA-3 and ICC was performed.

3.3.16 Animals: The Institute Ethics Committee authorized every experimental technique used in this investigation. Forty male Wistar rats were randomly separated

into four groups (n=10) for each of the four experimental groups (i) (Control) i.p. saline group, (ii) 5 mg/kg i.p. LPS, (iii) 5 mg/ kg i.p. LPS + 0.5 mg/kg i.p. Mito-TBA-3 and (iv) 5 mg/kg i.p. LPS + Aspirin 0.5 mg/kg. Aspirin was used as a positive control. In in vivo tests, we utilised 10 rats per group, for biochemical analysis and for histological study post-sacrifice. Three full coronal brain slices were obtained from each animal for histological evaluations and then prepared for staining or IHC. We analysed two specific regions—cortex and hippocampus in each tissue sample from every microtome-cut coronal segment (5µm). A predefined scoring system was employed to quantitatively evaluate histological alterations based on specific parameters (e.g., cellular architecture, inflammation, fibrosis), with each parameter rated from minimal/no change to severe changes, facilitating systematic and objective assessment of severity. Furthermore, to guarantee impartiality and reduce subjective bias, histological evaluations were performed utilising a blinding technique, with coded slides obscuring treatment groups from assessors. A number of independent observers engaged in scoring, with discrepancies reconciled by consensus to minimise inter-observer variability. The purpose of using male mice was to account for hormonal factors. The rats were housed in four animals per cage in a controlled confined setting with a 24-hour light and dark cycle, a temperature of 24 ± 1 °C, relative humidity 40-60% and free access to food and water.[40]

3.3.17 Serum Stability of Mito-TBA: Before using Mito-TBA-3 as a drug candidate for the treatment in rats the biostability of Mito-TBA-3 in human serum was assessed. Briefly, 150 µM of Mito-TBA-3 was co-incubated with human serum at 37 °C. Subsequently, 100 µL of this mixture of serum and Mito-TBA-3 was mixed with 100 µL of cold acetonitrile, and the resulting solution was stored at 4°C for 30 minutes. This mixture of acetonitrile and Mito-TBA-3 along with serum, was subsequently centrifuged for 10 minutes at 10,000 rpm at 4 °C, and the resulting filtrate was collected and analysed using HPLC. The aforementioned procedure was repeated at different time intervals 0, 12, 24, 48, 72, 96 and 120 hours.[31]

3.3.18 BBB Crossing: To assess the capability of our synthesised molecule (Mito-TBA-3) to cross the BBB, we performed a BBB experiment according to the previously reported protocol. For BBB crossing assessment, the rats were administered intraperitoneal injections of Mito-TBA-3, which was dissolved in a saline solution at a concentration of 0.5 mg / kg of body weight. Following a 6-hour treatment period, the animals were administered ketamine (i.p.) to induce anaesthesia and then sacrificed via transcardial perfusion. The brains were isolated and quickly placed in liquid nitrogen, and then homogenised using a mortar and pestle. In order to separate the soluble constituents, a solution consisting of a 1:1 ratio of acetonitrile and water was introduced to the homogenised brain tissue. The resultant mixture was subjected to centrifugation to remove the soluble portion and subsequently underwent filtration. Subsequently, the collected samples were subjected to HPLC and mass analysis for further examination.[31]

3.3.19 LPS-Induced Neuroinflammation Model Generation and Drug Administration: After acclimatization of animals for one week, four groups of animals were given dosage accordingly; (i) Control group received the only saline treatment, (ii) LPS group received LPS dissolved in Saline at a dose of 5 mg/kg intraperitoneally to achieve maximum inflammatory response, (iii) LPS + Mito-TBA group received LPS at a dose

of 5 mg/kg intraperitoneally and Mito-TBA-3 at a dose of 0.5 mg/kg 30 minutes' post-LPS administration, (iv) LPS + Aspirin group received LPS at dose of 0.5 mg/kg interperitonially and Aspirin positive control at a dose of 0.5 mg/kg 30 minutes' post-LPS administration. Further, animals were sacrificed at predetermined intervals, and their tissues (liver, brain, and serum) were utilized for morphological analysis.[40]

3.3.20 Open Field Test: An Open field test was performed to assess the anxiety and depression-like behaviour in rats after LPS administration according to the previously reported protocol with some modifications.[41] The apparatus consists of a specified translucent box (100 cm x 100 cm x 40 cm) with a black floor and a camera (ANYMAZE) installed directly above the open field arena to record the animal's behaviour and movement during the test. Rats were placed within the central area of the apparatus in a room illuminated with subdued lighting, and they were allowed to roam freely for a duration of 5 min. The movement of the animal was recorder for 5 min and the video-recorded data included the cumulative distance travelled, duration of time spent in the central area, and the number of entries made into the centre. After 5 min the rats were placed back into their home cage and the field was cleaned with 70% ethanol in order to reduce the possible impact of lingering smells from the previous group of rat, the equipment was left untouched for a minimum of 5 min before starting the subsequent tests.

3.3.21 Sucrose Preference Test: The assessment of depression-like behaviour or anhedonia in rats involves using a sucrose preference test (SPT) that uses a two-bottle choice paradigm. Depression or Anhedonia can be inferred when rats show a decrease in their sucrose preference ratio compared to control mice.[42] Animals were moved from the groups to the individual cages with a single animal per cage. In brief, in SPT, the rats first underwent adaptive training for 2 days, where rats were allowed to free access to two bottle of water for day 1, two bottles of 1% sucrose on day 2. The following day 3, the rats were given one bottle of water and another bottle of 1% sucrose solution for 24 hrs. The quantity of water and sucrose intake was calculated using the following formula:

$$Sucrose\ Preference\ (\%)$$

$$= \{[Sucrose\ Consumption] \,/\, Sucrose\ Consumption\ + waterConsumption\}\ x\ 100$$

3.3.22 Elevated Plus Maize: The elevated plus maze (EPM) was performed 24 hr after the LPS administration and is used to investigate anxiety-like behaviour in rats.[43] The apparatus consists of four arms in a cross shape, two open arms and two closed arms enclosed by a high wall facing each other. The EPM was raised approx. 90 cm from the ground, the rat was placed into the open arm and allowed to move freely for a time period of 3 min. During this time, the time spent in the open arm was calculated, and the entries into the open arm were measured. The maize was cleaned with 70% ethanol before the starting of new trial.

3.3.23 Forced Swimming Test: The forced swimming test (FST) was performed 48 hrs after LPS administration according to the previously reported protocol.[43] Rats were placed in an open cylinder (20 cm diameter x 40 cm height) filled with 30 cm of water at a temperature of 25 ± 1°C. The test was conducted for a duration of 5 minutes,

during which the assessment of immobility time was carried out by an observer blinded to the treatment conditions. After the completion of each experiment, the water in the container was replaced, and the mice were dried with towels and moved back to their initial cages.

3.3.24 Rotarod Test: Motor impairment in rats after LPS administration was assessed using a rotarod test, as reported previously, with little modifications.[44] This test uses a rotating rod of 30 cm in length to measure the balance and coordination of rats. Prior to LPS administration, all the rats from each group underwent a pre-training session for three consecutive days to run on a rod that rotated at the constant speed of around 15 rpm for a period of 3 minutes to acclimatize. After acclimatization and LPS administration, the final test was performed, and rats were placed on a rod rotating at a speed of 20 rpm, latency to fall for each group rat was recorded and analysed.

3.3.25 Novel Object Recognition Test: A Novel object recognition test was performed to assess the cognitive function after the LPS administration.[44] In order to perform the NORT, rats were first habituated to the same apparatus where OFT was carried out for an initial duration of 10 minutes. After habituation, two indistinguishable objects were placed in a counterbalanced manner in an open field arena, and rat were allowed to explore freely both the objects. The test session was carried out 24 hours after the training phase. In this session, one of the two identical objects was replaced with a new object at the same position but differed in colour and texture. After each trial, the open field arena and objects were cleaned using 70% ethanol to remove any remnants of urine or faeces odours. A different set of animals was used for NORT other than OFT-assigned animals. The total object exploration time of the animals with familiar and novel objects was recorded.

3.3.26 Pole Test: The climbing down pole test was performed according to the previously reported protocol with brief modifications.[45] The pole test consisted of a 50 cm long iron pole with a diameter of 0.5 cm, and a small platform covered with gauze was placed on top of the pole to prevent the animal from slipping. The pole was placed securely in the animal home cage. The animals were placed on the top of the pole, and time was recorded until the animal turned around to face downwards and climb down from top to bottom.

3.3.27 Morris Water Maze Test: The Morris water maze (MWM) test was performed to evaluate cognitive abilities like learning and memory in rats.[46] The water maze was divided into four directional quadrants, and the platform was concealed in the centre of the target quadrant, approximately one centimetre below the surface of the water. The standard training was continued for a total of 5 days. Each animal of every group was given a total of four separate trials every single day, with the beginning points of each test located in one of the tank's four distinct quadrants. The wall of the tank was also decorated with markers for spatial navigation, and the duration of the test was two minute for each trial. The rats that did not make it to the platform within two minutes were trained by placing them on the platform and keeping them there for around 20 seconds. Parameters like escape latency, distance travelled etc., were recorded as learning indicators over the course of 5 days. On the final day of testing, a space probe experiment was performed. The platform was removed, the animal was

placed on a contralateral platform, and their swimming pattern was observed for a period of 60 seconds.

3.3.28 Marble Burying Test: The Marble burying test (MBT) was performed according to the previously reported protocols with some modifications.[47] Fifteen ceramic black marbles, with a diameter of approx. 20 mm were placed in an animal standard home cage in a pattern of 5 rows and 4 columns on a 4 cm deep layer of wood chip bedding. Rats were placed in the cage facing the side wall of the cage, and it ensured that the rat could easily avoid coming into contact with the marbles while the test was about to start. The behaviour of the rat was recorded in a ANYMAZE software, and marble was considered to be buried when over two-thirds of its diameter was covered by bedding.

3.3.29 ELISA: After LPS administration and Mito-TBA-3 treatment, the whole brain of the different treatment groups was promptly extracted and placed on an ice-cold dish. The brain was thoroughly rinsed with ice-cold PBS (pH 7.4) and stored at -80 °C for future analysis. The brain tissue was pulverised entirely in a solution of ice-cold PBS with a concentration of 100 mg/mL. The quantification of several cytokines was conducted using commercially accessible ELISA assay kits (Quantikine ELISA).[40]

3.3.30 Tissue Processing & Histology: Following perfusion fixation, tissue samples were obtained and used for H & E (hematoxylin and eosin) and cresyl violet staining, using a procedure that has been previously described.[48] In summary, brain coronal tissue slices measuring 5 µm were subjected to a clearing process using xylene, followed by rehydration using a series of ethanol washes with varying concentrations. Subsequently, the sections were stained with hematoxylin and eosin for a duration of 2 minutes. Subsequently, the samples were mounted with DPX mounting medium. For Nissl staining, slides were initially hydrated using a decreasing gradient of alcohol and subsequently stained with a 0.5% solution of cresyl violet. Afterwards, the slices were cleaned, dehydrated using a progressive ethanol gradient, cleaned with xylene, and finally mounted in DPX.

3.3.31 Immunofluorescence: Immunofluorescence was conducted following a previously reported protocol with minor modifications.[49] After LPS administration and different treatments, animals were perfused to drain the blood and fixed using PBS and 10% formalin, respectively. The brain tissues were then taken and then fixed in formalin for an additional 24 hours. Then, the brain samples were moulded in paraffin blocks for further analysis. The paraffin-embedded blocks were then cut into 5 µm thickness for immunohistochemistry. The obtained sections were initially treated with xylene to remove the paraffin, followed by a gradual rehydration process using ethanol. Following blocking with BSA subsequently, the sections were exposed to primary antibodies (GFAP ab68428, 1:250; Iba1 ab178846, 1:2000; NeuN ab104225, 1:500) and incubated overnight at a temperature of 4 ℃. Prior to this, microwave-assisted antigen retrieval was performed using Tris-EDTA (pH=9) and citrate buffer (pH=6) for a duration of 30 minutes. Following that, brain sections were rinsed with PBST and then incubated with particular FITC-TRITC labelled secondary antibodies for 2h at RT. The sections were then further counter-stained with DAPI, and all images

were captured using an Olympus IX83 fluorescence microscope. The corrected total cell fluorescence (CTCF) intensities were quantified using NIH ImageJ software.[50]

$$CTCF = \{Integrated\ Density - Area\ of\ Selected\ Cell\ x\ Mean\ Fluroscence\ of\ Background\ Readings\}$$

3.3.32 Statistical Significance: All the cellular and animal experimental data in the chapter are shown as the average mean with the standard deviation (SD), which was derived from a minimum of three or six distinct experimental studies. Statistical significance across groups was analyzed using a one-way analysis of variance (ANOVA) with Tukey's post hoc test to account for multiple comparisons. All statistical analyses were conducted in GraphPad Prism (GraphPad Prism Software Inc., Version 8.0.2) to compare the mean values of every group with p-values designated as follows: *p < 0.05, **p < 0.01, and ****p < 0.0001", the p-value was below 0.05 was considered non-significant.

3.3.33 Figures: Some components of the figure are adapted from Servier Medical Art; Servier is licensed under a Creative Commons Attribution 3.0 unported license https://smart.servier.com/ and https://app.biorender.com/

3.4 RESULTS AND DISCUSSION

3.4.1 Design Strategy, Synthesis and Characterization of Mito-TBA: Therapeutics including bioactive small molecules that can specifically target mitochondria, are of the utmost importance to counteract mitochondrial-related disorders. These therapies involve the use of lipophilic cations carriers, such as TPP (triphenylphosphonium), which have the remarkable ability to cross mitochondrial membranes and concentrate in the mitochondrial matrix.[51] Two majorly well-known mitochondria targeting antioxidants, MitoQ10 and SkQ, which are currently undergoing clinical trials for a wide range of disorders such as illnesses, hepatitis C and dry-eye syndrome, also contain a covalently linked TPP to their backbone.[52,53] Moreover, additional bioactive compounds, such as quercetin, resveratrol, metformin, or vitamin E succinate, have also been utilized in conjunction with TPP to enhance their targeting to the mitochondria. Hence, along this framework of TPP and Gallic acid, we have synthesized a mitochondria-targeted antioxidant (Mito-TBA's) by substituting triazine ring with TPP for mitochondria targeting and Gallic acid as a polyphenolic group for neuroprotection, along with as an antioxidant against ROS and RNS (**Figure 3.2**).

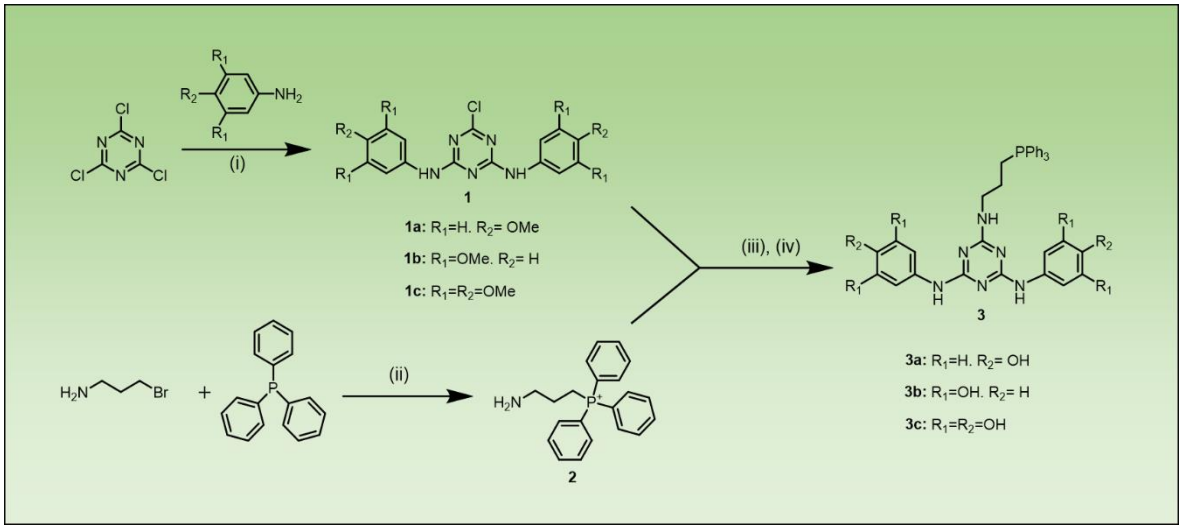


Figure 3.2 Synthetic route of substituted 1,3,5 triazine; Reagents and conditions: (i) Na_2CO_3, Acetone, from 0°C (2h) to room temperature (8h), (ii) ACN, Reflux, 15h, (iii) Triethylamine, Ethanol, Reflux, 18h, (iv) BBr_3, from –70 °C (10 min) to room temperature (12 h).

First, intermediate (1), substituted 1,3,5 triazine was synthesized under specific conditions using Na_2CO_3, and acetone and keeping temperature at 0°C for around 2h and then keeping the reaction at room temperature for 8h. Then, compound (2) was synthesized by attaching the 3-bromopropylamine hydrobromide to the TPP under reflux conditions for around 15 h. Then under an inert argon atmosphere, the compounds (1) and (2) were chemically attached and treated with BBr_3, from −70 °C (10 min) to room temperature (12 h) to afford the compound 3a-c with successively increasing a number of phenolic OH groups to evaluate it's role as ROS scavenger. The synthesized compounds are now called Mito-TBA's based on the count of –OH group. Mito-TBA-1, 2, 3 with one, two and three polyhydroxy groups respectively. Further, all Mito-TBA's was purified using column chromatography and characterized through 1H NMR, 13C NMR, and HRMS spectra analysis. The purity of all synthesized molecules was determined using RP-HPLC analysis, which revealed that the Mito-TBA's have a purity level above 95% (**Figure 3.3**).

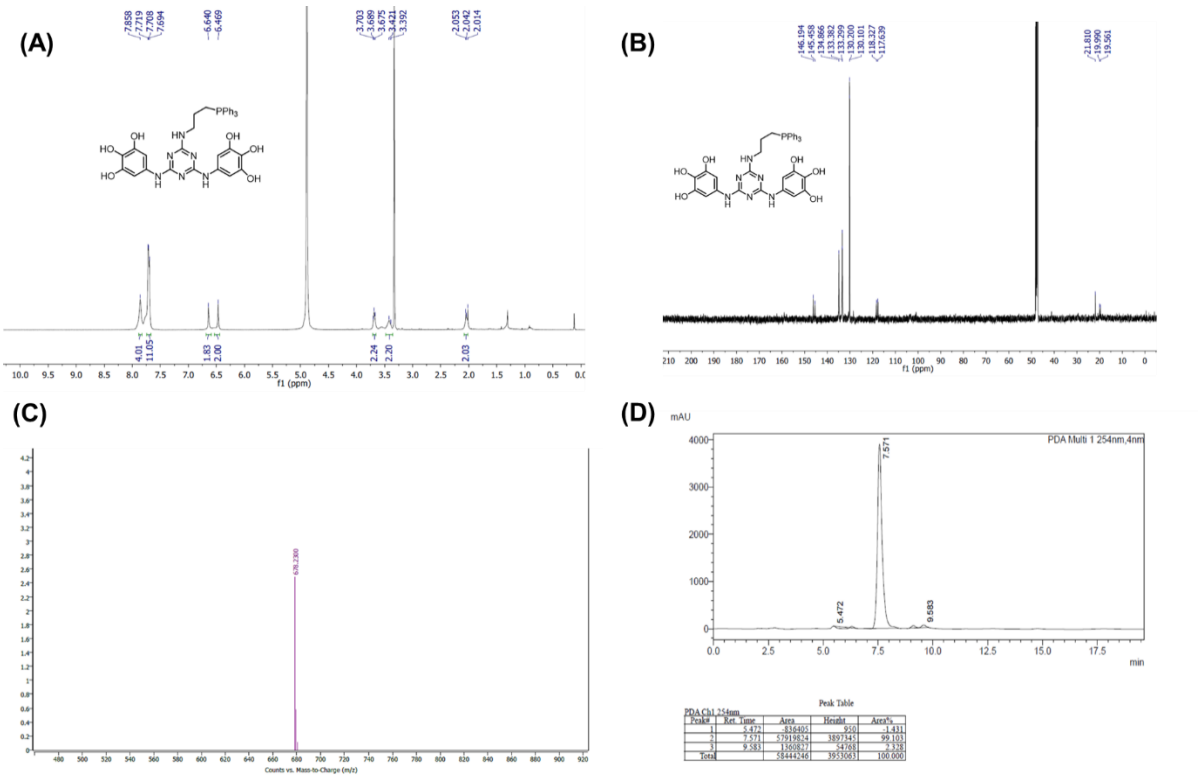


Figure 3.3 (A) 1H NMR of 3c (Mito-TBA-3), 13C NMR of 3c (Mito-TBA-3), (B) ESI-MS of 3c (Mito-TBA-3). (C) Expected 677.23 and observed 678.23 [M+H] mass, (D) HPLC spectra of 3c (Mito-TBA-3).

3.4.2 Free Radical Scavenging Ability of Mito-TBAs: After conducting a thorough characterization of Mito-TBA-1, Mito-TBA-2, Mito-TBA-3, their various antioxidant properties were evaluated. Owing to their poly-hydroxyl (-OH) moiety, the Mito-TBAs have an extraordinary ability to counteract free radicals, such as ROS and RNS. Firstly, the scavenging efficiency of all three compounds was measured using standard antioxidative assays, mainly 2,2′-azino-bis(3-ethylbenzothiazoline-6)-sulfonic acid (ABTS) and 2,2-diphenyl-1-picrylhydrazyl (DPPH).

In DPPH assay the purple colour DPPH free radical is being converted to a yellow color stable compound by an antioxidant compound (**Figure 3.4 A**). Moreover, the DPPH free radical also exhibits a distinct absorbance peak at around 517 nm.[29] However, this peak decreases when it comes into contact with an antioxidant. Evidently, when Mito-TBAs were mixed with DPPH the decrease in absorbance of DPPH free radicals was also seen in the reaction mixture, which can be attributed with the increasing concentration of Mito-TBAs, as seen in **Figures 3.4 A and B**. Further, as shown in **Figure 3.4 B**, the percentage of DPPH radical quenching was also calculated to assess the antioxidant ability of Mito-TBA's in comparison with the positive control gallic acid (0.19-50 µM). The results show that Mito-TBA-3 has the highest free radical scavenging ability and its effectively scavenges free radicals with an IC_{50} value of 4.33 µM, which is better than that of gallic acid at 5.60 µM (Table 1).

Compound	Precursor	MW (g mol^{-1})	DPPH (IC_{50})	ABTS (IC_{50})
Gallic acid	NA	180.16	8.79 μM	11.81 μM
Mito-TBA-1	Triazine	613.2481	55.91 μM	32.12 μM
Mito-TBA -2	Triazine	645.2396	32.04 μM	24.93 μM
Mito-TBA -3	Triazine	677.277	4.33 μM	5.60 μM

Table 3.1: Antioxidant property of Mito-TBAs and gallic acid.

Based upon the exceptional ROS scavenging capability of Mito-TBA's, we investigated their capacity to scavenge RNS. Some bioactive chemicals are insoluble in the reaction medium and so do not exhibit genuine free radical scavenging capabilities. Thus, in order to eliminate the possibility of antioxidant activity in the methanolic media using DPPH, we conducted an ABTS radical scavenging experiment, which is performed in an aqueous-based medium. In this particular assay, we utilized the ABTS test to evaluate their RNS scavenging ability. ABTS was incubated either alone or with different concentrations of Mito-TBA's and gallic acid (0.19-50 μM) for 30 minutes in the absence of light, and the absorbance at 734 nm was measured. As evident Mito-TBA-3 exhibited superior RNS scavenging action when compared to the other compounds (Mito-TBA-2, Mito-TBA-1) and positive control, gallic acid (**Figure 3.4 C and D**) due to having three polyhydroxyl groups. Moreover, the absorbance spectra of the $ABTS^{\cdot+}$ solution were measured in the range of 400-900 nm, and the addition of Mito-TBA and gallic acid resulted in a decrease in intensity of the detection of a distinct absorption peak at 734 nm. The IC_{50} value for Mito-TBAs was 8.79 μM, which is better than that of gallic acid, it was 11.8 μM (Table 1).

The potential of Mito-TBAs to mitigate ROS was also assessed using a coumarin-3-carboxylic acid (CCA) assay. The CCA test is a fluorescence-based detection technique employed for the identification of hydroxyl radicals (•OH) in water-based solutions. Ascorbate acts as a reducing agent, aiding in the conversion of Cu^{2+} to Cu^{+}. Nevertheless, Cu^{+} is extremely unstable and readily undergoes oxidation, rapidly returning to Cu^{2+} and producing H_2O_2, a significant ROS constituent. When exposed to H_2O_2, the non-fluorescent CCA component undergoes a chemical change and becomes fluorescent also known as 7-hydroxycoumarin-3-carboxylic acid (7-OH-CCA) with an excitation wavelength (λex) of 385 nm and an emission wavelength (λem) of 452 nm. Concentration of H_2O_2 in a solution can be quantified by assessing the strength of the fluorescent 7-OH-CCA. As anticipated, the control group (Control + Cu^{2+} + Ascorbate) exhibited high fluorescence, indicating the lack of any antioxidants. However, the addition of gallic acid and Mito-TBAs resulted in a decrease in fluorescent intensity (**Figure 3.4 E**). These results conclusively demonstrate that Mito-TBAs are highly antioxidant and have an exceptional ROS scavenging ability.

3.4.3 Protective Effect of Mito-TBA-3 on LPS-Induced Oxidative Stress Injury in Differentiated PC12 (dPC12) Cells: In order to check the potential of Mito-TBAs to reduce the multifarious toxicity of ROS and RNS *in vitro*, we proceeded to explore their potential for use in a cellular system. To examine the bio-potential of Mito-TBAs first, the cytocompatibility of Mito-TBA's was assessed in PC-12 cells derived neuronal model (dPC12) by using 3-(4,5-dimethylthiazol-2-yl)2,5-diphenyltetrazolium bromide (MTT) assay. dPC-12 cells were treated with increasing concentrations of Mito-TBA's (1.5 to 200 μM) and it was observed that Mito-TBA's had no observable toxicity at concentrations of up to 12.5 μM, as evidenced by a cell survival rate over 90% relative to untreated cells after 24 hours (**Figure 3.4 H, 3.5 A and B**).

Commonly, various *in vitro* models were created to induce oxidative stress using inducers such as phorbol 12-myristate 13-acetate (PMA), diallyl trisulfide (DATS), H_2O_2, cisplatin (CDDP), lipopolysaccharide (LPS), amyloid beta (Aβ), UV irradiation, oxidised low-density lipoprotein (OxLDL), hypoxia-hypoglycemia and reoxygenation (HR) and many others. Therefore, to stimulate the *in vitro* model of neuroinflammation, an oxidative stress injury model was established in dPC12 cells with the help of LPS. Firstly, the analysis of the cytotoxic effects of LPS on dPC12 cells was evaluated to identify the most effective concentration for the neuroinflammation model. In this regard, we have treated the dPC-12 cells with different concentrations of LPS (20-500 μg/mL) for 4 h, to determine the IC_{50} value. In comparison to the control group, treatment with 50 μg/mL of LPS showed significant cytotoxicity by almost 50%. Therefore, 50 μg/mL of LPS was used for further experiments.

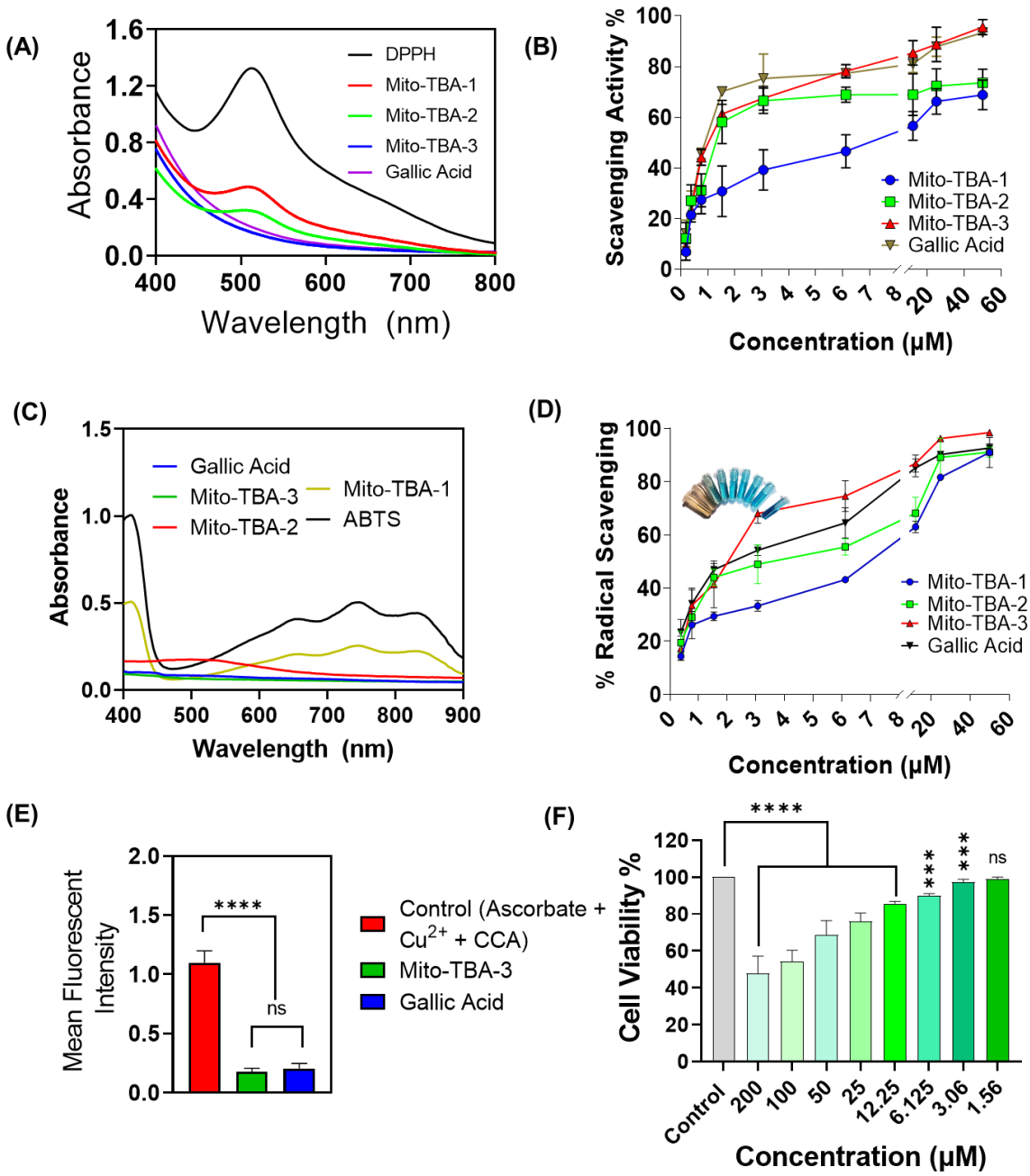


Figure 3.4 Evaluation of *in vitro* effectiveness of Mito-TBA's in scavenging free radicals. (A) Absorbance of DPPH following treatment with Mito-TBA's (B) The radical scavenging rates of DPPH• were plotted as a percentage of the scavenging rate (%) of Mito-TBA's at different concentrations along with the positive control Gallic acid. (C) Absorbance of ABTS following treatment with Mito-TBA's. (D) The radical scavenging rates of ABTS• were plotted as a percentage of the scavenging rate (%) of Mito-TBA's at different concentrations along with the positive control Gallic acid. (E) Bar graph illustrating the normalized mean fluorescence intensity (452 nm) of 7-OH–CCA under various treatment conditions. (F) Cell viability (MTT assay) of Mito-TBA-3 with dPC12 at different concentrations (1.5-200 μM) after 24 hrs. Data represent mean ± SD of three independent experiments. The statistical significance of all the results was calculated by using a one-way analysis of variance (ANOVA) with Tukey's post hoc test. *$p < 0.05$, **$p < 0.01$, ***$p < 0.001$ and ****$p < 0.0001$ in GraphPad Prism.

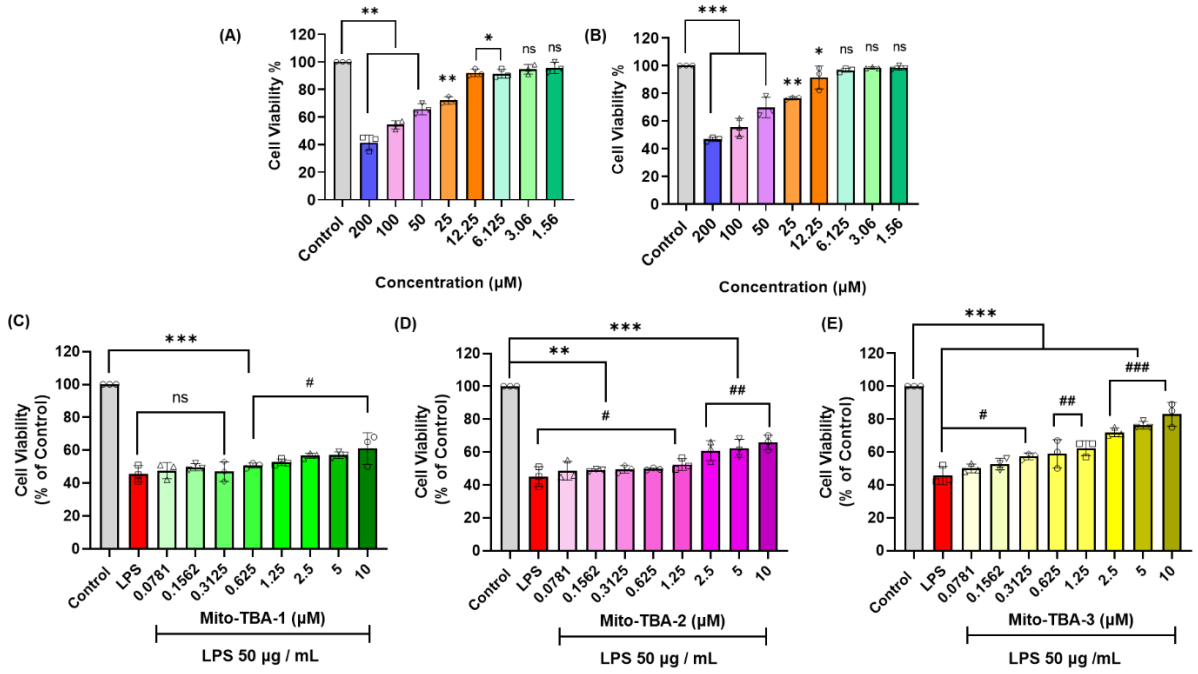


Figure 3.5 (A) and (B) Cell viability (MTT assay) of Mito-TBA-1 and Mito-TBA-2 with dPC12 at different concentrations (1.5-200 μM) after 24 hrs. (C), (D) and (E) Cell viability (MTT assay) of dPC12 with LPS (50 μg / mL) and Mito-TBA-1, Mito-TBA-2 and Mito-TBA-3 respectively to determine the neuroprotective effect of Mito-TBA's. Data represent mean ± SD of three independent experiments. The statistical significance of all the results was calculated by using a one-way analysis of variance (ANOVA) with Tukey's post hoc test. The results are represented as the mean ± SD, n = 3 per group from three independent experiments. Significances are marked as *P< 0.05, **P< 0.01, ***P< 0.001, **** P < 0.0001 versus the control group, $^{\#}$P<0.05, $^{\#\#}$P<0.01, $^{\#\#\#}$P<0.001, $^{\#\#\#\#}$ P < 0.0001 versus the LPS treatment group. Here, 'ns' is nonsignificant when compared to control.

Further, to assess the ability of Mito-TBA's to rescue cells from cellular apoptosis induced by LPS, dPC12 cells were first exposed to 50 μg/mL LPS and subsequently treated with progressively increasing concentrations of Mito-TBA's. The results obtained from the MTT cell viability assay clearly indicate that treatment with Mito-TBA's effectively mitigates the cell death induced by LPS in a dose-dependent manner (**Figure 3.5 C, D and E**). However, among all compounds (Mito-TBA-1,2,3), Mito-TBA-3 showed the highest neuroprotection at a concentration of 10 μM with almost 80% recovery. Hence, from the results of both *in vitro* antioxidant assays and cellular investigations, we unequivocally discovered that Mito-TBA-3 exhibits superior antioxidant properties and effectively modulates ROS levels.

3.4.4 Mito-TBA's Rescues dPC12 Cells from LPS-Induced Cytotoxicity: The Calcein-AM and Propidium Iodide (PI) assay is a widely employed technique for evaluating cell viability and measuring the capacity of compounds to rescue cells from oxidative damage. Calcein-AM is a non-fluorescent substance capable of permeating cellular membranes. Upon entering live cells, it undergoes hydrolysis by cellular esterases, resulting in the formation of a highly fluorescent green compound. While, Propidium Iodide (PI) is a red fluorescent dye that cannot enter live cells, but can enter cells with damaged or dead cell membranes. In this experiment, viable cells would display green

fluorescence as a result of the conversion of Calcein-AM, but dead cells would exhibit red fluorescence due to the presence of PI. Moreover, the green-to-red fluorescence ratio can be utilised to evaluate cell viability and the efficacy of compounds in rescuing cells under oxidative stress conditions.

To further observe the inhibitory impact of Mito-TBA-3 on cellular apoptosis, cells were stained using a Calcein-AM / propidium iodide (PI). **Figure 3.6** shows that there was a significant increase in the number of red-stained dead cells in the group that were pretreated with LPS. On the contrary, the number of dead cells decreased significantly in the Mito-TBA-3 treatment group. Moreover, treatment with Mito-TBA-3 alone does not induce any apoptosis as evident from the negligible red stained cells (**Figure 3.7A**). These findings of Calcein-AM/ PI imaging are in accordance with the results of the MTT and the quantitative analysis of live-dead fluorescence images. The One-way ANOVA statistical method was utilised to ascertain the significance of the differences that existed among LPS and treatment groups. These results provided more understanding of the process by which antioxidants protect against oxidative stress, which was subsequently investigated in more depth with DCFDH-DA assay.

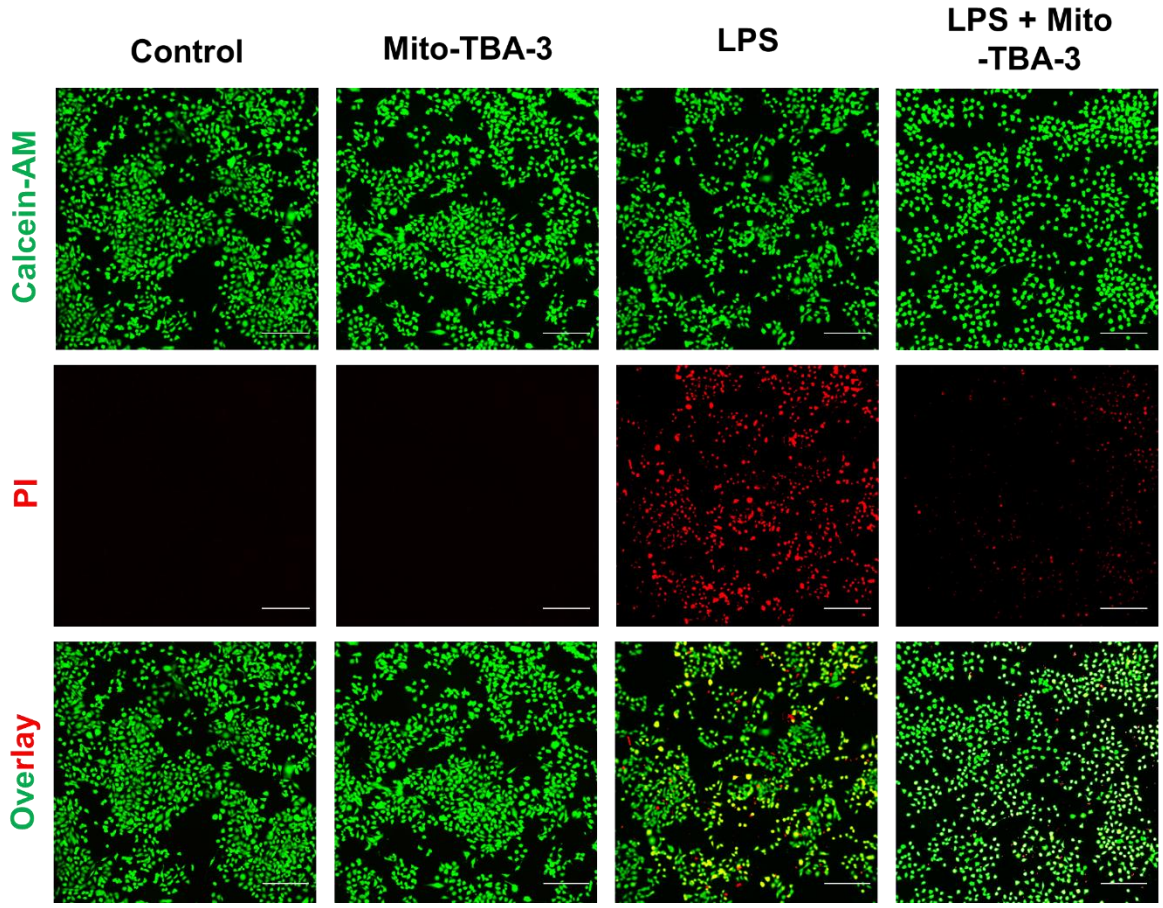


Figure 3.6 Neuroprotective effect of Mito-TBA-3 against LPS-induced oxidative stress in dPC12 rat pheochromocytoma cells. (A) Calcein-AM / PI images of dPC12 cells treated with, Mito-TBA-3 alone, LPS, and LPS + Mito-TBA-3. Scale bar corresponds to 200 µm.

Further, the DCFH-DA probe is used to measure the baseline levels of ROS in cells. Crucially, the DCFH-DA probe allows for the continuous tracking of ROS generation in living cells, providing important information about the ever-changing cellular oxidative stress. The intracellular esterase in live cells cleaves the probe DCFH-DA into DCFH, which further interacts with the cell's free radicals and results in the formation of a fluorescent compound known as DCF. An accurate measurement of the baseline cellular ROS levels can be obtained by quantifying the fluorescence intensity of this fluorescent probe DCF.

The intracellular ROS level was measured using fluorescence intensity in different groups. The control group and cells cultivated with only Mito-TBA-3 had approximately the same ROS levels as a control group, demonstrating that Mito-TBA-3 do not cause ROS in dPC12 cells. Meanwhile, LPS pretreatment increased cellular oxidative stress, indicating ROS overproduction (**Figure 3.7 B**). Mito-TBA-3 significantly reduced overproduced ROS in LPS pretreated dPC12 cells compared to the other groups, suggesting a scavenging function.

We also compare the level of ROS in different experimental conditions using fluorescent microscopy. As shown in **Figure 3.7 C**, negligible levels of green fluorescence were detected in the control group of cells and cells treated with only Mito-TBA-3. This clearly indicates that Mito-TBA-3 itself does not have any role in ROS generation, and it maintains the basal ROS level required for normal homeostasis. However, cells that were pre-exposed to LPS exhibited a remarkably intense green fluorescence, which clearly signifies a substantial presence of ROS. Upon treating the LPS pretreated cells with Mito-TBA 3, a reduction in intracellular ROS was seen, as indicated by the decrease in the intensity of the green signal (**Figure 3.7 C**).

Further, in addition, a secondary assay was conducted to confirm if Mito-TBA-3 can alleviate the excessive intracellular ROS in LPS induced dPC-12 cells. The amount of intracellular ROS produced was measured using CellROX dye. **Figure 3.8** demonstrates an elevation in red fluorescence following LPS pretreatment. Conversely, LPS pretreated cells, when treated with Mito-TBA-3, exhibited a significant decrease in red intensity, as depicted in **Figure 3.8**. Thus, these findings suggest that Mito-TBA-3 have the ability to efficiently remove excessive intracellular ROS.

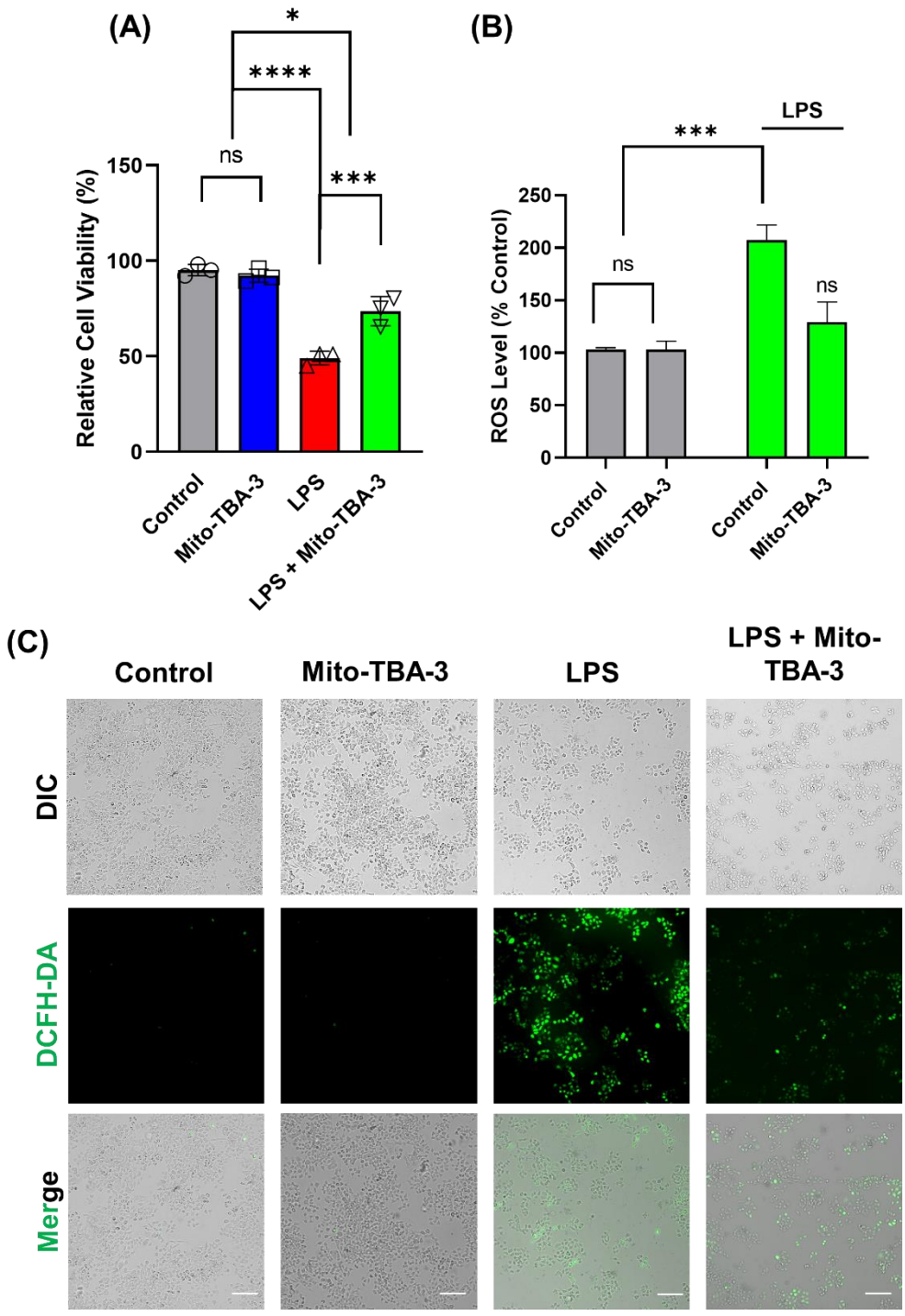


Figure 3.7 Neuroprotective effect of Mito-TBA-3 against LPS-induced oxidative stress in dPC12 rat pheochromocytoma cells. (A) The relative cell viability of dPC12 cells, quantitatively analyzed using Image J software. (B) Bar graph showing the quantitatively analysed levels of DCFH-DA staining in dPC12 cells using a microplate reader. The cells were treated with Mito-TBA-3 individually as well as with LPS pretreated dPC12 cells treated with Mito-TBA-3. (C) DIC and Fluorescent Images of DCFH-DA assay were used to determine the overall level of ROS in PC12 cells after Mito-TBA-3 treatment. Scale bar corresponds 200 µm. Data represent mean ± SD of three independent experiments. The statistical significance of all the results was calculated by using a one-way analysis of variance (ANOVA) with Tukey's post hoc test. The results are represented as the mean ± SD, n = 3 per group from three independent experiments. Significances are marked as *P< 0.05, **P< 0.01, ***P< 0.001, **** P < 0.0001 versus the control group, $^{\#}$P<0.05, $^{\#\#}$P<0.01, $^{\#\#\#}$P<0.001, $^{\#\#\#\#}$ P < 0.0001 versus the LPS treatment group. Here, 'ns' is nonsignificant when compared to control.

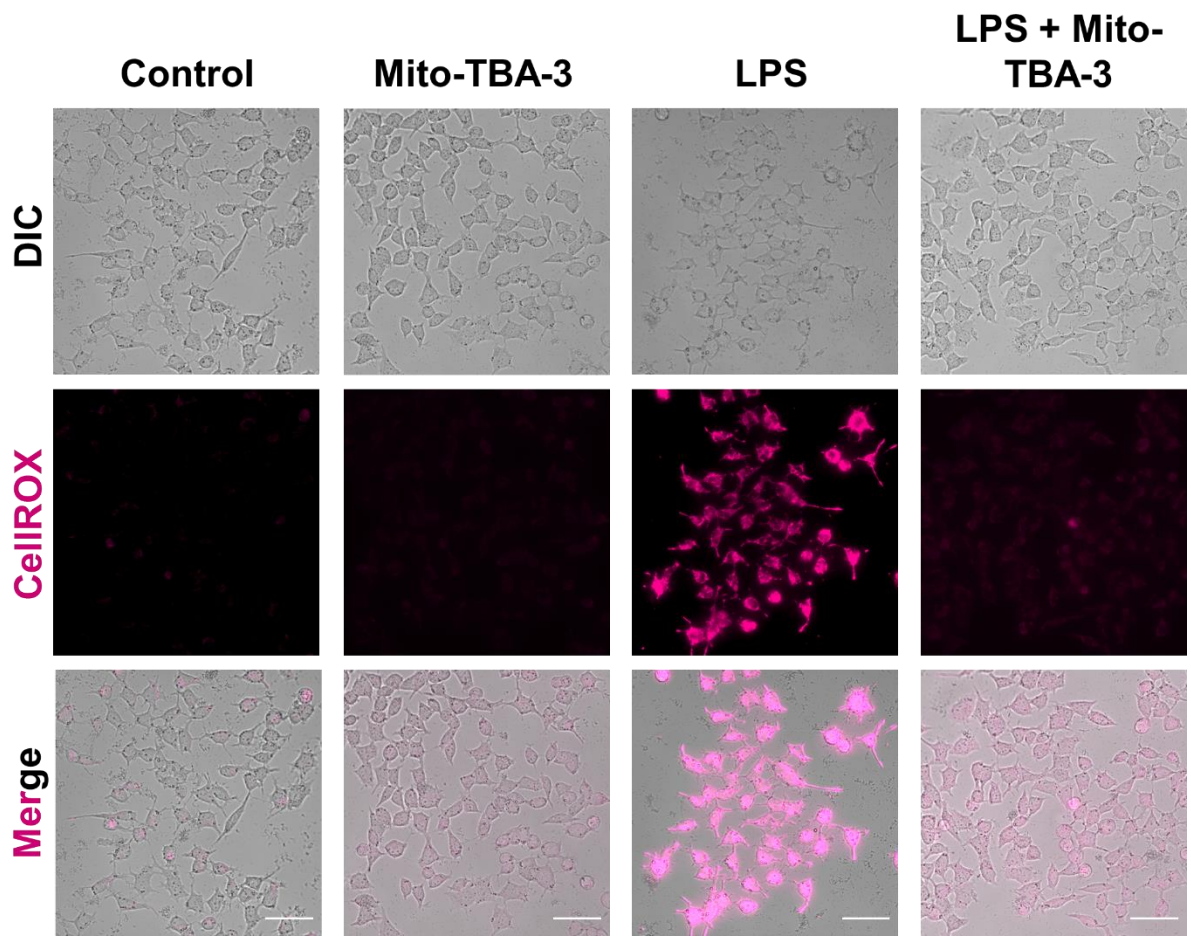


Figure 3.8 Neuroprotective effect of Mito-TBA-3 against LPS-induced oxidative stress in dPC12 rat pheochromocytoma cells. DIC and Fluorescent microscopic images of dPC12 cells stained with CellROX under different treatment conditions. Scale bar corresponds to 50 µm.

3.4.5 Mito-TBA's Mitigates Oxidative Stress due to $A\beta_{42}$ and Inhibits Cellular ROS Production in SHSY-5Y Neuroblastoma Cells: First, the biocompatibility of Mito-TBAs was assessed using MTT assay and to our expectation, none of the compounds showed any cytotoxic behaviour towards SH-SY5Y cells (**Figure 3.9 A, B, C**). The Mito-TBAs were further assessed for their capacity to protect cells against the harmful effects of $A\beta_{42}$. The SH-SY5Y cells were cultured with $A\beta_{42}$ (10 µM) and LPS (50 µg /mL) alone for about 24 h and 4 h, respectively, which decreased cell viability to approximately 50%. The cells were further treated with compounds (0.07-10 µM), and the viability of the cells was then evaluated using the MTT assay to determine if any rescue effect was observed. The cells cultured with $A\beta_{42}$ in the presence of Mito-TBA-3 demonstrated an excellent substantial increase in cell viability to around 82%, while other compounds Mito-TBA-1, Mito-TBA-2 rescue cell viability at around 75 and 71%, respectively (**Figure 3.9 D, E, F**). However, with LPS-treated cells the Mito-TBA-3 showed the best scavenging ability to rescue the SH-SY5Y from the oxidative damage caused due to LPS (**Figure 3.9 G, H, I**). From all the above results, it was obvious that Mito-TBA-3 has the highest free radical scavenging activity. Therefore, further experiments were conducted with the lead molecule Mito-TBA-3.

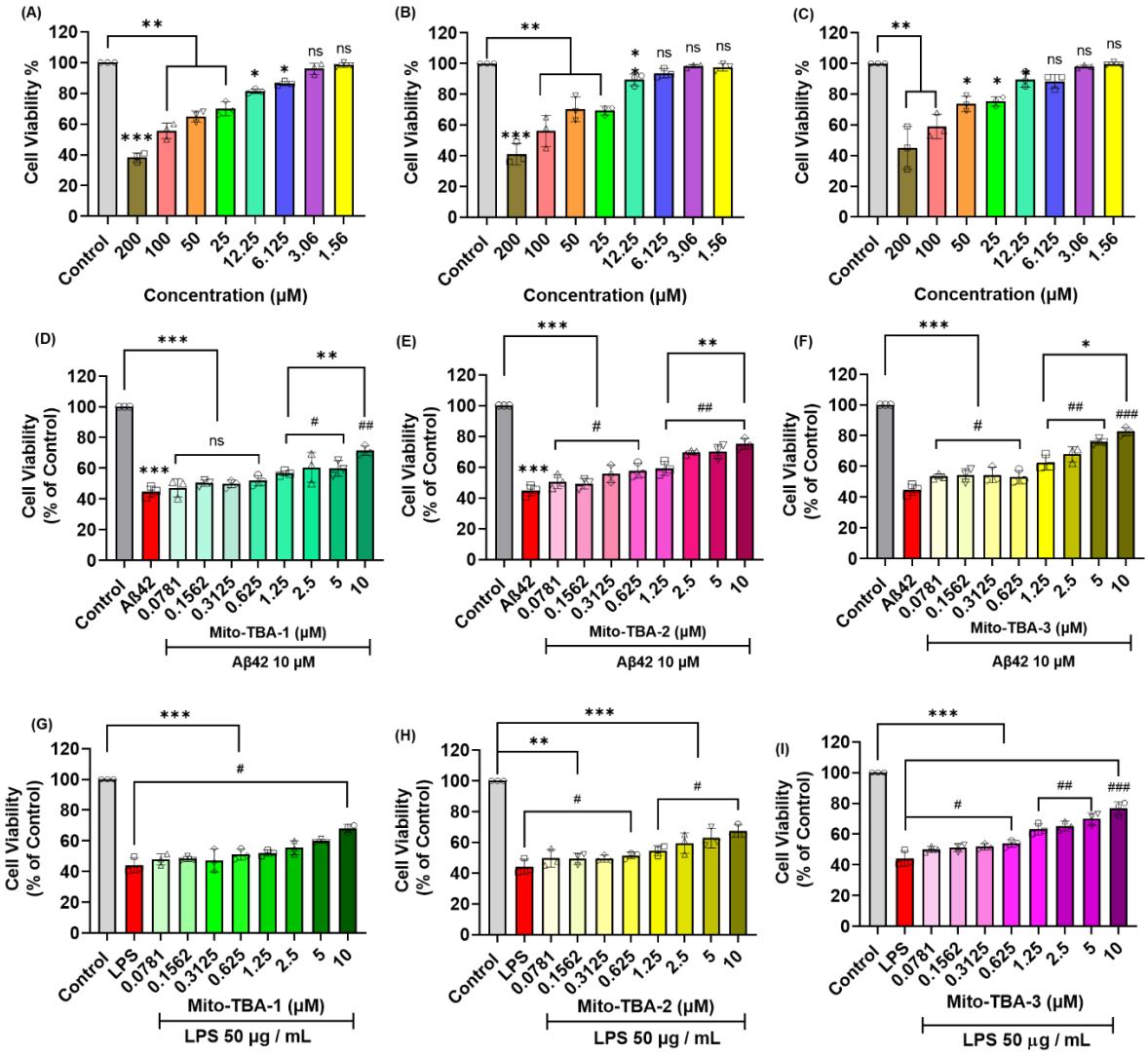


Figure 3.9 (A), (B) and (C) Cell viability (MTT assay) of Mito-TBA-1, Mito-TBA-2 and Mito-TBA-3 with SH-SY5Y at different concentrations (1.5-200 μM) after 24 hrs. (D), (E) and (F) Cell viability (MTT assay) of SH-SY5Y cells with Aβ42 (10 μM) and Mito-TBA-1, Mito-TBA-2 and Mito-TBA-3 (0.018-10 μM) respectively to determine the neuroprotective effect of Mito-TBA's. (G), (H) and (I) Cell viability (MTT assay) of SH-SY5Y cells with LPS (50 μg / mL) and Mito-TBA-1, Mito-TBA-2 and Mito-TBA-3 (0.018-10 μM) respectively to determine the neuroprotective effect of Mito-TBA's. Data represent mean ± SD of three independent experiments. The statistical significance of all the results was calculated by using a one-way analysis of variance (ANOVA) with Tukey's post hoc test. The results are represented as the mean ± SD, n = 3 per group from three independent experiments. Significances are marked as *P< 0.05, **P< 0.01, ***P< 0.001, **** P < 0.0001 versus the control group, #P<0.05, ##P<0.01, ###P<0.001, #### P < 0.0001 versus the LPS treatment group. Here, 'ns' is nonsignificant when compared to control.

The generation of ROS from the amyloid has been known as a significant factor contributing to neuronal death in people with AD. Further, the accumulation of ROS ultimately leads to a rise in oxidative stress, resulting in damage to several cellular components, including proteins, lipids, and DNA. Hence, the excellent neuroprotective effect of Mito-TBA-3 encouraged us to investigate further the role of Mito-TBA-3 in rescuing the cells from the oxidative stress caused due to the Aβ42 cytotoxicity. We have performed the DCFHDA assay on differentiated SH-SY5Y cells

to check the effect of Mito-TBA-3 in mitigating the excessive ROS produced due to $A\beta_{42}$. The results have shown that in the control group of cells, the green fluorescent intensity was minimal due to the absence of any ROS, however, a substantial increase in green fluorescent was observed in the $A\beta_{42}$ group of treated SH-SY5Y cells, which is due to the oxidative stress and neuronal cell death due to $A\beta_{42}$ cytotoxicity (**Figure 3.10**).

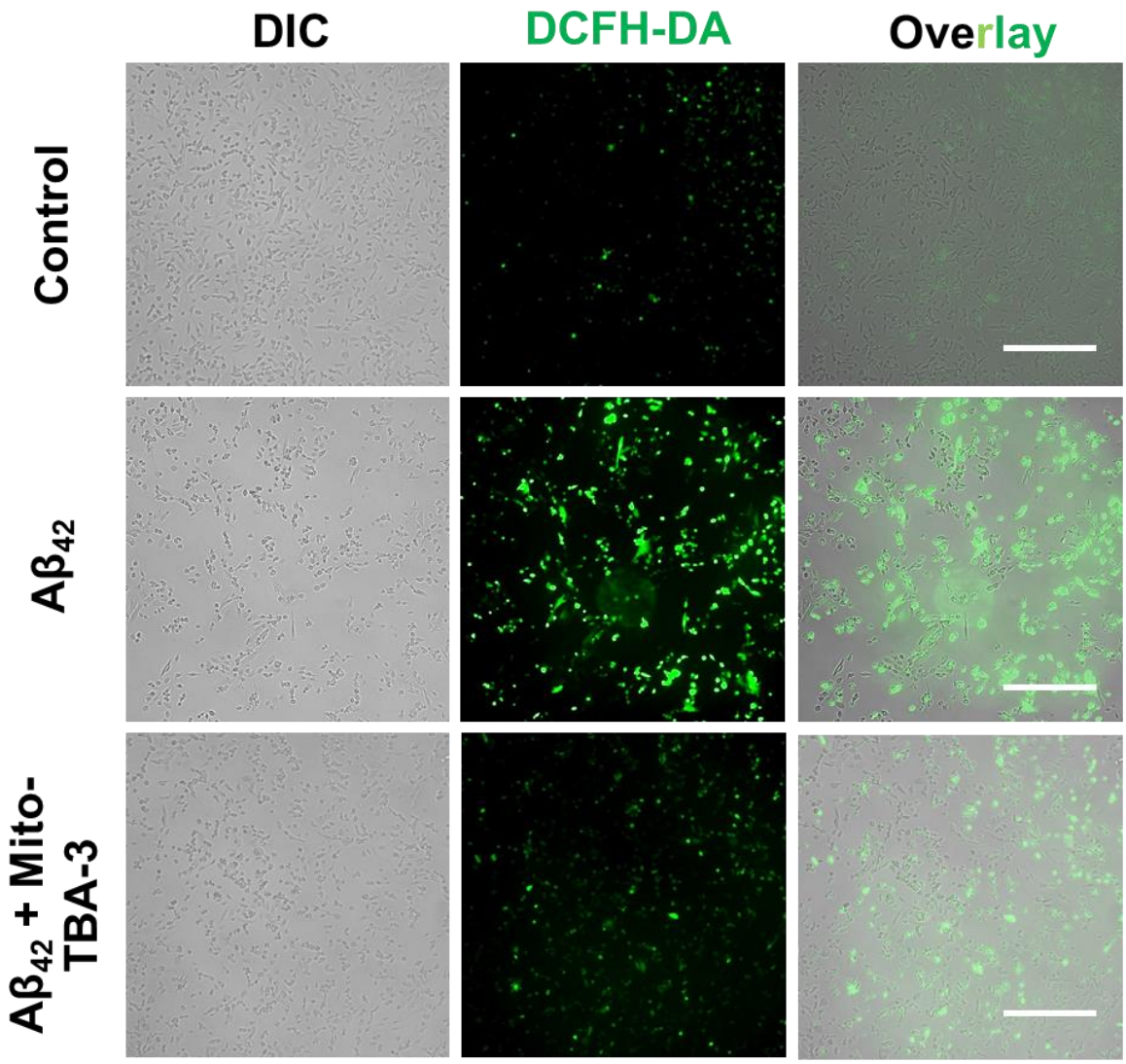


Figure 3.10 Neuroprotective effect of Mito-TBA-3 against LPS-induced oxidative stress in dPC12 rat pheochromocytoma cells DIC and Fluorescent Images of DCFH-DA assay used to determine the overall level of ROS in SH-SY5Y cells after Mito-TBA-3 treatment. Scale bar corresponds to 200 µm.

Further analysis was performed to verify whether Mito-TBA-3 can reduce the excessive levels of intracellular ROS in differentiated SH-SY5Y cells caused by $A\beta_{42}$. The quantity of intracellular ROS generated was assessed using CellROX dye. **Figure 3.11** shows an increase in red fluorescence after $A\beta_{42}$ pretreatment. In contrast, cells that were pretreated with $A\beta_{42}$ and then treated with Mito-TBA-3 showed a notable reduction in red intensity, as seen in (**Figure 3.12 A**). Therefore, our data indicate that Mito-TBA-3 possesses the capacity to effectively eliminate excessive ROS.

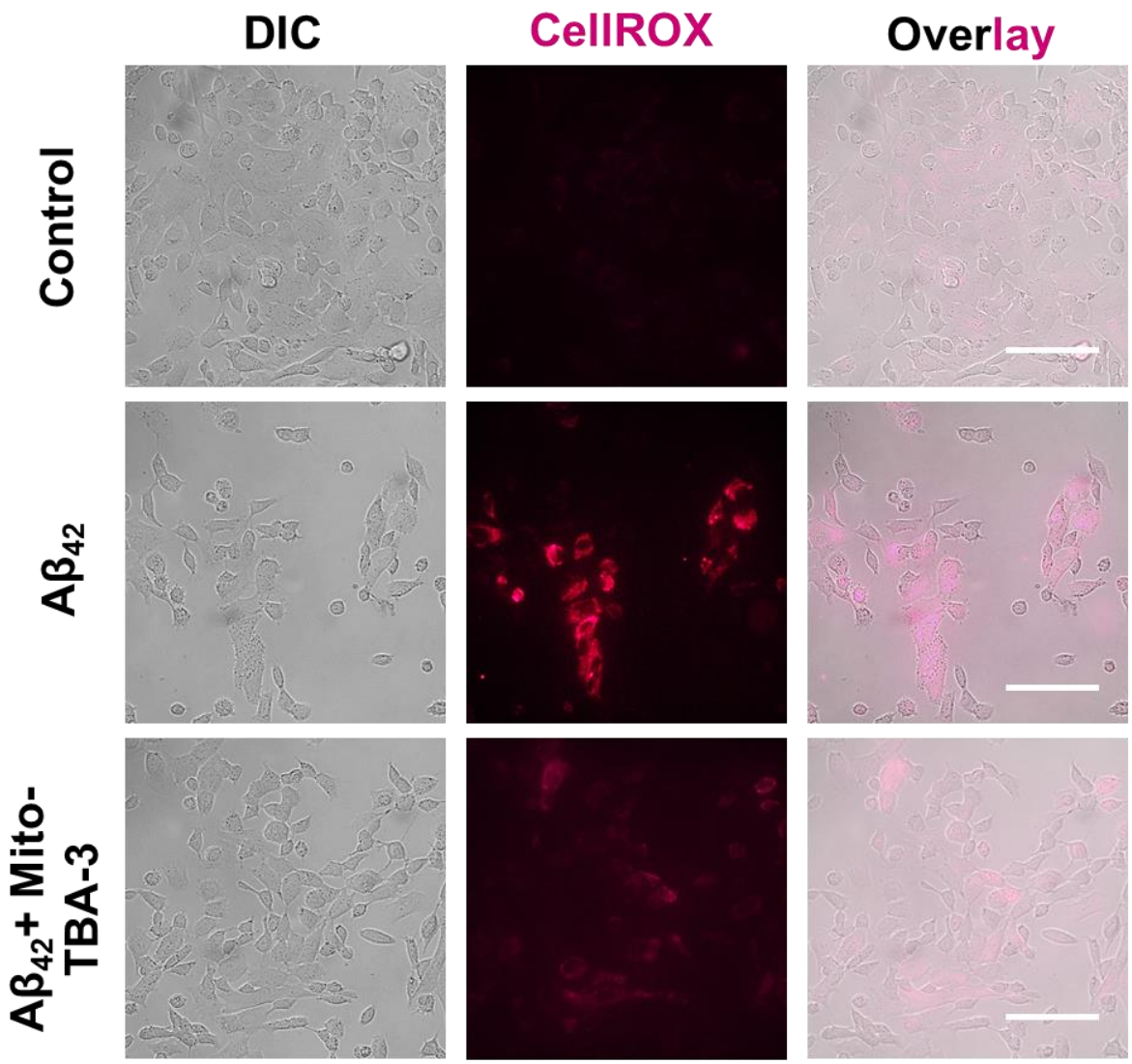


Figure 3.11 Neuroprotective effect of Mito-TBA-3 against LPS-induced oxidative stress in dPC12 rat pheochromocytoma cells. DIC and Fluorescent microscopic images of SH-SY5Y cells stained with CellROX under different treatment conditions. Scale bar corresponds to 50 µm.

The Calcein-AM and PI assay is a commonly used method for assessing cell viability and quantifying the potential of substances to protect cells from oxidative harm. In order to further investigate the suppressive effect of Mito-TBA-3 on cellular apoptosis due to $A\beta_{42}$ toxicity, the cells were subjected to staining with Calcein-AM and PI. **Figure 3.12 B** demonstrates a notable rise in the quantity of red-stained deceased cells in the group that received $A\beta_{42}$ pretreatment. In contrast, the Mito-TBA-3 therapy group exhibited a substantial drop in the number of deceased cells (**Figure 3.12 C**). The findings of Calcein-AM/PI imaging align with the results obtained by MTT and the quantitative analysis of live-dead fluorescence images.

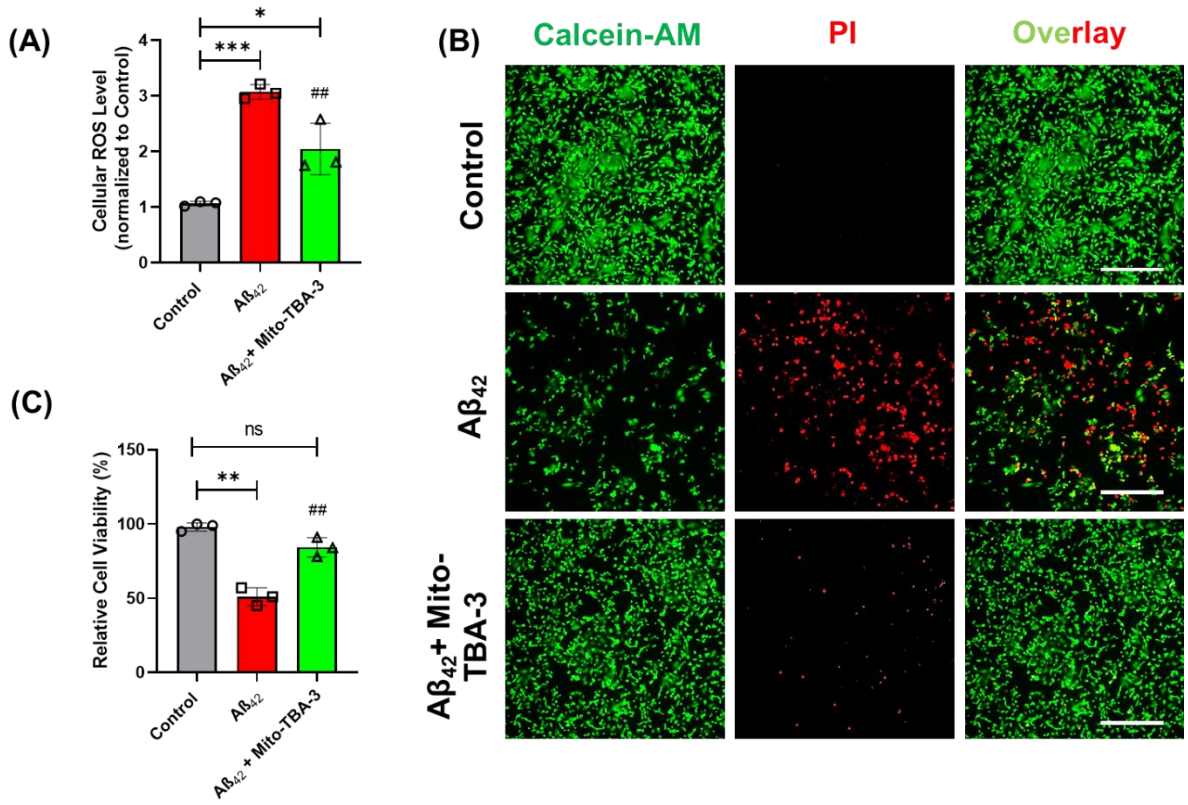


Figure 3.12 (A) Representative bar showing quantification of CellROX results to determine the total ROS, obtained from fluorescent microscopy images under different treatment conditions. (B) Calcein-AM / PI images of SH-SY5Y cells pretreated with Aβ42 (10 µM) alone, and Aβ42 (10 µM) + Mito-TBA-3 (C) The relative cell viability of SH-SY5Y cells, quantitatively analyzed using Image J software. Scale bar corresponds to 200 µm. Data represent mean ± SD of three independent experiments. The statistical significance of all the results was calculated by using a one-way analysis of variance (ANOVA) with Tukey's post hoc test. The results are represented as the mean ± SD, n = 3 per group from three independent experiments. Significances are marked as *P< 0.05, **P< 0.01, ***P< 0.001, **** P < 0.0001 versus the control group, #P<0.05, ##P<0.01, ###P<0.001, #### P < 0.0001 versus the LPS treatment group. Here, 'ns' is nonsignificant when compared to control.

3.4.6 Impact of Mito-TBA-3 on Mitochondria Morphofunction Impairment and ROS in LPS-induced Oxidative Stress Injury: The buildup of ROS can result in various damage to cellular constituents and can lead to a range of disorders, starting from DNA damage and mutations to mitophagy of mitochondria, hence potentially elevating the susceptibility of cellular apoptosis. Due to its role in oxidative phosphorylation and electron transport chain, mitochondria also serve as a major source of superoxide and other ROS. The excessive generation of these ROS results in the disturbance of mitochondria shape and membrane potential. Furthermore, the overabundance of ROS generated in mitochondria has been associated with the process of ageing and other neurological disorders. Therefore, the significance of preserving a harmonious level of ROS within cytoplasmic and mitochondrial microenvironment is of atmost importance to ensure optimal cellular well-being.

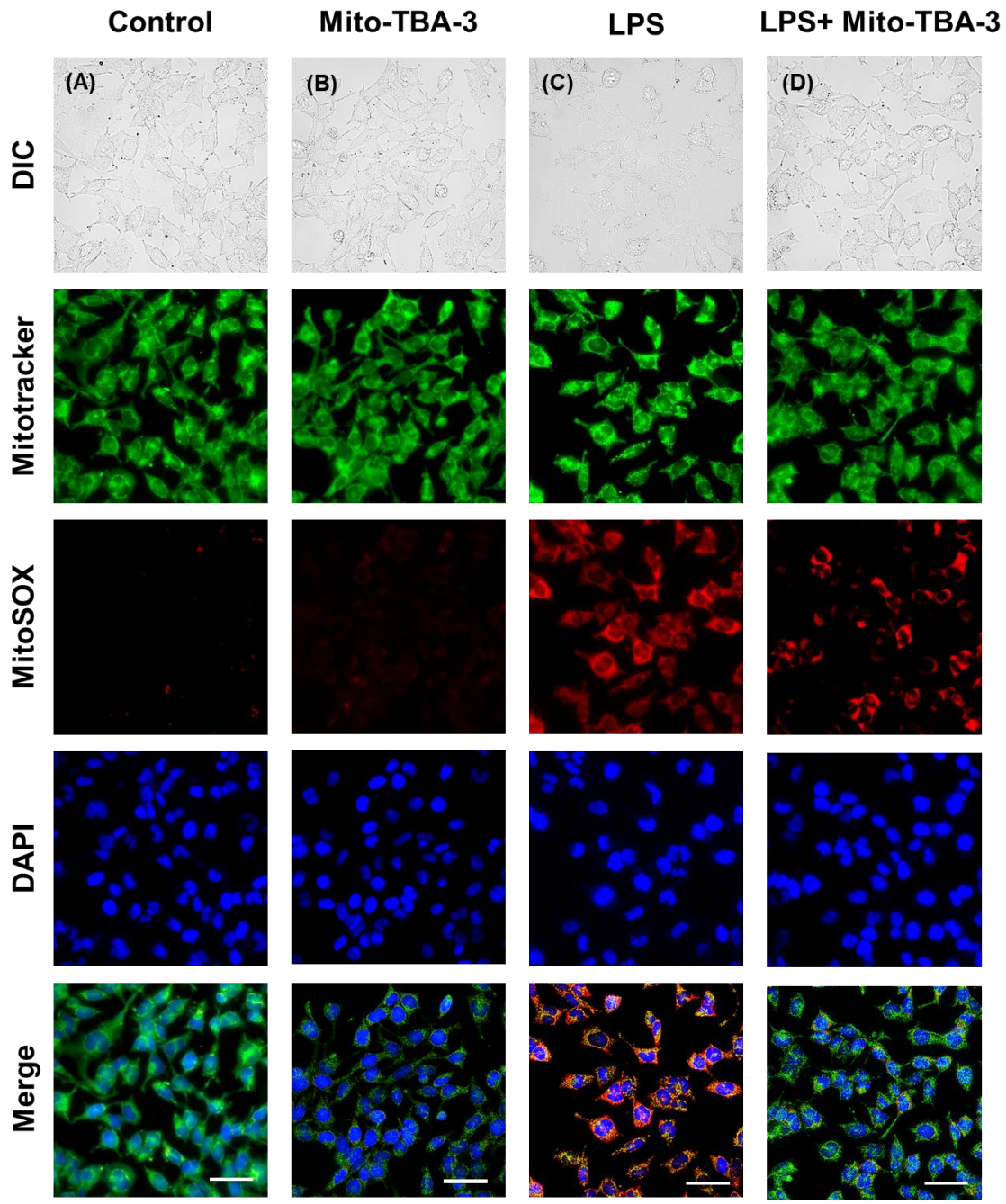


Figure 3.13 Mito-TBA-3 mitigates mitochondrial oxidative stress, restores mitochondria morphology and alleviates LPS induced oxidative stress in dPC12 cells. Fluorescent microscopy images of Mitotracker-Green (200 nM) and MitoSox-Red (5 µM) staining in live dPC12 cells, counter stained with DAPI under (A) control, (B) Mito-TBA-3, (C) LPS and (D) LPS + Mito-TBA-3. Scale bar corresponds to 20 µm.

In this study, we assessed the potential of Mito-TBA-3 to eradicate ROS in mitochondria, specifically using MitoSOX (Red) dye. dPC12 cells were pretreated with 50 µg / mL of LPS for approximately 4 h to induce oxidative stress following treatment with Mito-TBA-3 (10 µM) for an additional 24 h.

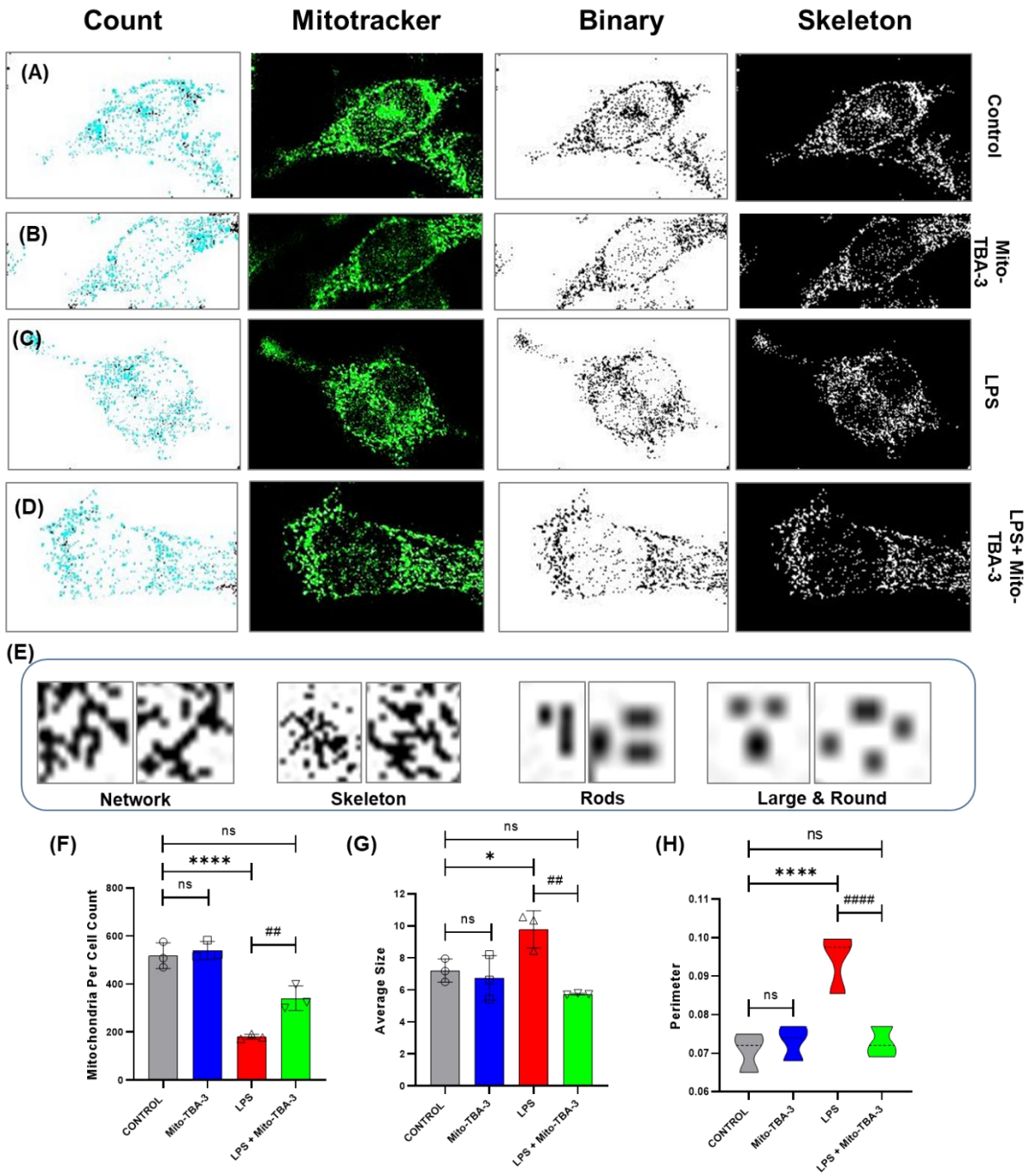


Figure 3.14 Representative fluorescent microscopic image of dPC12 cells stained with the MitoTracker green, Lysotracker red, and Hoechst 33342 under different treated condition (A) control, (B) Mito-TBA-3, (C) LPS and (D) LPS + Mito-TBA-3, (E) Mitochondria dynamic shape, (F) Mitochondria Per cell count, (G) Average Size and (H) Mitochondrial parameters like Perimeter, under different treatment conditions (n=3 per group). Data represent mean ± SD of three independent experiments. The statistical significance of all the results was calculated by using a one-way analysis of variance (ANOVA) with Tukey's post hoc test. The results are represented as the mean ± SD, n = 3 per group from three independent experiments. Significances are marked as *P< 0.05, **P< 0.01, ***P< 0.001, **** P < 0.0001 versus the control group, $^{\#}$P<0.05, $^{\#\#}$P<0.01, $^{\#\#\#}$P<0.001, $^{\#\#\#\#}$ P < 0.0001 versus the LPS treatment group. Here, 'ns' is nonsignificant when compared to control.

Following that cells were stained with 5 µM of MitoSox in colorless DMEM under dark condition at 37°C for 15 minutes to determine the superoxide generation in

mitochondria. MitoSOX is a highly selective fluorescent superoxide dye for the detection of superoxide in live cells. It has been observed that the fluorescence intensity of MitoSOX was higher in cells pretreated with LPS, which might be due to the disruption of mitochondrial morphology and integrity, which ultimately leads to superoxide generation in mitochondria, where the MitoSOX intensity in Mito-TBA-3 treatment was comparatively low as compared to the LPS group (**Figure 3.13 A-D**). This unequivocally demonstrates the exceptional capacity of Mito-TBA-3 to scavenge mitochondria-specific ROS, highlighting their potential as a strong antioxidant for alleviating oxidative stress. Moreover, the observed decrease in MitoSOX fluorescence intensity indicates that Mito-TBA-3 possess a notable ability to specifically target ROS within mitochondria.

Furthermore, in addition, to assess both the overall mitochondrial content and structure, cells were simultaneously labelled with Mitotracker Green (**Figure 3.13**). To determine the mitochondria morphology, cells were stained with Mitotracker Green. Cells were pretreated with LPS (50 µg / mL for 4 h) to induce oxidative stress following treatment with Mito-TBA-3 (10 µM) for an additional 24 h. After that cells were stained with 200 nM of Mitotracker green in colourless DMEM media under dark condition for 15 minutes at 37°C. Further cells were counterstained with DAPI to stain the nucleus. Here, our observation revealed that the mitochondria in the control untreated group were predominantly in a healthy filamentous, tubular, and hyperfused form (**Figure 3.14 A, E**). However, when cells were pretreated with LPS (**Figure 3.14 B**), there was an increase in the proportion of mitochondria with a round shape, accompanied with increased swelling, creation of punctiform structures, and disintegration of filamentous structures (**Figure 3.14 C**). These results clearly indicates that exposure to LPS results in mitochondrial malfunction and changes in shape, potentially suggesting damage to the mitochondria. Furthermore, treatment with Mito-TBA-3 have averted the transition of mitochondria morphology from a complex branching structure to a more spherical shape (**Figure 3.14 D**). Moreover, in order to assess the changes in the shape of mitochondria, we analyzed the raw Mitotracker Green images using the Mitochondria analyzer in Fiji/Image J. This allowed us to calculate indices such as mitochondria count, perimeter, circularity, and average size. Based on our data, pretreatment with LPS resulted in increased levels of ROS, which caused irregularities in the shape of the mitochondria (**Figure 3.14 F**). This was indicated by a decrease in the number of mitochondria per cell, an increase in average size and the perimeter of the mitochondria (**Figure 3.14 G, H**).

3.4.7 Mito-TBA-3 Inhibits the LPS-Induced Auto-Mitophagy and Restores Mitochondria Network Dynamics: Autophagy is a vital cellular phenomenon in which cells dismantle their own components to maintain homeostasis. Autophagy is a process in which misfolded or aggregated proteins and malfunctioning cellular organelles are enclosed within a doubled membraned vesicle. Then, this vesicle subsequently transports the loaded cargo to the lysosome, where it is broken down. Mitophagy is a quality control mechanism that selectively removes malfunctioning or damaged mitochondria by autophagy. It serves to minimize inflammation, suppress cell death signals, and prevent unnecessary cell loss upon exposure to different stressors. Additionally, LPS

has been known to trigger mitochondrial dysfunction, mitochondria-mediated inflammation and autophagy in neurons, cardiomyocytes and osteoclasts

Mitochondrial autophagy, also known as mitophagy, is a crucial process that ensures the upkeep of mitochondrial quality by removing malfunctioning mitochondria. As no single characteristic alone is enough to confirm mitophagy conclusively, hence in order to establish whether Mito-TBA-3 can inhibit the LPS-induced mitophagy definitively, we examined the co-localization of Lysotracker red-labeled acidic bodies with Mitotracker Green-labeled mitochondria using ICC, this approach is beneficial in identifying the first stages of mitophagy that can occur in the presence of LPS. As evident from the cells in the control group (**Figure 3.15 A**) and Mito-TBA-3 treatment group (**Figure 3.15 B**), there are no signs of mitophagy, which suggests that Mito-TBA-3 does not have any adverse effect on mitochondria. Interestingly, as shown in **Figure 3.15 D** Mito-TBA-3 treatment significantly alleviates the auto(mito)phagy compared to the LPS-treated group (**Figure 3.15 C**). Overall, the imaging data suggests that Mito-TBA-3 might be involved in the cellular adaptive response.

3.4.8 Inhibition of Apoptosis and Inflammation by Mito-TBA-3: Apoptotic cell death can be easily recognized based on the shape of the nuceli. During apoptotic cell death, the organelles and cell membrane are preserved for a short span of time, whereas the nucleus suffers preliminary degeneration. Cap-shaped chromatin margination is commonly observed as an early indicator of apoptosis. Additionally, one may see the condensation of cytosol, pyknosis, and the formation of cell membrane blebs. Moreover, the nucleus subsequently forms several electron-dense micronuclei, which are frequently discharged into the extracellular environment. The changes in the shape of the nucleus during apoptosis are noticeable signs that programmed cell death is happening. In addition, apoptosis is often accompanied by nuclear fragmentation and membrane blebbing. Labelling techniques, such as DAPI labelling, help us to visualise morphological changes, making it easier to distinguish apoptotic cells from healthy ones. Examining these morphological characteristics provides the essential understanding of the fundamental processes and control of apoptosis. The change in the shape of the nucleus and its roundness has been identified as an early indicator of cell death. Researchers studying cell death mechanisms find this quantitative measure simply calculable using image analysis software, making it a practical tool.

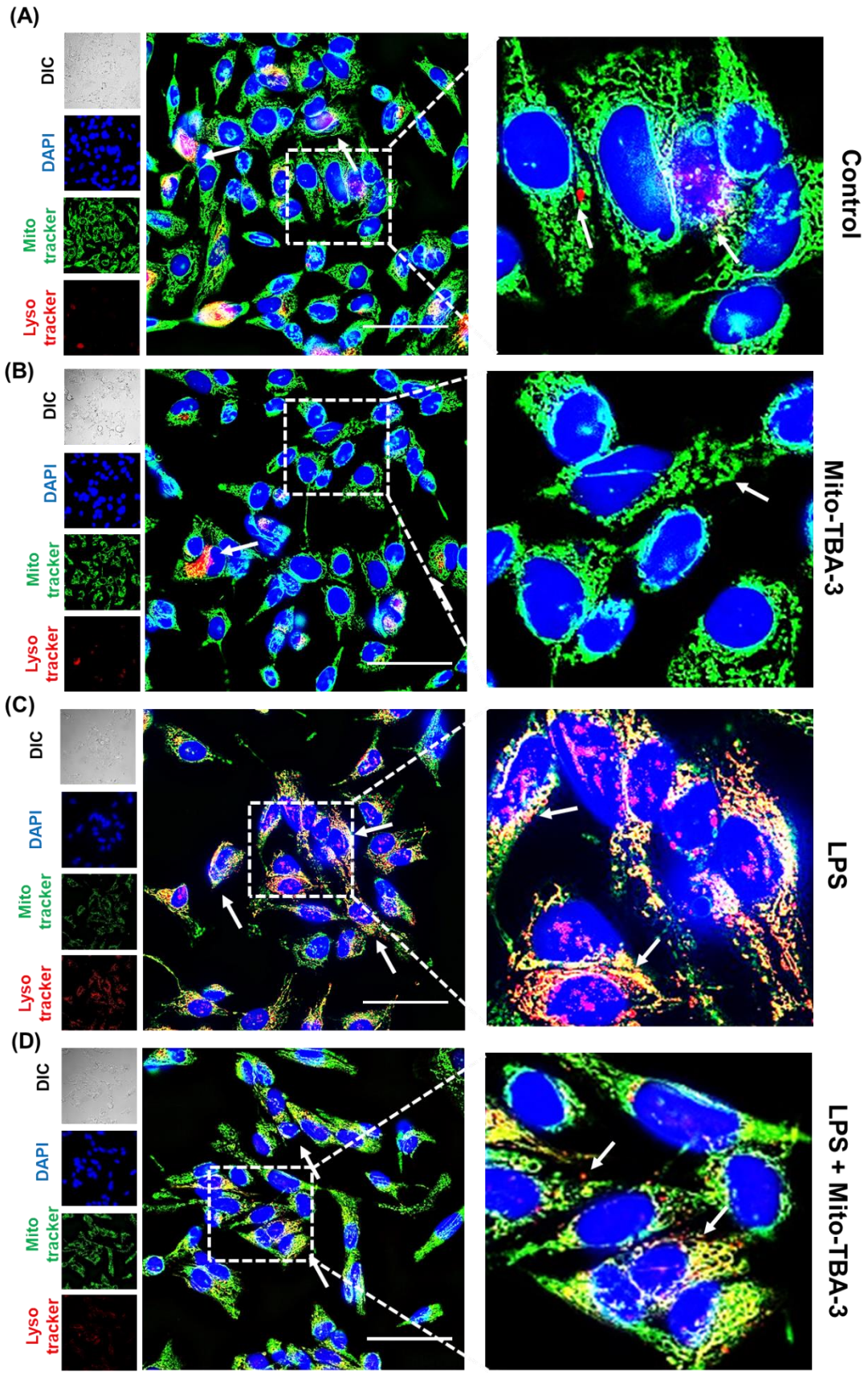


Figure 3.15 Representative fluorescent microscopic image of dPC12 cells stained with the MitoTracker green, Lysotracker red, and Hoechst 33342 under different treated condition (A) control, (B) Mito-TBA-3, (C) LPS and (D) LPS + Mito-TBA-3. Scale bar corresponds to 20 µm

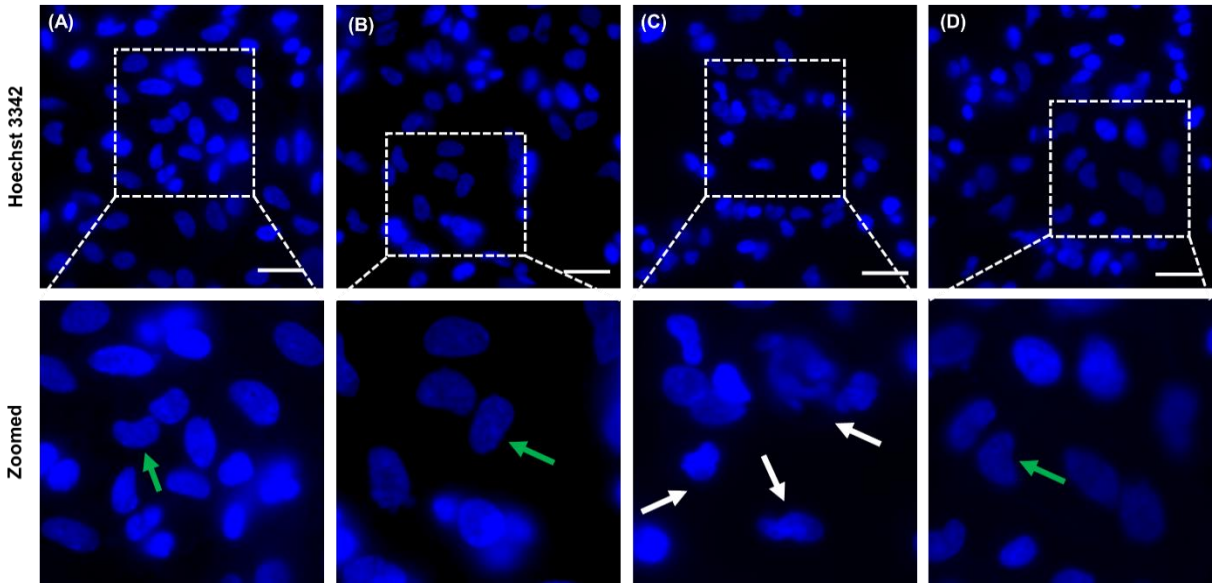


Figure 3.16 Representative fluorescent microscopic image of dPC12 cells stained with Hoechst 33342 to check the nuclear pyknosis under different treated conditions (A) control, (B) Mito-TBA-3, (C) LPS and (D) LPS + Mito-TBA-3. Scale bar corresponds 50µm.

3.4.9 Mito-TBA-3 Inhibits the LPS-Induced Mitochondrial Membrane Potential Disruption and Hyperpolarization in dPC12 Cells: Subsequently, we wondered if our observations on the fragmentation of mitochondria under oxidative stress caused by LPS were also applicable to the hypothesis that excessive oxidative stress also results in a decline in mitochondrial membrane potential ($\Delta\Psi_M$, MMP). Thus, we performed fluorescent JC-1 staining to detect both the quantitative and qualitative changes in $\Delta\Psi_M$. Within healthy cells, JC-1 molecules assemble in the mitochondria's matrix to create J-aggregates when the $\Delta\Psi_M$ is high. These J-aggregates emit a robust red fluorescence when excited at 560 nm and emit light at 595 nm. However, in apoptotic cells, JC-1 is unable to accumulate in the matrix. As a result, it resides in the matrix as monomers, which emit a strong green fluorescence under low $\Delta\Psi_M$ conditions.

Hence, the assessment of mitochondrial membrane depolarization can be accomplished by measuring the extent of the transition from red to green fluorescence. The fluorescent images acquired of mitochondria stained with JC-1 dye (**Figure 3.17**) exhibited red fluorescence in both the control and Mito-TBA-3 treated group of dPC12 cells, indicating the presence of healthy and functioning mitochondria and Mito-TBA-3 does not impart any adverse change in the $\Delta\Psi_M$ and mitochondria morphology. Nevertheless, the presence of LPS resulted in a notable alteration from red to green in the fluorescence of JC-1 dye, in comparison to the control group. Therefore, it can be concluded that the integrity of the mitochondrial membrane is compromised by causing a reduction in the electrical potential across the membrane and the mitochondrial membrane potential (MMP) due to the presence of LPS. However, this effect has been reversed after administering treatment with Mito-TBA-3. Therefore, the $\Delta\Psi_M$ of cells treated with Mito-TBA-3 exhibited a gradual restoration, as evidenced by the increase in red-stained mitochondria and decrease in green fluorescent mitochondria. Further, fluorescence intensity was measured in each treatment group using Image J, NIH analysis software (USA).

3.4.10 Effect of Mito-TBA-3 on F-actin levels in LPS-stimulated dPC12 Cells: It has been shown in the literature that upon stimulation with LPS, LPS induces reorganization of the actin cytoskeleton, leading to the creation of a contractile ring at the outer edge of the cell and the rupture of stress fibres in the centre. This results in reduced cell adhesion and an increased tendency for cells to detach. Furthermore, the increased occurrence of F-actin bundles and a decrease in neurite outlength and aggregates imply that LPS may alter the stability and rigidity of the actin cytoskeleton, thus impacting the mechanical characteristics of cells.

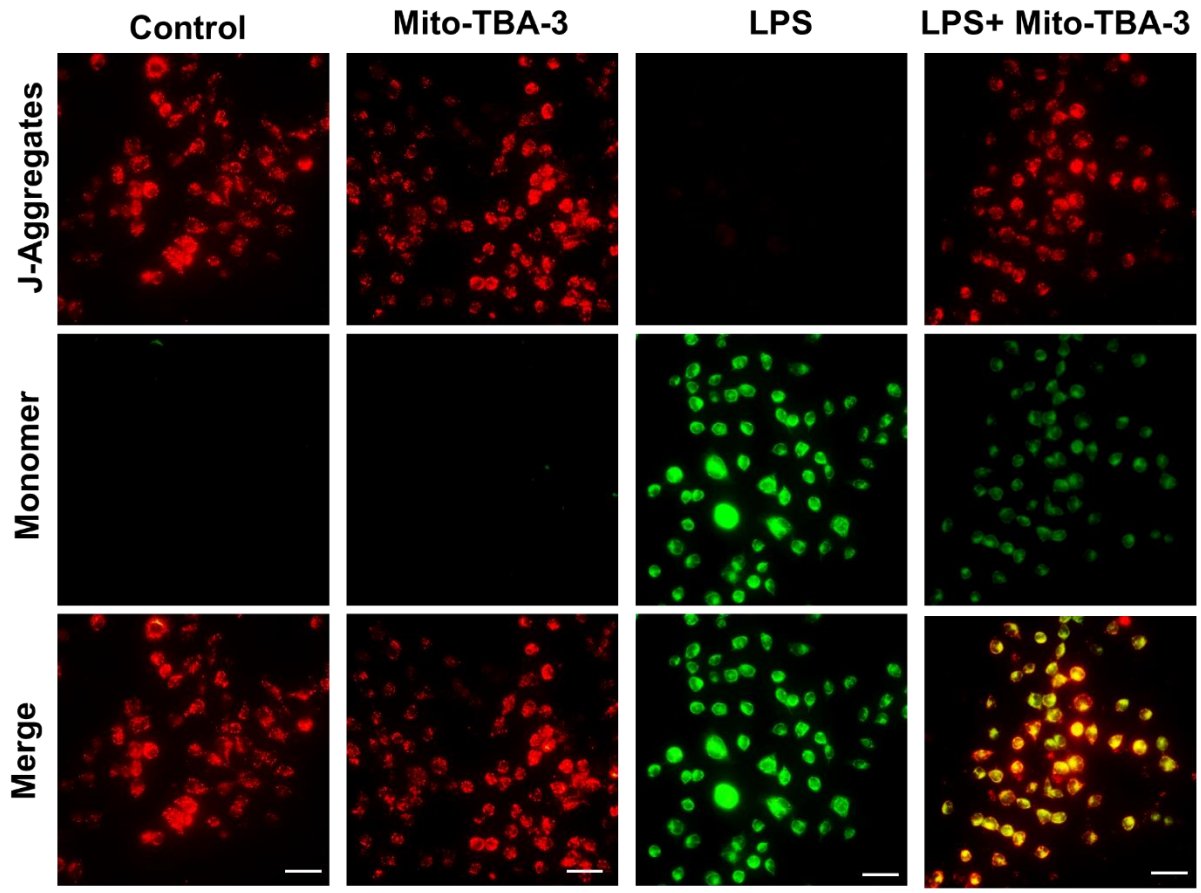


Figure 3.17 Determination of MMP using JC-1 staining, actin filament organization and microtubule structure using Phalloidin staining. Fluorescent microscopic images show JC-1 aggregates (Red, healthy cells) and JC-1 monomers (Green, apoptotic cells) of dPC12 cells stained with JC-1 dye under different treatment conditions control, Mito-TBA-3, LPS and LPS + Mito-TBA-3. Scale Bar corresponds to 50µm.

Hence, in view of the antioxidative property of Mito-TBA-3, we have checked whether Mito-TBA-3 can suppress the disruption of actin cytoskeleton. As expected, treatment with Mito-TBA-3 prevented the LPS-induced loss of the F-actin cytoskeleton. Moreover, there were no discernible variations in F-actin levels between the control group or the Mito-TBA group without LPS stimulation (**Figure 3.18**).

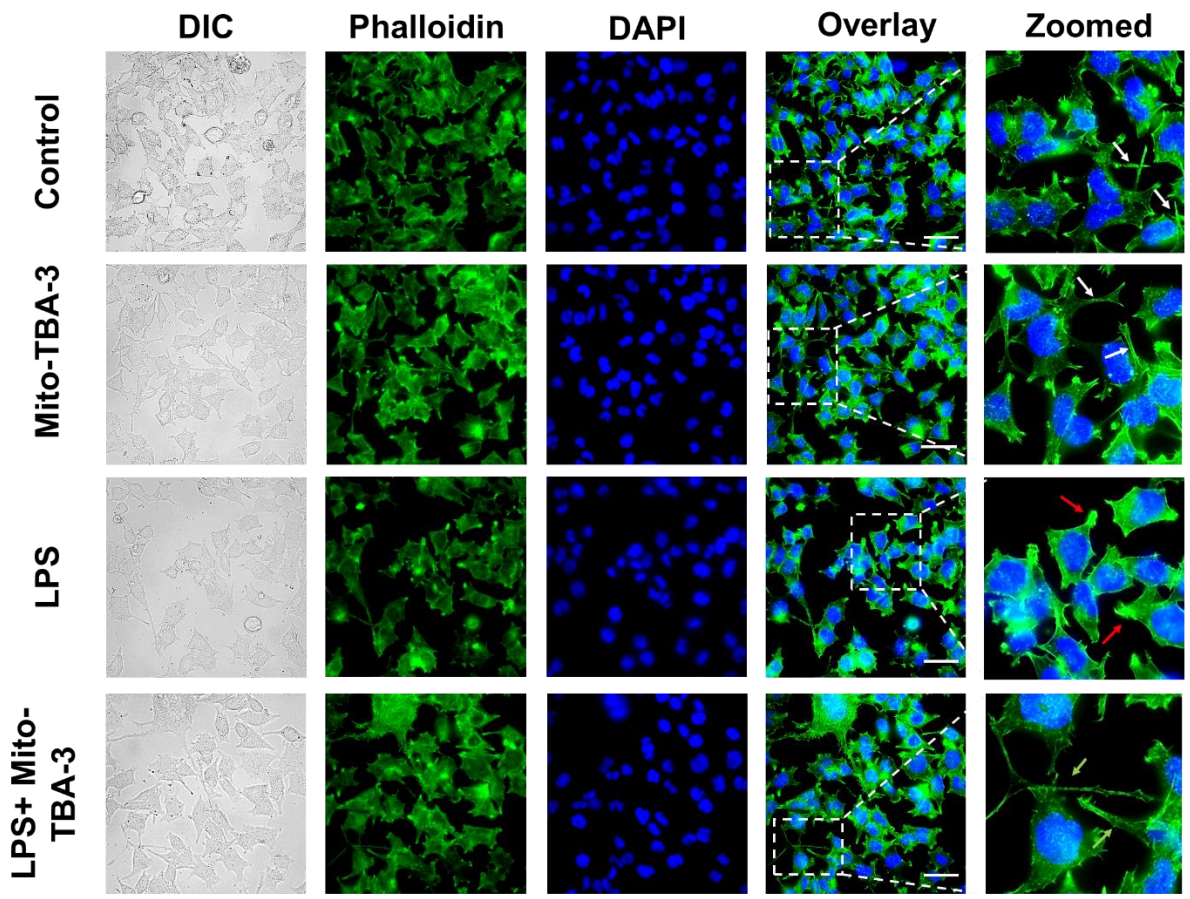


Figure 3.18 Neuroprotective effect of Mito-TBA-3 against LPS-induced oxidative stress in dPC12 rat pheochromocytoma cells. Analysis of actin fillopodia outgrowth using Phalloidin staining in control, Mito-TBA-3, LPS and LPS + Mito-TBA-3. Scale Bar corresponds to 50µm.

3.4.11 Molecular Docking Analysis: Prior to further pathway analysis, we validated the design concept of our lead molecule using *in-silico* method to determine their potential binding affinity to the Nrf-2 gene. The validation process includes conducting a molecular docking analysis between our specifically designed small molecule and the Nrf-2 protein (PDB ID: 2DYH). An examination of molecular docking showed that the proposed molecule interacted with a specific pocket in the structure of the Nrf-2 protein, mostly through π−π stacking interaction (**Figure 3.19 A, B**).

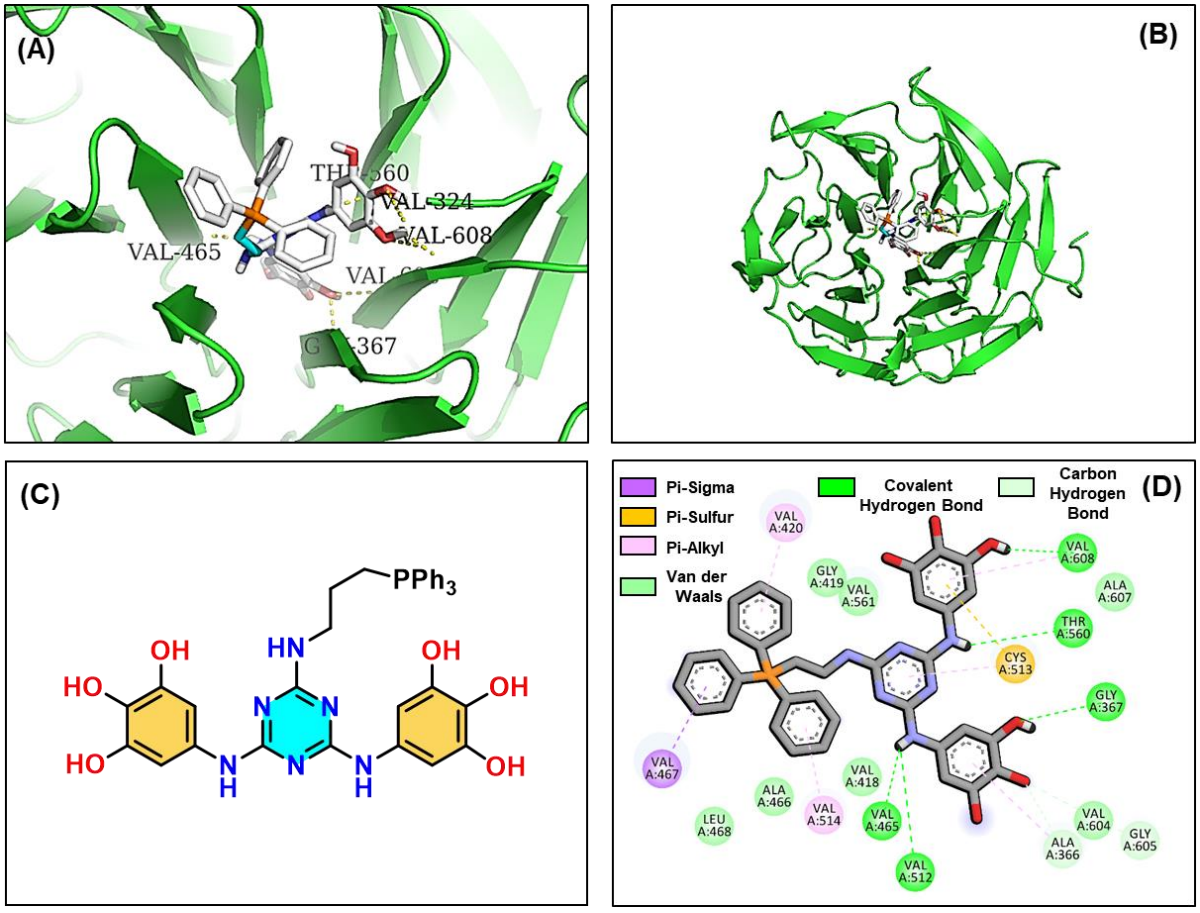


Figure 3.19 (A) Binding site of Mito-TBA-3 with Nrf-2 / Keap1 complex protein (PDB ID: 5NJ8) showing possible binding interactions with key amino acids. (B) Binding model of Mito-TBA-3 with Nrf-2 / Keap1 complex protein (C) Structure of Mito-TBA-3(D) 2D binding interactions of Mito-TBA-3with the important amino acid residues. Purple circles reflects pi-sigma interaction, Pink circles reflects pi-alkyl interaction, yellow circle represent pi-sulfur interaction, light green circle indicates carbon hydrogen bonding, dark green circle indicates covalent hydrogen bonding, sea green circle indicates van der Waals interaction of amino acid residues with ligand.

The lead molecule Mito-TBA-3, when docked, demonstrates interacting with the Nrf-2 protein through a complex network of interactions, with a binding affinity of -10.2 kcal/mol. The ligand molecule Mito-TBA-3 formed a binding relationship with the Nrf-2 protein by attaching to a specific pocket. It engaged in π−π stacked interactions with Ala-366, Val-604 and Gly-605. Additionally, it participated in a pi-sulfur interaction with Cys-513. In addition, Mito-TBA-3 also established typical hydrogen bonding contacts with Val-608, Thr-560, Gly-367, Val-465 and Val-512, which were made possible by the presence of a polyhydroxy group (**Figure 3.19 C, D**).

3.4.12 Inhibition of LPS-Induced Neuronal Loss and TLR-4 Pathway Mediated Inflammation by Mito-TBA-3: Toll-like receptors (TLRs) are a type of pattern recognition receptors (PRRs) that identify pathogen-associated molecular patterns (PAMPs) and elicit prompt inflammatory reactions in response to any foreign antigen. TLR-signalling is known to trigger the recruitment of specific adaptor molecules, which in turn activates various transcription factors in response to any infection. These transcription factors enhance the production of different inflammatory mediators,

including cytokines and chemokines such as IL-1α, IL-6, TNF-α, IL-23, IL-1β, IL-8 and IL-12. There are different subtypes of TLRs, these subtypes vary in terms of ligand specificity, cellular location, method of multimerization upon activation, and downstream signalling pathway. TLR-4 is generally localized on the surface of the cell. Within the CNS, TLR-4 is mainly present on microglia and astrocytes, although they can also be found on neurons, oligodendrocytes and Schwann cells. When TLR-4 gets activated, these microglia generate proinflammatory cytokines, including TNF-α, IL-1β, prostaglandin E2 (PGE2), NO and several other cytokines. These cytokines play a crucial role in the neuro-inflammatory process. TLR-4 has a crucial role in causing the widespread death of neuronal cells.

LPS a component of cell walls of gram-negative bacteria, is initially recognized as a ligand for Toll-like receptor 4 (TLR-4). It has been well-known as a stimulant of the immune system. Its potent ability to cause inflammation and the extensively studied immune system activation pathways have led to the widespread use of LPS as a model for studying sepsis and inflammation in mammals. In modern times, advanced medical research employs more precise in vitro and in vivo models to study LPS-induced inflammation and oxidative stress like cardiac dysfunction, acute septic renal injury, acute lung injury, periodontitis, endometritis, uveitis, mastitis, preeclampsia and other CNS disorders.

In addition, the injection of LPS to animals causes cognitive impairment, as well as a variety of behaviours such as anorexia, reduced movement, weight loss, exploratory behaviour, heightened anxiety, drowsiness, and overall behavioural depression. Many of these symptoms are believed to closely resemble the clinically significant symptoms of neurodegenerative illness in people. Consequently, the administration of LPS is commonly employed to investigate disorders in mice that are related with neuroinflammation. Nevertheless, the LPS model of neuroinflammation also has been extensively utilized in the field of brain research.

Therefore, in order to determine whether or not our designed molecule was capable of reducing the inflammation that was caused by LPS through the TLR-4 pathway, we examined the mRNA expression of a number of downstream signalling molecules that are associated with the TLR-4 pathway (**Figure 3.20**). The Mito-TBA-3 has, as anticipated, been found to decrease the expression of the key intermediates of the TLR-4 pathway, which include TLR-4 and MyD88. The expression of TLR-4 and MyD88 were found to be significantly increased in the LPS group as compared to the control group (**Figure 3.20 A-C**). This increase in the expression of TLR-4 is known to cause an increase in phosphorylation of IκBα and IκB kinase (IKK), which will ultimately induce the translocation of NF-κB p65 subunit into the nucleus. An increase in translocation of NF-κB p65 subunit into the nucleus is known to increase the expression of various proinflammatory cytokines like TNF-α, IL-1β, IL-6, iNOS and various other cytokines. Furthermore, it has been observed to limit the overexpression of several proinflammatory cytokines, while simultaneously enhancing the expression of anti-inflammatory cytokines, specifically IL-4 and IL-10 (**Figure 3.20 D-H**).

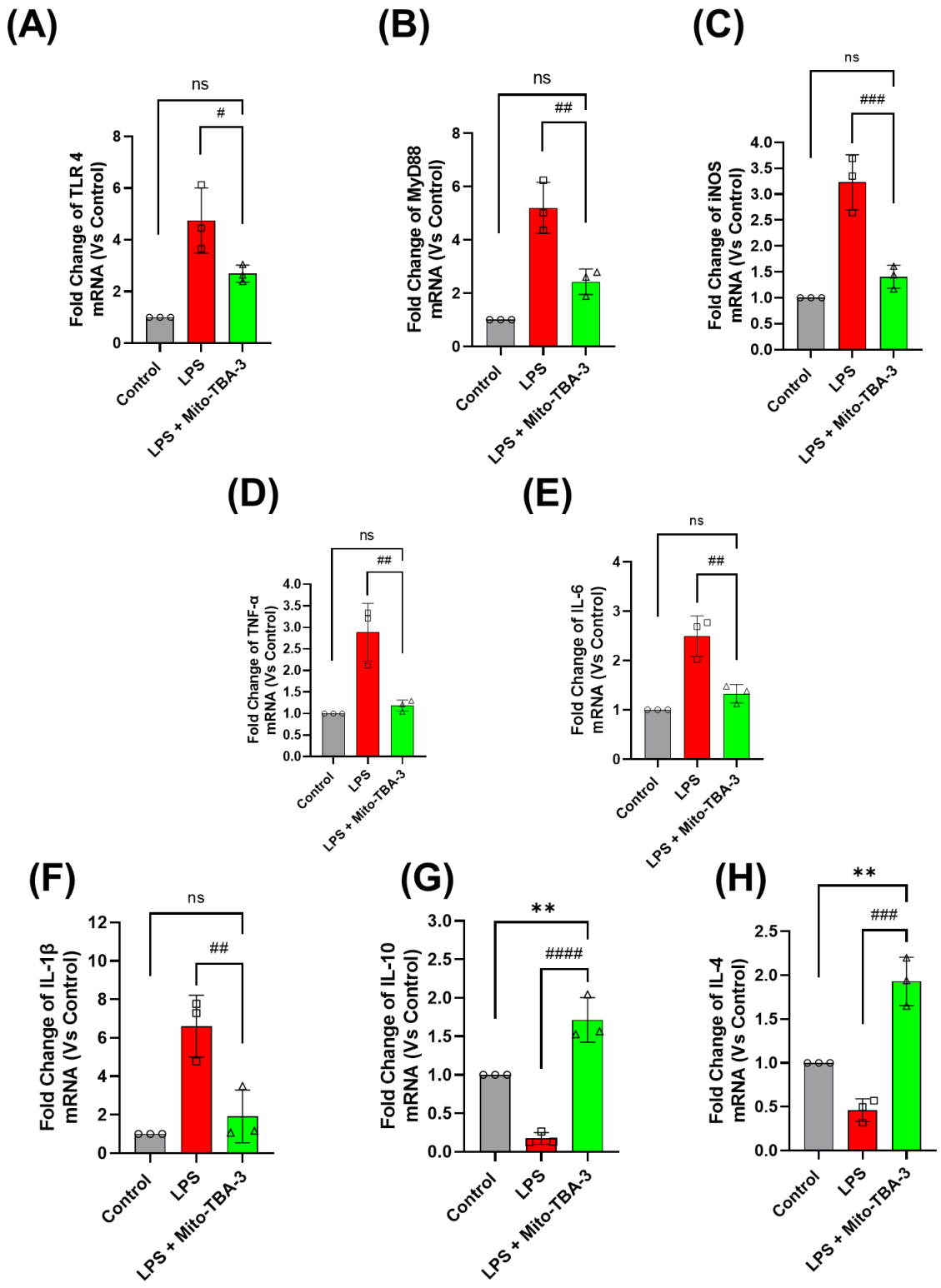


Figure 3.20 Mito-TBA-3 attenuates pro-inflammatory responses and promotes cytoprotective Effect in dPC12 Cell Lines via Pre-activation of Toll-Like Receptor-4 Signaling Pathway Leading to the Inhibition of Caspase-3/Nuclear Factor-κappa B Pathway. Effect of Mito-TBA-3 on mRNA expression levels of different mediators of TLR-4 / NF-Kb pathway like total (A) TLR 4, (B) MyD88, (C) iNOS, (D) TNFα, (E) IL-6, (F) IL-1β, (G) IL-10, (H) IL-4 with LPS and Mito-TBA-3 treatment using RT-qPCR analysis.

3.4.13 Mito-TBA-3 Suppresses LPS-Induced Stress via NFκB Signaling Pathway: In order to explore the role of NFκB in LPS-induced neuroinflammation and oxidative stress and to confirm the effectiveness of Mito-TBA-3 in reducing neurodegeneration by regulating these pathways, we carried out further experiments. The ICC results indicated that PC12 cells, when exposed to LPS, had enhanced translocation of the NF-κB p65 component of NFκB protein into the nucleus, as shown with the arrow in **Figure 3.21 A-C**. Nevertheless, the administration of Mito-TBA-3 after to LPS exposure resulted in a notable decrease in the movement of NFκB into the nucleus, as observed in **Figure 3.21 D**.

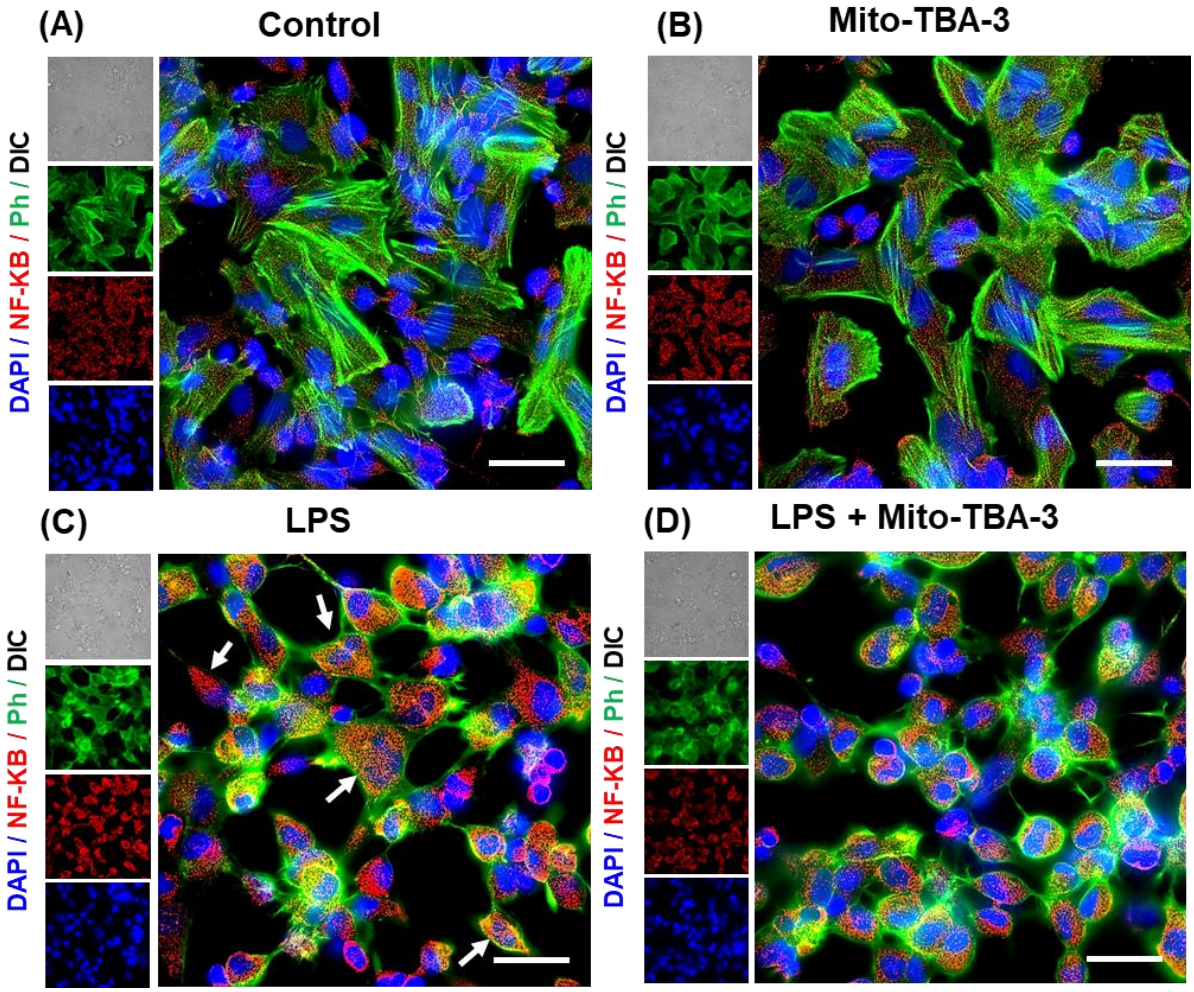


Figure 3.21 Ttranslocation of the NF-κB p65 component of NFκB protein into the nucleus under different treatment condition (A) control, (B) Mito-TBA-3, (C) LPS and (D) LPS + Mito-TBA-3. Scale bar corresponds 50µm. Scale bar corresponds to 50 µm.

3.4.14 Mito-TBA-3 attenuates Oxidative Stress Injury by activating the Keap1-Nrf-2/ARE Pathway during Selective Autophagy: In response to oxidative stress, antioxidant defence systems have undergone adaptive changes, wherein the transcription factor Nuclear factor erythroid 2-related factor (Nrf-2) has emerged as a key regulator. Nrf-2 is a transcription factor that relocates to the nucleus and stimulates the transcription of antioxidants-related genes in response to oxidative stress. Under homeostasis conditions, Nrf-2 is captured in the cytoplasm by Keap1 (Kelch-like ECH-associated protein 1). However, under oxidative stress, Nrf-2 is released from Keap1 inhibition.

This allows Nrf-2 to translocate into the nucleus, where it binds to antioxidant response elements (AREs) in the DNA, where it is known to subsequently initiate the transcription of phase-II antioxidant enzymes related genes (NQO1, HO-1, GCLC, and GCLM). The activation of Nrf-2 is essential for protecting cells from oxidative damage and maintaining a balanced redox state. Nrf-2 also plays a crucial role in regulating a wide range of antioxidant enzymes (SOD, CAT) that are involved in the process of detoxifying and removing free radicals (**Figure 3.22 A**). Disruption of Nrf-2 signalling has been linked to the development of specific impairments ranging from cardiovascular to neurological disorders. Moreover, Nrf2 has also been recognized as a promising therapeutic target for neurodegenerative disorders such as Alzheimer's, in which oxidative stress exerts a substantial influence on the advancement of the disease.

This indicates that focusing on Nrf-2 signalling pathways may be a favourable approach for creating new therapeutic treatments for disorders characterized by oxidative stress. Hence, underscoring its significance as a possible target for therapeutic approaches is of utmost need. Hence, here in this study, we further explored whether our designed molecule Mito-TBA-3 effectively promotes the activation of the Nrf-2/ARE signalling pathway and activates the translocation of Nrf-2 in the nucleus, which will ultimately increase the activation of oxidative stress and inhibit the apoptosis-mediated cell death.

To verify this hypothesis, we have performed RT-qPCR analysis of the various phase-II antioxidant enzymes related genes (NQO1, HO-1, GCLC, and GCLM) to check the impact of Mito-TBA-3 on the mRNA levels of Nrf2, NQO1, HO-1, GCLC, and GCLM in both the control and experimental groups of dPC12 cells. In LPS-treated dPC12 cells, the mRNA expression of Nrf2, NQO1, HO-1, and its downstream proteins GCLC and GCLM showed a considerable decrease under oxidative stress generated by LPS. However, these altered expressions of various antioxidants (SOD and CAT) are conversely prevented by Mito-TBA-3 treatment (**Figure 3.22 A**).

We have also performed an indirect immunofluorescence labelling of LPS pretreated dPC12 cells. The cells that were exposed to LPS exhibit significant oxidative stress, which triggers the translocation and increased accumulation of Nrf-2 in the nucleus from cytoplasm, in comparison to the control cells (**Figure 3.22 B-E**). However, Mito-TBA-3 conclusively enhances the translocation of Nrf-2 in the nucleus, as is evident from the microscopic images shown in **Figure 3.22 E**.

Gene	Forward 5´-3´	Reverse 5´-3´	Accession No.
Nrf2	GGTTGCCCACATTCCCAAAC	ATCCAGGGCAAGCGACTCAT	NM_031789.3
NQO1	AAACGACATCACAGGGGAGC	GGGCACCCCAAACCAATACA	NM_017000.3
HMOX-1	CTAAGACCGCCTTCCTGCTC	GGTAGTATCCTGGGCTCTAAGG	XM_039097469.1
GCLC	GCAGCTCTTAGAGGAAGTGTGA	GGCACTGGTGTGGACCTAGA	XM_039080870.1
GCLM	CCCTGATTTGGTCAGGGAGTTT	GTCCAGCTGTGCAACTCCAA	NM_017305.2
GAPDH	CTCCAACCCAACCCTCAACAG	CCGATACGGCCAAATCCGTTC	XM_039107008.1
iNOS	CCTAGTCAACTACAAGCCCCAC	GGGGTTTTCTCCACGTTGTTG	NM_012611.3
TLR-4	ATCTGAGCTTCAACCCCCTG	TGTCTCAATTTCACACCTGGAT	NM_019178.2
TNF-α	GATCGGTCCCAACAAGGAGG	CTTGGTGGTTTGCTACGACG	NM_012675.3
IL-1β	CAGCTTTCGACAGTGAGGAGA	TTGTCGAGATGCTGCTGTGA	NM_031512.2
IL-6	GCCCACCAGGAACGAAAGTC	TGGCTGGAAGTCTCTTGCGG	NM_012675.3
IL-4	GGAACGGTATCCACGGATGT	CTCCGTGGTGTTCCTTGTTG	NM_201270.1
SOD-1	TTGGCCGTACTATGGTGGTCC	TGGGCAATCCCAATCACACC	NM_017050.1
CAT	CTGACTGACGCGATTGCCTA	AGGACATCGGGTTTCTGAGG	NM_012520.2
IL-10	CATTCCATCCGGGGTGACAA	TGTTGTCCAGCTGGTCCTTC	NM_012854.2
Myd88	TGTCCGTGGACTCCTACTTGT	ACAAACTGCGAGTGGGATCG	NM_198130.2

Tbale 3.2 Primers Sequence Used for qRT-PCR

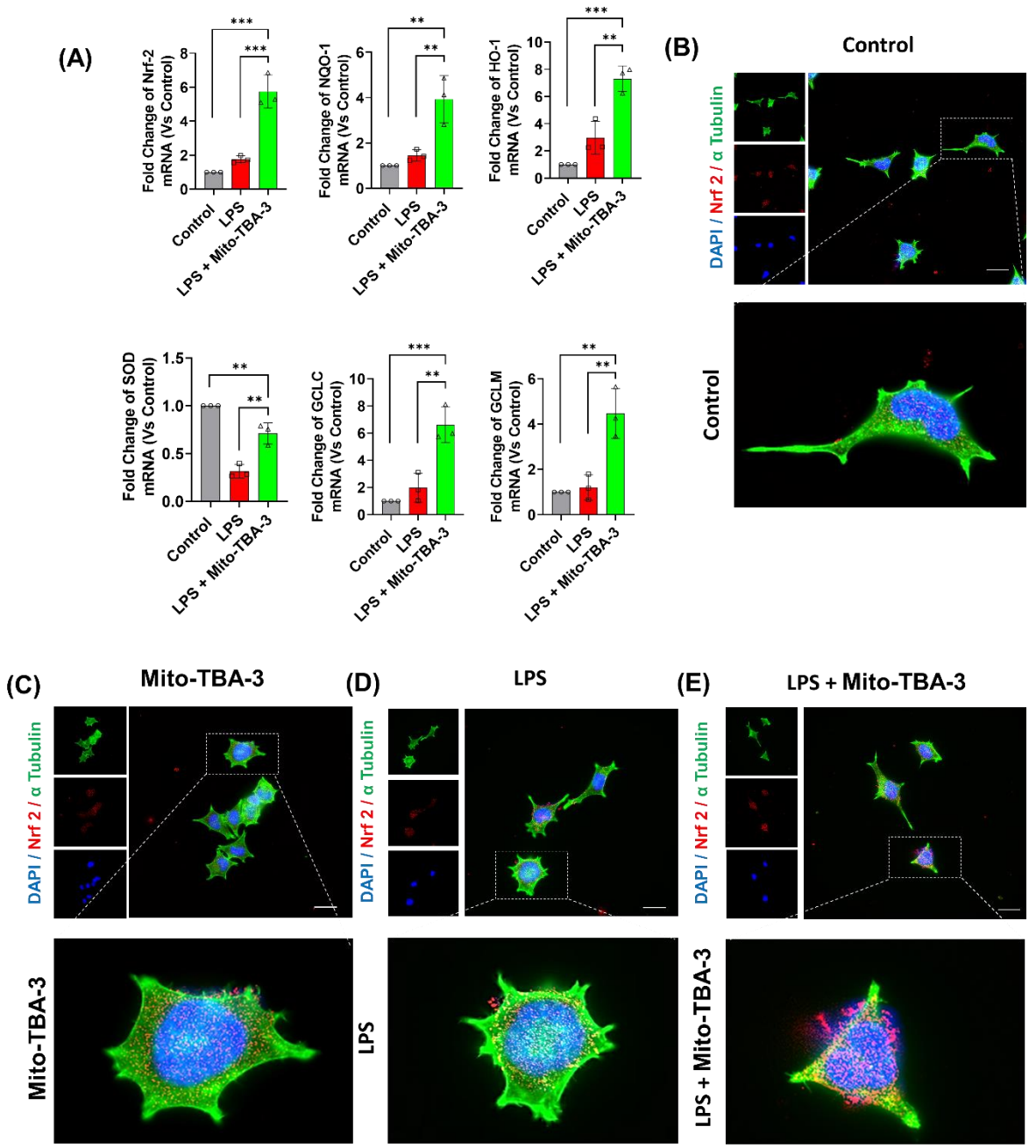


Figure 3.22 Investigating the mechanism by which Mito-TBA-3 mitigates the production of ROS through the Nrf2/ARE signalling pathway and neuroprotective potential of Mito-TBA-3. (A) Effect of Mito-TBA-3 on mRNA expression levels of different antioxidant enzymes like total Nrf2, HO-1, NQO1, GCLC and GCLM in dPC12 cells treated with LPS using qRT-PCR. Immunocytochemical analysis of Nrf-2 expression in the cytoplasm and nucleus under different treatment conditions (B) Control, (C) Mito-TAB-3, (D) LPS and (E) LPS + Mito-TAB-3. Scale bar corresponds to 50 µm. The results are represented as the mean ± SEM. n = 3 per group from three independent experiments. The statistical significance of all the results was calculated by using a one-way analysis of variance (ANOVA) with Tukey's post hoc test. Significances are marked as *P< 0.05, **P< 0.01, ***P< 0.001, **** P < 0.0001 versus the control group, $^{\#}$P<0.05, $^{\#\#}$P<0.01, $^{\#\#\#}$P<0.001, $^{\#\#\#\#}$ P < 0.0001 versus the LPS treatment group, $^{@}$P<0.05, $^{@@}$P<0.01, $^{@@@}$P<0.001 $^{@@@@}$P < 0.0001 versus the Aspirin treatment group. Here, 'ns' is nonsignificant when compared to control. Scale bar corresponds to 20 µm. Some component of the figure is adapted from Servier Medical Art; Servier is licensed under a creative commons attribution 3.0 unported license https://smart.servier.com/ and https://app.biorender.com/s.

3.4.15 Anti-Apoptotic and Anti-inflammatory Analysis: The Bcl-2 and caspase families control the intrinsic apoptotic process. Changing the expression levels of pro- and anti-apoptotic gene family members can significantly affect programmed cell death. Moreover, in many neurodegenerative disorders, pro-inflammatory cytokines, including IL-6, IL-1β, and TNF-α are crucial in causing neuroinflammation and neuronal death. Western blot analysis was used to evaluate the protein levels of pro-apoptotic genes (Bax and Bad) and proinflammatory cytokine (IL-6) to determine if Mito-TBA-3 could rescue LPS-induced apoptosis by modifying apoptotic protein abundance. Both proinflammatory makers (IL-6) and apoptotic markers (Bax and Bad) level were found to be increased significantly in cells pretreated with just LPS. However, LPS-pretreated cells when treated with Mito-TBA-3 showed dramatically reduced pro-apoptotic gene expression (**Figure 3.23 A-D**). These findings suggest that Mito-TBA-3 inhibits the LPS-induced apoptosis and neuroinflammation.

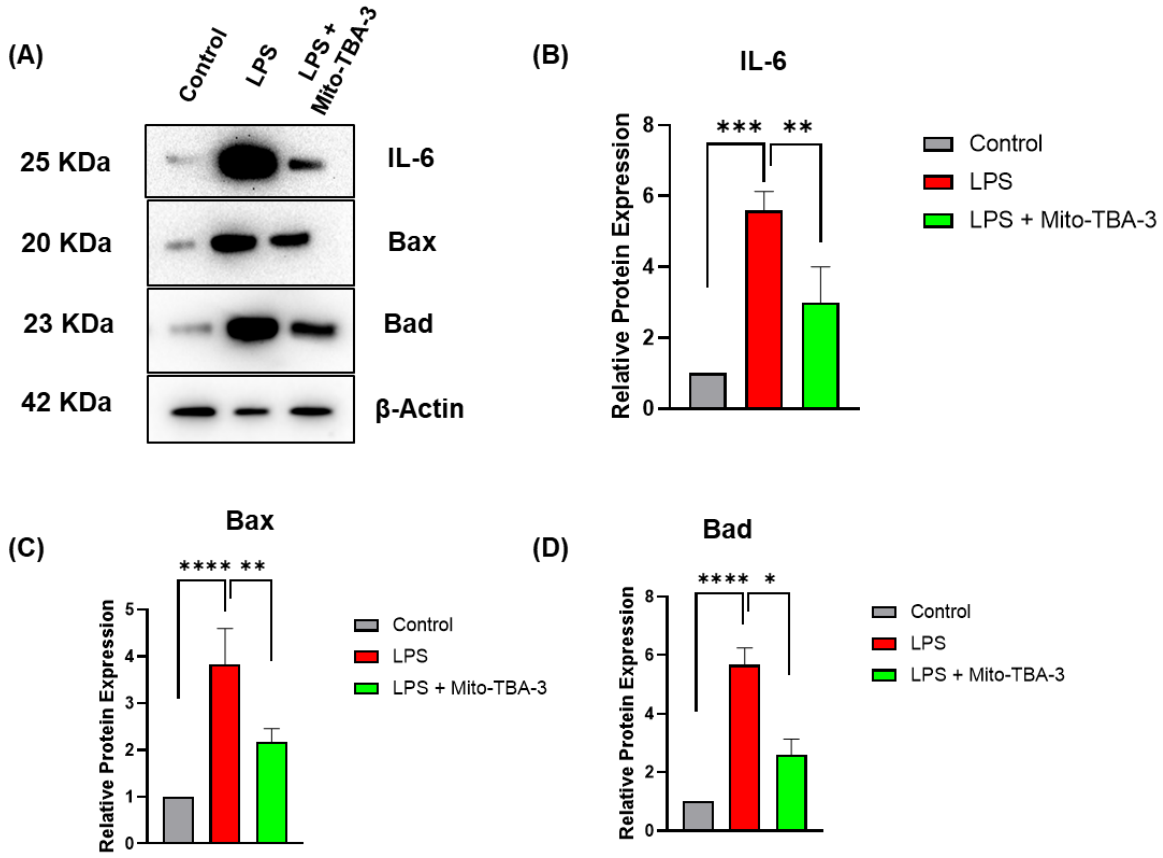


Figure 3.23 Determination of expression of proinflammatory cytokines and apoptotic markers (A) Western blot analysis of different apoptotic (Bax and Bad) and inflammatory (IL-6) markers in dPC12 cells and its densitometry analysis (B) IL-6, (C) Bax and (D) Bad calculated using Image Lab software of Biorad. Data represent mean ± SD of three independent experiments. The statistical significance of all the results was calculated by using a one-way analysis of variance (ANOVA) with Tukey's post hoc test. The results are represented as the mean ± SD, n = 3 per group from three independent experiments. Significances are marked as *P< 0.05, **P< 0.01, ***P< 0.001, **** P < 0.0001 versus the control group. Here, 'ns' is nonsignificant when compared to control.

3.4.16 Neuroprotective Effect of Mito-TBA-3 on $A\beta_{42}$ Induced Toxicity Primary Neuronal Culture: Next, we examined the impact of Mito-TBA-3 on inhibiting the development of neuroinflammation by utilizing the primary neuronal culture model. Previous research has shown that Aβ is known to cause synaptic denegation in primary hippocampal neurons, which are widely recognized as a model for Alzheimer's disease (AD) and neuroinflammation and known to display similar pathological characteristics to those reported in AD patients, which include significant neuronal cell death and an elevated buildup of Aβ plaques in the subiculum.

However, reactivation of the cell cycle in mature neurons is an initial characteristic of neurodegeneration. Oxidative stress induced by Aβ is a widely recognized to stimulate the release of pro-inflammatory substances that induce the death of neuronal cells by activating glial cells. Further, the stimulation of glial cells results in the secretion of pro-inflammatory cytokines, which exacerbate the process of neurodegeneration. Moreover, studies have demonstrated that neuroinflammation generated by oxidative free radicals interferes with the regular operation of neuronal networks and hampers synaptic plasticity, ultimately resulting in cognitive deterioration and other signs of neurodegeneration.

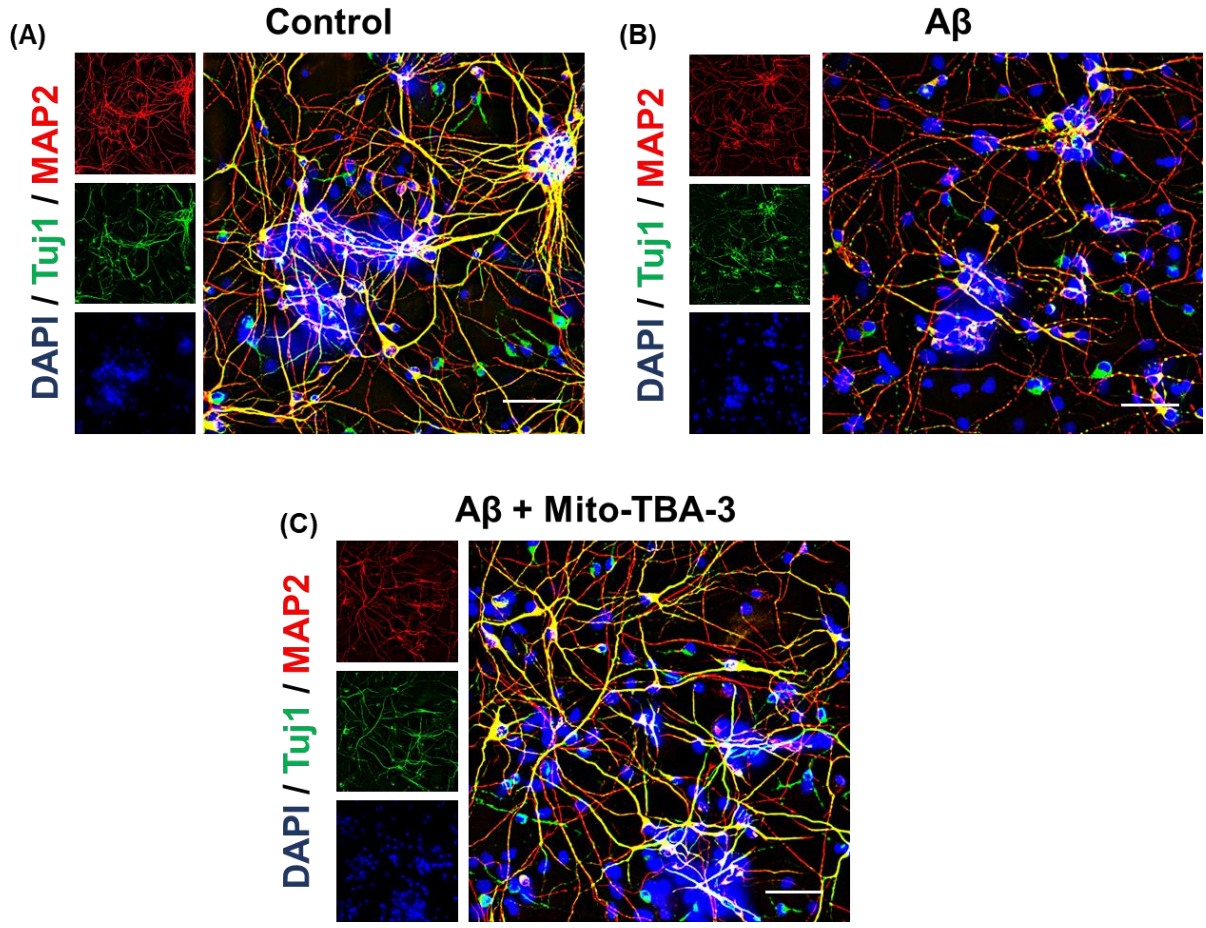


Figure 3.24 ICC of E18 primary cortical neurons stained with TUJ1, MAP2 and counterstained with Hoechst 33342, under (A) control condition and when treated alone with (B) Aβ and (C) Aβ + Mito-TBA-3. Scale bar corresponds to 50 µm.

Hence, in this study, we aimed to evaluate the neuroprotective effect of Mito-TBA-3 on the inflammatory effect of Aβ on neuronally developed cells. We used immunocytochemistry to examined whether the inflammatory response induced by Aβ can be reverted back by Mito-TBA 3 (**Figure 3.24 A-C**). The findings of our study demonstrated that exposure to Aβ did led to the reactivation of the cell cycle in differentiated neuronal cells, as evidenced by decrease in neuronal cell length and decrease in expression of mature synapatodendrtitc marker MAP2. However, when this Aβ pretreated primary neuronal culture was treated with Mito-TBA-3 it has been shown to restore the complex neurite network. Hence, alleviated the Aβ induced cytotoxicity.

***3.4.17 In Vivo* Validation of LPS-Induced Neuroinflammation Rat Model:** Encouraged by the promising antioxidant properties exhibited by Mito-TBA-3 *in vitro*, we proceeded to investigate their potential use in alleviating inflammation-induced depression, induced by LPS administration. Depressed individuals often exhibit anxiety-related behaviours, including restlessness, irritability, and impaired concentration. These behaviours frequently appear as persistent anxiety and an intensified feeling of apprehension or distress. In addition, persons suffering from depression may also have bodily manifestations such as tachycardia, tremors, and dyspnea as a result of their anxiety. Nevertheless, the simultaneous presence of anxiety symptoms and depression can have a substantial effect on the general state of well-being and quality of life for these persons. Therefore, it is essential to discover proper medication in order to effectively manage both depression and anxiety. In the context of these symptoms here, we have performed various behavioural experiments like open field test (OFT), elevated maze test (EPM), and sucrose preference test (SPT) in LPS-induced rats to check the potential of Mito-TBA-3 to rescue depression and anxiety-like behaviour.

Glial fibrillary acidic protein (GFAP) and ionised calcium-binding adaptor molecule-1 (Iba-1) is widely recognized as indicators of active microglia and astrocytes, respectively, and administration of LPS is well known to elevated expression levels of Iba-1 and GFAP. Hence, to validate the *in vivo* LPS model of neuroinflammation and to find out the efficient dose of LPS to generate a mouse model of neuroinflammation, we have checked the protein expression level of GFAP in rat brain. Results from western blot revealed an upregulation in GFAP expression in rats with increasing concentrations of LPS, the highest expression was observed in LPS dose of 5 mg / Kg (**Figure 3.25 A, B**). Therefore, a dose of 5 mg / Kg was used as an effective dose to generate a neuroinflammatory rat model

In addition, we performed an additional assay to find the most effective dosage of Mito-TBA-3 for future animal research. A preliminary western blotting analysis was performed to evaluate the effects of three different dosages (0.1, 0.5, and 1.0 mg/kg of rat body weight) of Mito-TBA-3 on inhibiting the overexpression of GFAP in LPS-induced rats. The results of our study showed that Mito-TBA-3, when injected at a dose of 0.1 mg/kg, did not produce any significant impact on the expression of GFAP. However, the concentrations of 0.5 mg/kg and 1.0 mg/kg showed almost same effect

on GFAP expressions. Therefore, we chose a dosage of 0.5 mg/kg (**Figure 3.26 A, B**) as the lead dosage for the further studies.

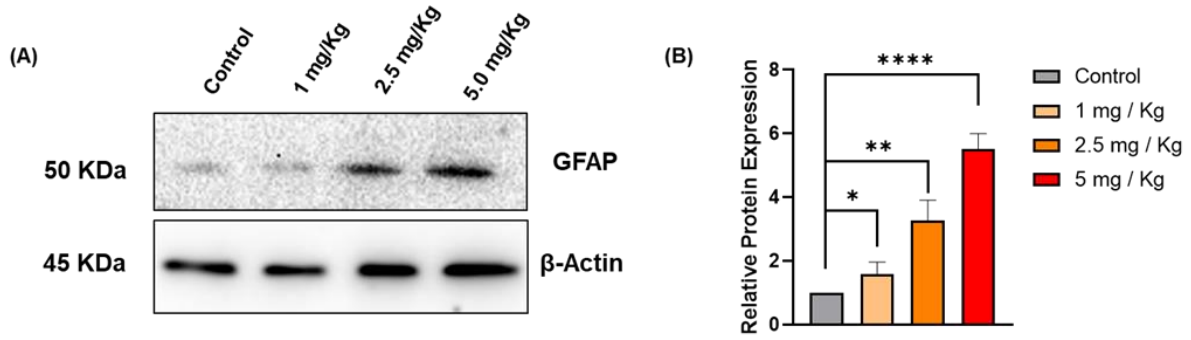


Figure 3.25 Determination of expression of GFAP with different doses of LPS, (A) Western blot analysis of GFAP in LPS induced rat brain and its (B) densitometry analysis calculated using Image Lab software of Biorad. Data represent mean ± SD of three independent experiments. The statistical significance of all the results was calculated by using a one-way analysis of variance (ANOVA) with Tukey's post hoc test. The results are represented as the mean ± SD, n = 3 per group from three independent experiments. Significances are marked as *P< 0.05, **P< 0.01, ***P< 0.001, **** P < 0.0001 versus the control group. Here, 'ns' is nonsignificant when compared to control.

3.4.18 Assessment of Serum Stability of Mito-TBA-3: Data from previous *in vitro* analysis strongly emphasized the remarkable neuroprotective capacity of the compound Mito-TBA-3 against neuroinflammation. Prior to proceeding with *in vivo* analysis involving animal models, it is crucial to do a serum stability evaluation of compound Mito-TBA-3 as a preliminary measure to check the stability of the molecule under *in vivo* conditions. Serum stability is crucial in various applications, such as clinical diagnosis, medication development, medical research, and sample storage. Serum stability is a critical factor in medical research since it directly impacts the accuracy and reliability of experimental outcomes. The levels of crucial analytes or biomolecules in serum samples may vary due to degradation, denaturation, or chemical modification. This has the potential to result in incorrect positive or negative results, which could lead to wrong interpretations and inefficient use of resources. The stability of serum is essential for drug development as it directly affects the pharmacokinetics of dosing.

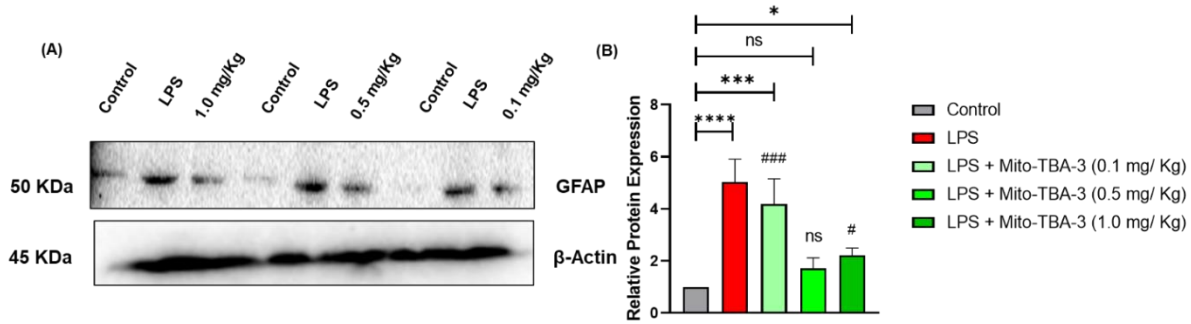


Figure 3.26 Estimation of effective dose of Mito-TBA-3, (A) Western blot analysis of GFAP in LPS-induced rat brain after treatment with different doses of Mito-TBA-3, and its (B) densitometry analysis. Data represent mean ± SD of three independent experiments. The statistical significance of all the results was calculated by using a one-way analysis of variance (ANOVA) with Tukey's post hoc test. The results are represented as the

mean ± SD, n = 3 per group from three independent experiments. Significances are marked as *P< 0.05, **P< 0.01, ***P< 0.001, **** P < 0.0001 versus the control group, #P<0.05, ##P<0.01, ###P<0.001, #### P < 0.0001 versus the LPS treatment group. Here, 'ns' is nonsignificant when compared to control.

This investigation involves the incubation of Mito-TBA-3 with human blood serum and assessing its stability for a duration of 96 hours using reverse-phase high-performance liquid chromatography (RP-HPLC). The results indicate that the molecule remained stable in serum, up to 95% of its stability within the first 24 hours (**Figure 3.27**). As a result, compound Mito-TBA-3 has been identified as a very stable contender that is acceptable for future analysis in *in vivo* animal models. This discovery opens up possibilities of using Mito-TBA-3 for the development of novel therapies for neuroinflammation.

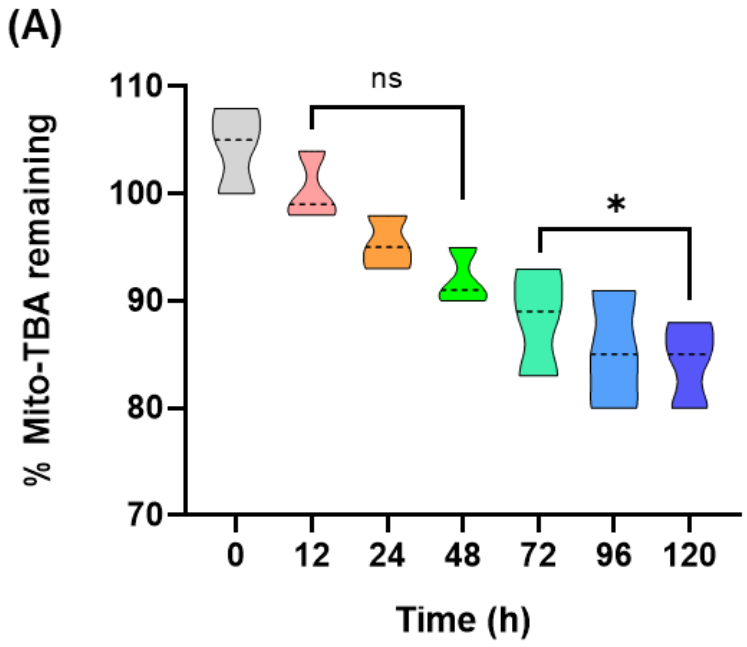


Figure 3.27 Estimation of serum stability of Mito-TBA-3, (A) Serum stability of Mito-TBA-3 for 120 h. Data represent mean ± SD of three independent experiments. The statistical significance of all the results was calculated by using a one-way analysis of variance (ANOVA) with Tukey's post hoc test. The results are represented as the mean ± SD, n = 3 per group from three independent experiments. Significances are marked as *P< 0.05, **P< 0.01, ***P< 0.001, **** P < 0.0001 versus the control group, #P<0.05, ##P<0.01, ###P<0.001, #### P < 0.0001 versus the LPS treatment group. Here, 'ns' is nonsignificant when compared to control.

3.4.19 Assessment of BBB Crossing efficacy of Mito-TBA-3: A significant obstacle for any molecule or drug to function as a neuroprotective medication is its capacity to cross the BBB. In order to determine if Mito-TBA-3 can pass through the BBB, Mito-

TBA-3 at a concentration of 0.5 mg / kg was administered into rats via intraperitoneal injection. After a duration of 6 hours, the rats were euthanized, and the brains were isolated for HPLC analysis followed by mass spectrometry. The electrospray ionisation (ESI) mass spectrum of the homogenate displayed the Mito-TBA-3 peak at m/z 677.2311 [M] and 675.2154 [M-2H], as shown in **Figure 3.28**. This confirms the presence of Mito-TBA-3 in the brain extract and its ability to cross BBB.

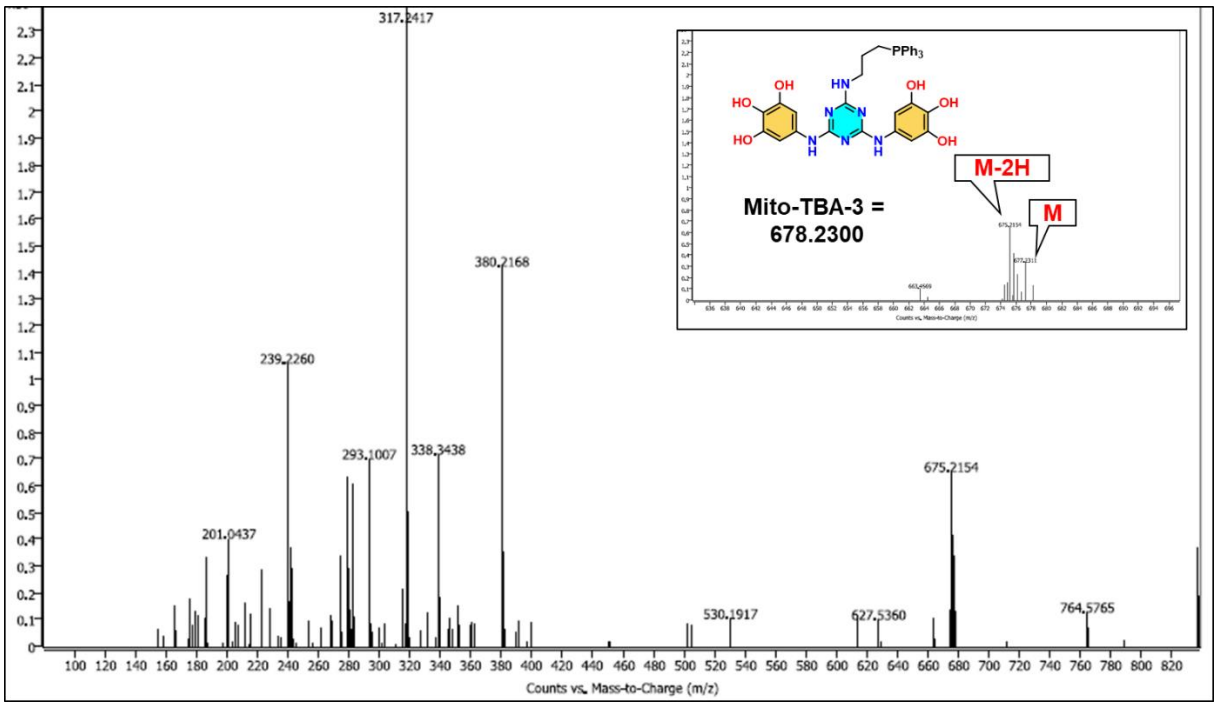


Figure 3.28 ESI-MS of rat brain homogenate for Mito-TBA-3, molecular peak at the inset image indicated Mito-TBA-3 crosses the BBB. Expected mass 677.2300 Da, observed mass 677.2311 Da [M] and 675.2154 Da [M-2H].

3.4.20 Mito-TBA-3 Improved Depression and Anxiety-like Behaviors in LPS-Induced Neuroinflammation Rat Model: EPM paradigm is frequently used to evaluate anxiety-like behaviour. The main objective of this study is to effectively examine the relationship between conditioned fear in generalized anxiety disorders and unconditioned fear in panic disorders as distinct constructs (**Figure 3.29 A, B)**. The administration of LPS is known to result in an anxiety-like behaviour, which is also evidenced by a significant decrease in the entries into the open arm (6.33 ± 1.24 vs 3.00 ± 0.81, **Figure 3.29 C**), a decrease in the time spent in open arms (**Figure 3.29 D**) compared to the group treated with the Mito-TBA-3 and Aspirin, a common nonsteroidal anti-inflammatory drug (NSAID). However, treatment with Mito -TBA-3 at a dosage of 0.5 mg/kg effectively reversed the changes produced by LPS, which is significantly better than that of aspirin. Compared to the LPS-control group, the group treated with Mito -TBA 3 exhibited a significant increase in the number of entries into the open arms (**Figure 3.29 C, D**).

As the anxiogenic effects of different treatments may vary depending on the specific characteristics of the test situation. An additional experimental test was conducted to evaluate the impact of LPS on rat performance in a forced swimming test (FST), and the inclination to escape-related mobility behaviour in rats was observed. In this acute

study, using the FST paradigm, rats treated with LPS exhibited a significant increase (54.00 ± 5.59 vs. 30.88 ± 6.74, **Figure 3.29 E**) in the amount of time spent immobile compared to the normal control group. This increase was significantly reduced by Mito-TBA 3 (31.00 ± 2.64) and Aspirin (36.80 ± 5.17), indicating that both Mito-TBA-3 and positive control aspirin have anti-depressant effects. However, Mito-TBA-3 showed significantly better results than the aspirin.

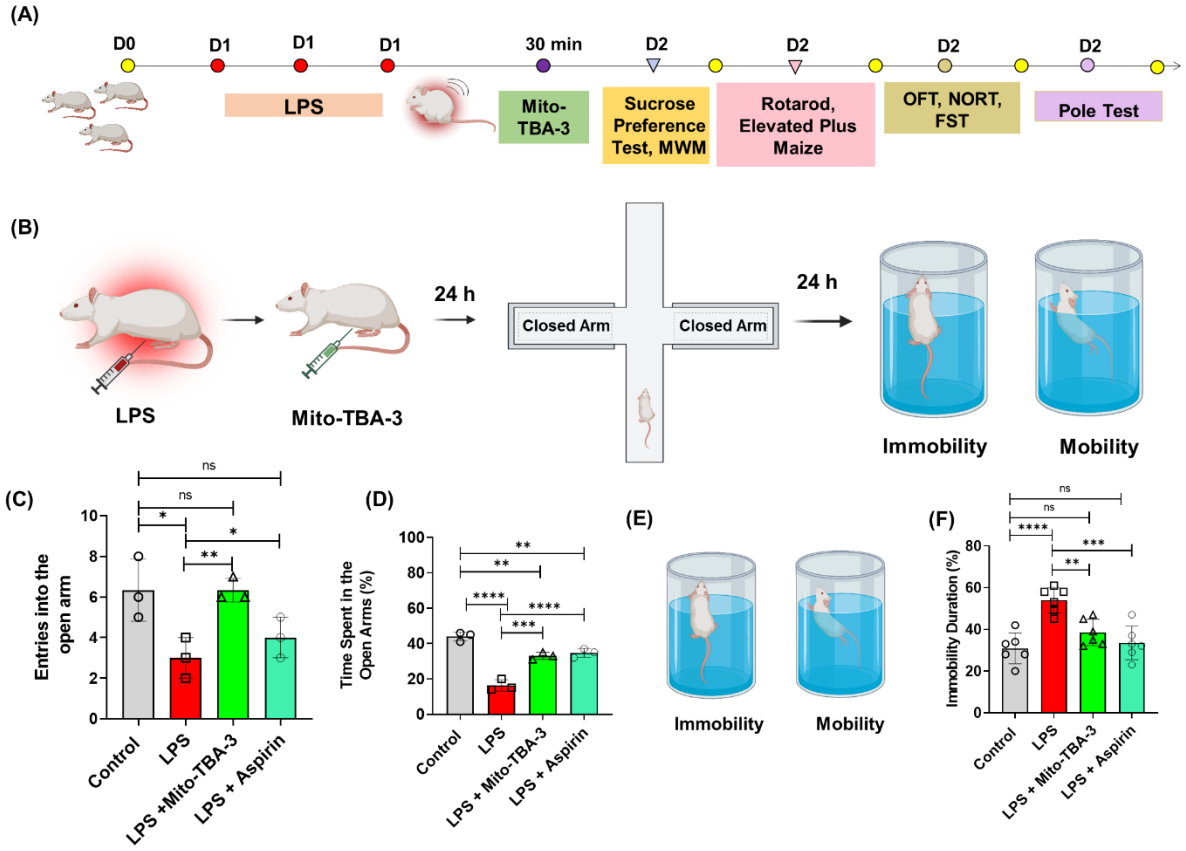


Figure 3.29 Mito-TBA-3 attenuated depression and anxiety-like behavior in LPS-induced neuroinflammatory model rats. (A) Schematic depiction of the experimental procedure followed to generate neuroinflammatory model rats: rats were intraperitoneally injected with LPS to induce neuroinflammatory-mediated anxiety and depression-like behaviour, which was successfully alleviated by Mito-TBA-3. The therapeutic effect of Mito-TBA-3 was evaluated by anxiety and depression-like behaviour tests, including sucrose preference test (SPT), Rotarod test, Elevated Plus Maze test (EPM), Open field test (OFT), Novel object recognition test (NORT), Forced Swimming test (FST) and pole test. (B) Schematic illustration of the experimental procedure followed to evaluate anxiety behaviour. Corresponding bar graph with data points showing (C) entries into the open arm and (D) time spent in the open arm. (E) Illustration of rat in the FST paradiagm, (F) Corresponding bar graph showing immobility duration shown by rats in FST. The results are represented as the mean ± SEM. n = 6 per group from three independent experiments. Significances are marked as *P< 0.05, **P< 0.01, ***P< 0.001, **** P < 0.0001 versus the control group, $^{\#}$P<0.05, $^{\#\#}$P<0.01, $^{\#\#\#}$P<0.001, $^{\#\#\#\#}$ P < 0.0001 versus the LPS treatment group, $^{@@}$P<0.05, $^{@@}$P<0.01, $^{@@@}$P<0.001, $^{@@@@}$P < 0.0001 versus the Aspirin treatment group. Here, 'ns' is nonsignificant when compared to control. The statistical significance of all the results was calculated by using a one-way analysis of variance (ANOVA) with Tukey's post hoc test.

3.4.21 Mito-TBA-3 Effectively Mitigates the Locomotive Balance and Motor Impairment in LPS-Induced Neuroinflammation: LPS has been demonstrated to induce abnormal behaviour in rats, including the suppression of locomotor and exploratory activity, depressive-like behaviour, and alterations in social behaviour. Furthermore, LPS has been known to provoke neuroinflammation and modify neurotransmitter levels in the brain, hence contributing to neuroinflammation. Recent findings have also shown that the abnormal behaviour generated by LPS in rats can be reversed or reduced by administering anti-inflammatory agents or pharmaceuticals that target specific neurotransmitter systems.

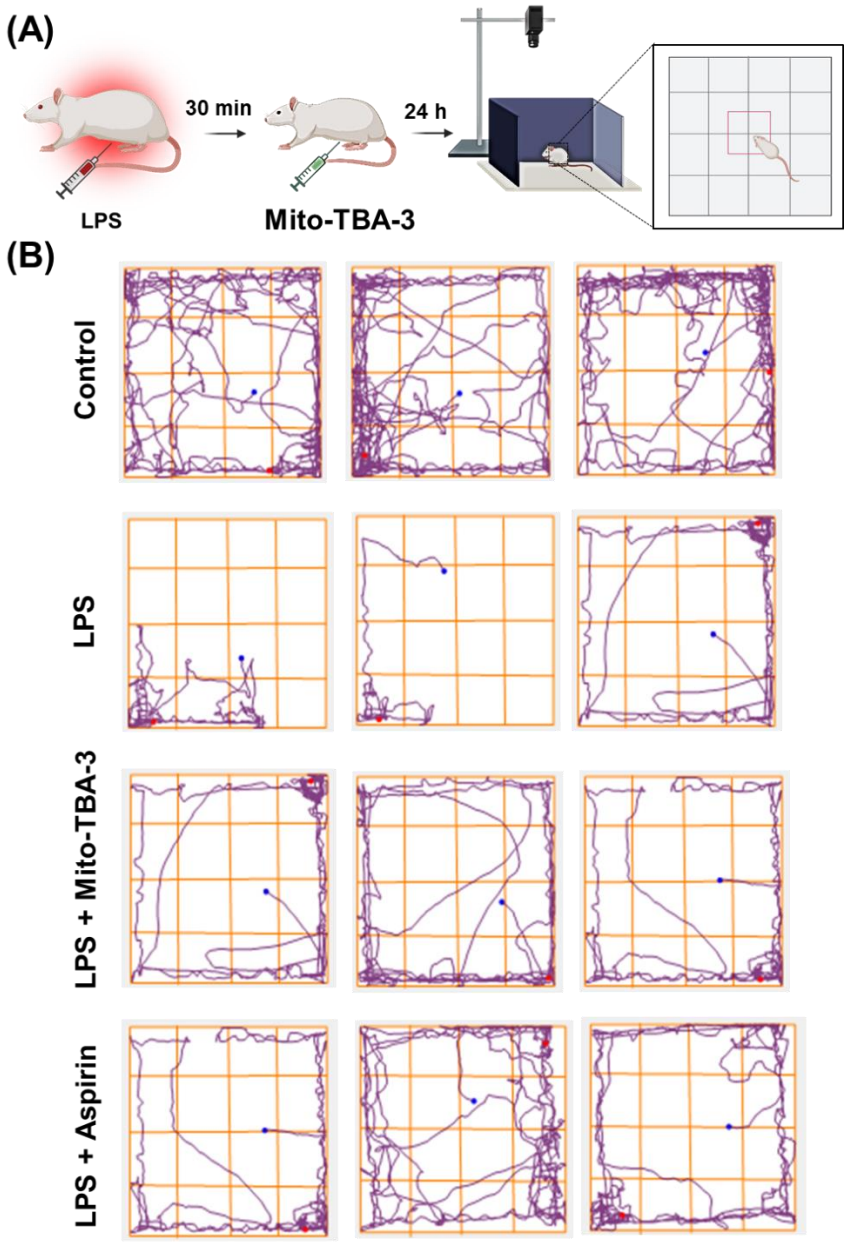


Figure 3.30 (A) Schematic illustration of the procedure followed to assess locomotor and anxiety-like behaviour in LPS-induced neuroinflammatory model rats. (B) Representative activity tracking plot of the rats under different treatment conditions.

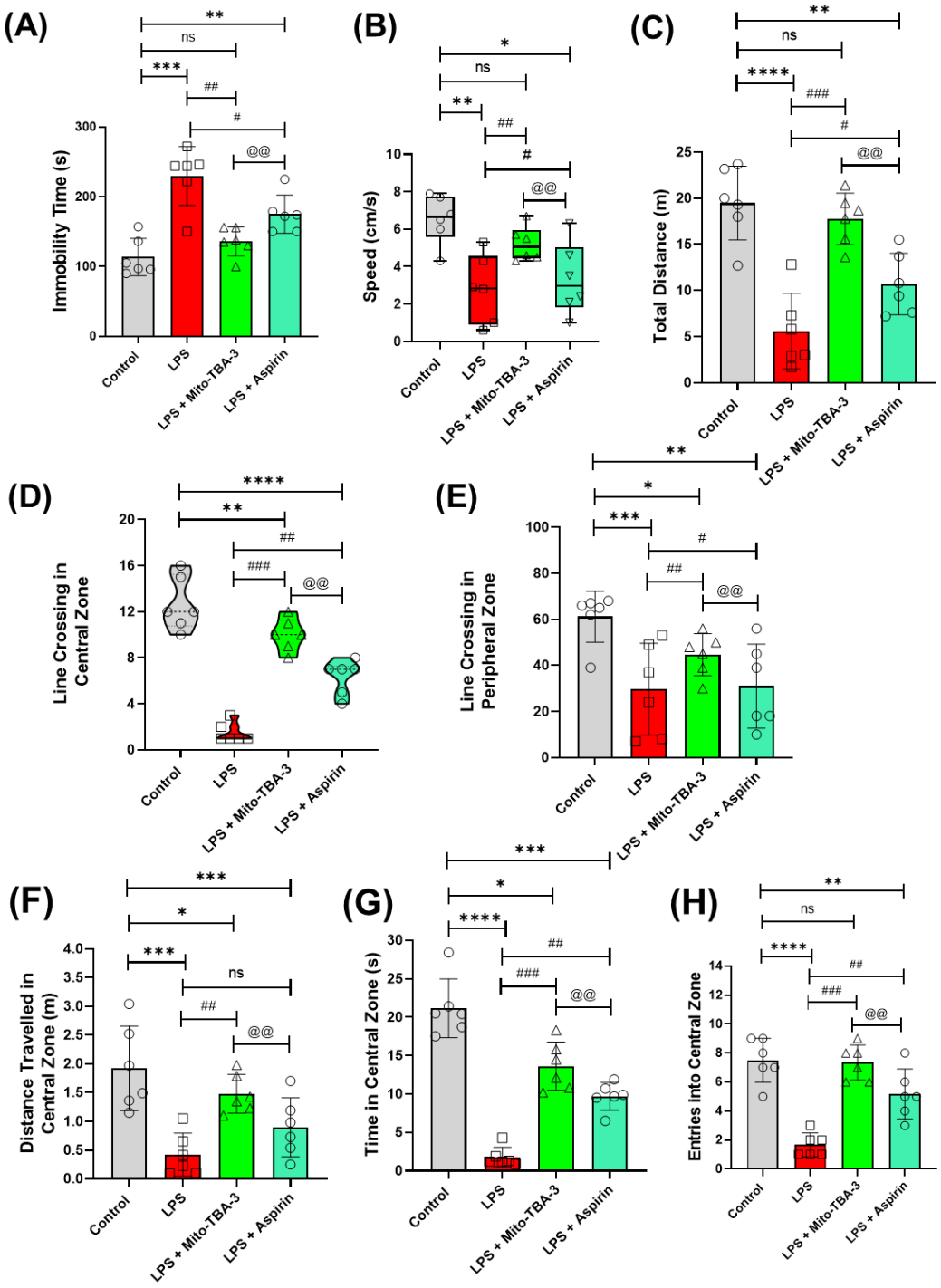


Figure 3.31 Representative activity tracking and the corresponding bar graph showing (A) immobility time, (B) speed, (C) total distance travelled in the OF arena, (D) total lines crossed in the central zone of the OF, (E) total lines crossed in the peripheral zone of the OF, (F) total distance travelled in the central zone, (G) total time spent the central zone, (H) total number of entries made into the central zone. The results are represented as the mean ± SEM. n = 6 per group from three independent experiments. Significances are marked as *P< 0.05, **P< 0.01, ***P< 0.001, **** P < 0.0001 versus the control group, $^{\#}$P<0.05, $^{\#\#}$P<0.01, $^{\#\#\#}$P<0.001, $^{\#\#\#\#}$ P < 0.0001 versus the LPS treatment group, $^{@@}$P<0.05, $^{@@}$P<0.01, $^{@@@}$P<0.001, $^{@@@@}$P < 0.0001 versus the Aspirin treatment group. Here, 'ns' is nonsignificant when compared to control. The statistical significance of all the results was calculated by using a one-way analysis of variance (ANOVA) with Tukey's post hoc test.

Hence, locomotor activity, stress, and locomotion impairment were evaluated using OFT after LPS administration (**Figure 3.30 A**). Here, we have determined whether an LPS treatment could induce aberrant behaviour and whether Mito-TBA-3 can mitigate the side effects of LPS. We found that treatment with Mito-TBA 3 indeed attenuated the aberrant behaviour induced by LPS injection. Briefly, the track plots shown in Figure 6H indicate that the control group exhibit comparable activity in the open field. The majority of the time is spent either in all four corners of the field or moving between and around the corners. Nevertheless, within the LPS group, a significant portion of the time was spent to a single corner of the open field (**Figure 3.30 B**). Moreover, the LPS group exhibited significant decreases in activity as measured by an increase in total immobility time (**Figure 3.31 A**), decrease in speed (**Figure 3.31 B**) and total distance covered (**Figure 3.31 C**) in comparison to the control group. However, the rats that received Mito-TBA-3 treatment did not exhibit any disparity due to LPS administration as seen from the decrease in total immobility time, increase in speed and total distance covered when compared to the control group. The Mito-TBA-3 group exhibited statistically significant alterations in distance or duration of immobility as compared to the Aspirin group. Moreover, there was a significant difference in the line crossing in the central and peripheral zone (**Figure 3.31 D, E**), distance travelled in the central zone (**Figure 3.31 F**), time spent in the central zone (**Figure 3.31 G**) and entries in the central zone (**Figure 3.31 H**) in Mito-TBA-3 group as compared to the LPS group and aspirin group.

In order to assess the appropriateness of the LPS-based rat model of neuroinflammation, we verified motor impairments in the model by conducting rotarod tests. The rotarod test is a well-established method for assessing muscle coordination and movement in animals. **Figure 3.32 A** shows the schematic illustration of the study. **Figure 3.32 B** demonstrates that LPS alone significantly impaired locomotor activity, which resulted in a decrease in the duration of time spent on the rod, as compared to the control group. During the experimental procedure, it was seen that rats frequently exhibited jumping behavior and attempted to evade the rod. Nevertheless, this behaviour tends to diminish in naïve rats after the second day, as they become more composed and remain affixed to the rod during the entirety of the test. However, rats injected with LPS displayed this form of nervous behaviour until the final day of the experiment. However, the combination of LPS and Mito-TBA-3 resulted in a considerable decrease in the duration of time spent on the rod, as compared to the group treated with LPS alone and aspirin group.

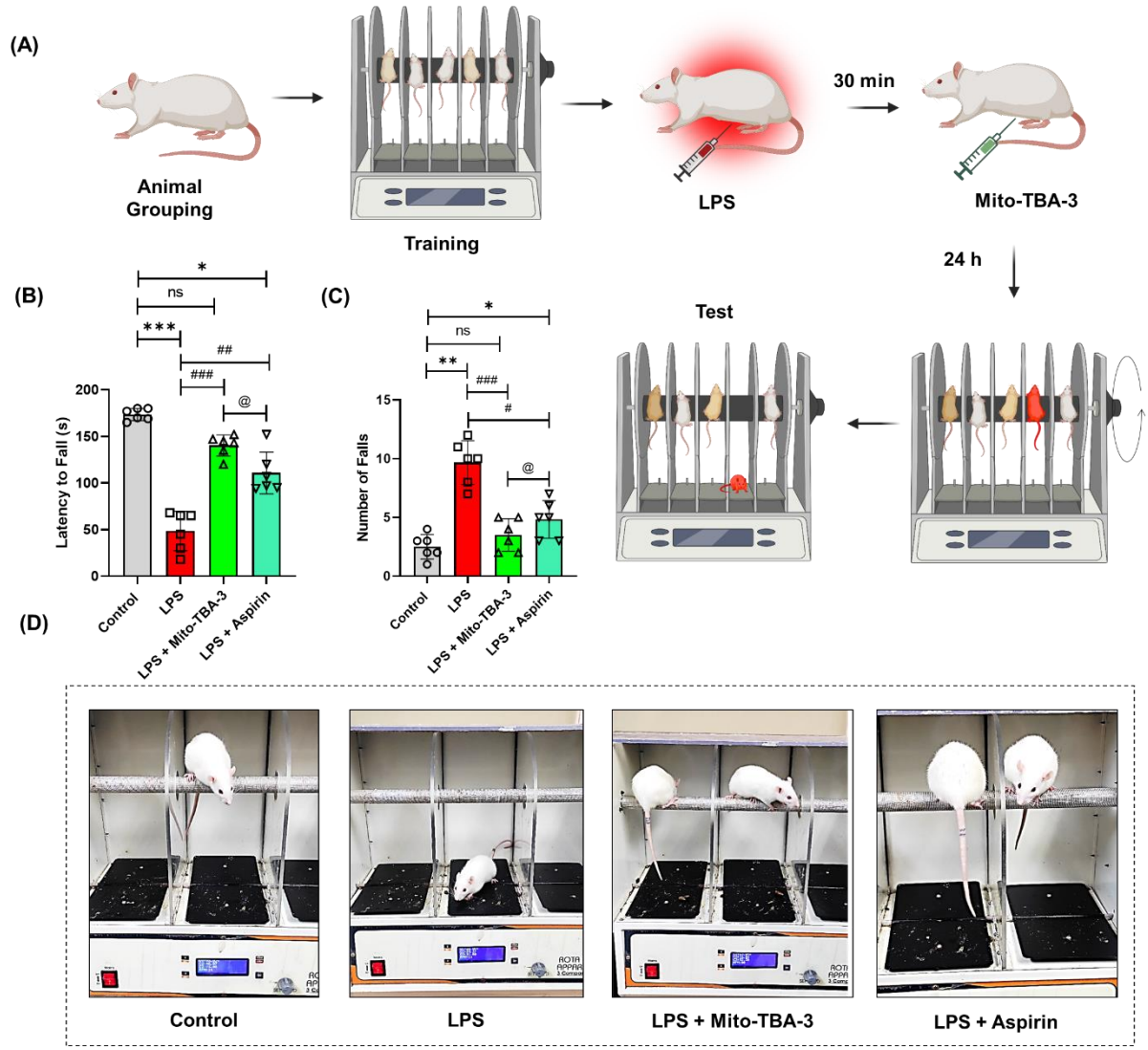


Figure 3.32 Assessment of motor coordination, locomotor activity and cognitive impairment in LPS induced rats. (A) Schematic illustration of the experimental procedure followed to perform the rotarod test, starting from training on day 0 to the final day of test performance. Rats were trained as described in the Figure, and different parameters were assessed during the test. LPS administration caused a significant loss in motor coordination in rats, as shown by a decrease in (B) Latency to fall from the rod and (C) an increase in a total number of falls. (D) Representative images of the rat performance on rotarod test. The results are represented as the mean ± SEM. n = 6 per group from three independent experiments. Significances are marked as *P< 0.05, **P< 0.01, ***P< 0.001, **** P < 0.0001 versus the control group, $^{\#}$P<0.05, $^{\#\#}$P<0.01, $^{\#\#\#}$P<0.001, $^{\#\#\#\#}$ P < 0.0001 versus the LPS treatment group, $^{@@}$P<0.05, $^{@@}$P<0.01, $^{@@@}$P<0.001, $^{@@@@}$P < 0.0001 versus the Aspirin treatment group. Here, 'ns' is nonsignificant when compared to control. The statistical significance of all the results was calculated by using a one-way analysis of variance (ANOVA) with Tukey's post hoc test.

Additionally, we also calculated the number of falls from the rod after LPS administration. While there was few falls in the control group showing excellent motor coordination, LPS-injected rats showed impaired coordination and abnormal movement as evident form the increase in fall from the rod (**Figure 3.32 C**). However, administration of Mito-TBA-3 after LPS injection alleviated the motor coordination

imbalance, as evident with a decrease in the number of falls from the rotarod (**Figure 3.32 D**).

3.4.22 Effective Amelioration of Cognitive Impairment in LPS-Induced Model Rats by Mito-TBA-3: Findings in the rotarod and OFT indicate that administration of LPS leads to an increase in the anxiety levels of the rats, which ultimately results in extended durations of tension and restlessness throughout the experiment. Additional investigation is required in order to comprehensively comprehend the effects of LPS on anxiety-related behaviours.

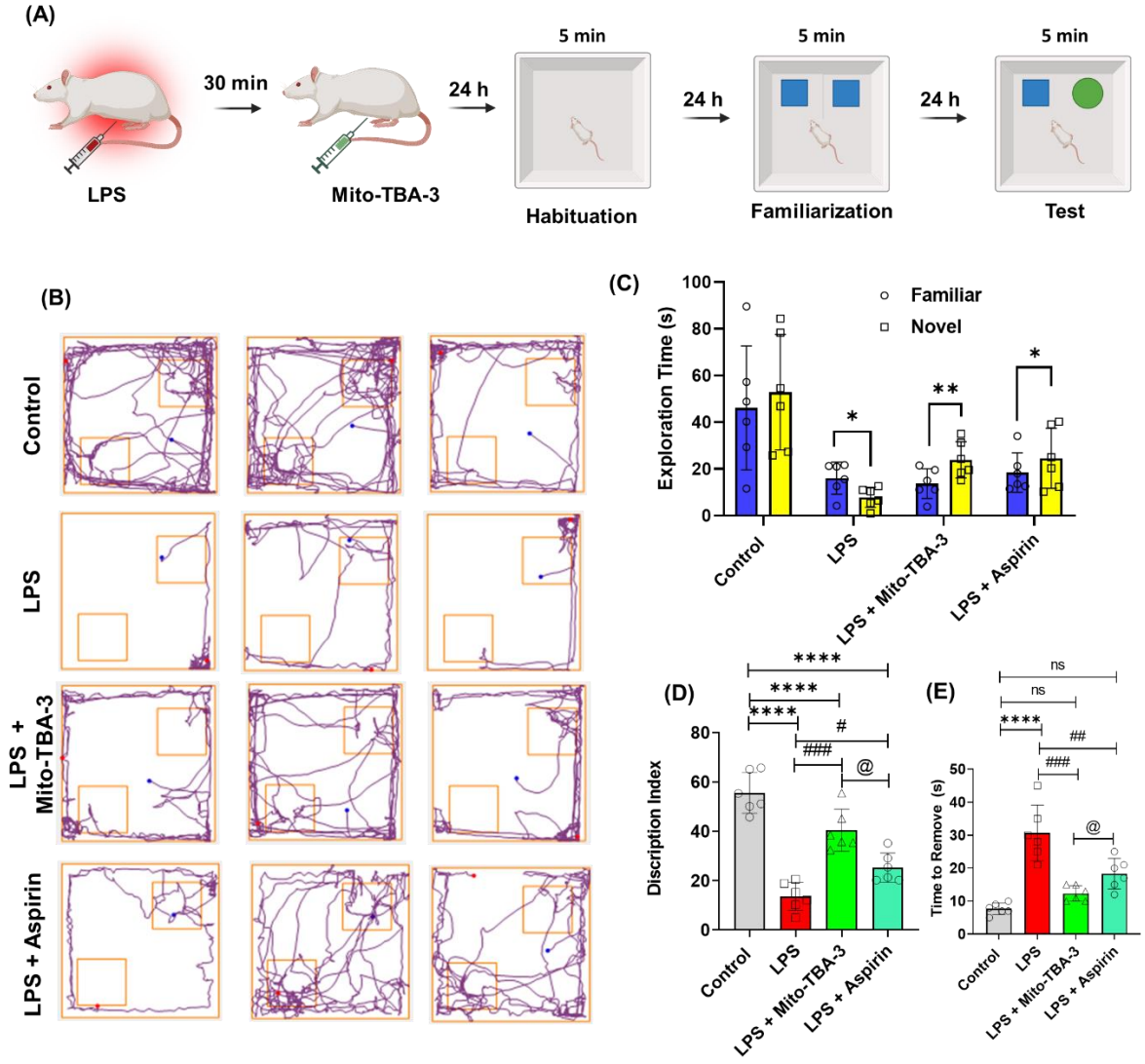


Figure 3.33 (A) Schematic illustration of the experimental procedure followed to assess the cognitive behaviour in LPS-induced rats. (B) Representative tracking plot of the NORT, (C) Bar graph showing exploration time spent by rats with novel and familiar objects, (D) Discrimination index showing the amount of time spent exploring the novel object as compared to the familiar object. (E) Bar graph showing the time to remove the adhesive test from the forelimb. The results are represented as the mean ± SEM. n = 6 per group from three independent experiments. Significances are marked as *P< 0.05, **P< 0.01, ***P< 0.001, **** P < 0.0001 versus the control group, $^{\#}$P<0.05, $^{\#\#}$P<0.01, $^{\#\#\#}$P<0.001, $^{\#\#\#\#}$ P < 0.0001 versus the LPS treatment group, $^{@@}$P<0.05, $^{@@}$P<0.01, $^{@@@}$P<0.001, $^{@@@@}$P < 0.0001 versus the Aspirin treatment group. Here, 'ns' is nonsignificant when compared to control. The statistical significance of all the results was calculated by using a one-way analysis of variance (ANOVA) with Tukey's post hoc test.

In this study, the NOR test (NORT) was employed to assess the effect of LPS on cognitive impairment, mainly recognition memory. We next investigate whether treatment with Mito-TBA-3 after LPS administration, could mitigate the impact of LPS on long-term memory function. To assess this, we employed NORT, a commonly used test for investigating memory impairment in rats. This test measures recognition memory, attention, and preference for novelty.

As shown in **Figure 3.33** An illustration shows a typical experimental configuration for the NORT. On the first day of habituation (T0), rats are placed in an empty arena for a duration of 5 minutes. After 24 hrs the rats were returned to the same arena with two identical objects and allow to explore the arena for a period of 10 minutes (T1). During the second day of testing (T2), the rats were once again placed into the arena, with one familiar object and one novel object and they are allowed to explore for a duration of 10 minutes. No disparity was observed between the control group rats in exploration time of novel and familiar objects, suggesting that the animals in the control group possess a non-comparable level of differentiation. However, after LPS administration, the preference for novelty has been shown to decrease as evident from the less exploration time in novel object. Treatment with Mito-TBA-3, after LPS administration, resulted in an enhanced inclination towards exploring the new object, as seen in **Figure 3.33 B, D**. This outcome was also observed in form of track plots as shown in **Figure 3.33 B**, it has been clearly seen the preference of LPS-induced rats with familiar object. Moreover, when comparing the preference score for exploration as DI (**Figure 3.33 C),** Mito-TBA 3 treated rats exhibiting a substantially higher DI score compared to LPS group ($p<0.05$, unpaired t-test) and aspirin group. The findings of this study suggest that the treatment with Mito-TBA 3 has a protective effect against cognitive impairment generated by inflammation.

3.4.23 Mito-TBA-3 Restores the Sensorimotor Co-ordination Deficits: The evaluation of functional recovery following LPS-induced neuroinflammation was conducted via the "adhesive-tape removal" test. In the experimental procedure, a minute small adhesive tape is affixed to the paw of the right forelimb, and the duration required for the rat to detach the tape is calculated. The results of this experiment indicate that the induced rat had a prolonged tape removal time in comparison to a control group of rats (**Figure 3.33 E**). The observed phenomenon in the control group of rats may be attributed to neuronal plasticity, which seems to be compromised in LPS-induced rats. This impairment may also be a result of secondary damage to neurons (such as dendritic spine development) and glia (including microglia and astrocytes) caused by the generation of free radicals.

The pole test is particularly for studying motor coordination in rats with degenerative brain diseases. The rats underwent the test on a daily basis until they learnt to climb down the pole (**Figure 3.34 A**). There is a notable correlation between degenerative brain disorders, such as memory impairment and neuroinflammation, and a decline in motor function, encompassing a diminished sense of balance and coordination. Hence, there will be a substantial drop in motor coordination of rats injected with LPS compared to the control group (**Figure 3.34 A**).

As shown in **Figure 3.34 A, B** the duration of time spent on a slanted pole was significantly shorter in the control group (7.16 ± 1.95 s) compared to the LPS group (23.00 ± 2.23 s). However, it was significantly longer in the Mito-TBA-3 group (10.66 ± 1.69 s) and aspirin group (13.00 ± 3.16 s). In particular, the pole results clearly demonstrated that the administration of Mito-TBA-3 to an animal afflicted with neuroinflammation and neuronal death has shown exceptional efficacy in enhancing motor function and exhibiting neuroprotective properties.

Considering the evidence that an LPS administration usually causes immune-inflammatory responses throughout the body, leading to the disruption of the blood-brain barrier (BBB) and causing significant astrogliosis and neuronal cell death, it is clear that these factors also contribute to the decline in cognitive performance and motor function. The Morris water maze (MWM) is a well-known behavioural experiment used to study long-term learning and memory in rats. For this study, we conducted behavioural tests to evaluate spatial navigation and reference memory for a duration of 5 days. Each group of rats underwent training and acquired learning over a period of 5 days. During this phase, the swimming pattern of the rats was assessed and Mito-TBA-3 treatment group showed a less chaotic swimming pattern and reached the platform in a short time duration as compared to the LPS group, which showed a more chaotic swimming pattern (**Figure 3.34 C, D**). Remarkably, the group that received Mito-TBA-3 treatment displayed the most significant improvement, indicating that these rats showed the highest amount of recovery in their ability to learn spatially after the treatment. In addition, when evaluating factors such as the amount of time spent in the target quadrant, the Mito-TBA-3 group showed the most favourable results compared to the other groups (**Figures 3.34 E**) (Aspirin).

After finishing the learning phase, the rat was subjected to a testing procedure where their ability to remember the platform was assessed. The testing results demonstrated that the rat in the Mito-TBA-3 group have the capacity to accurately remember the location of the platform which is evident from the shortest swimming distance needed to reach the platform (**Figures 3.34 F**).

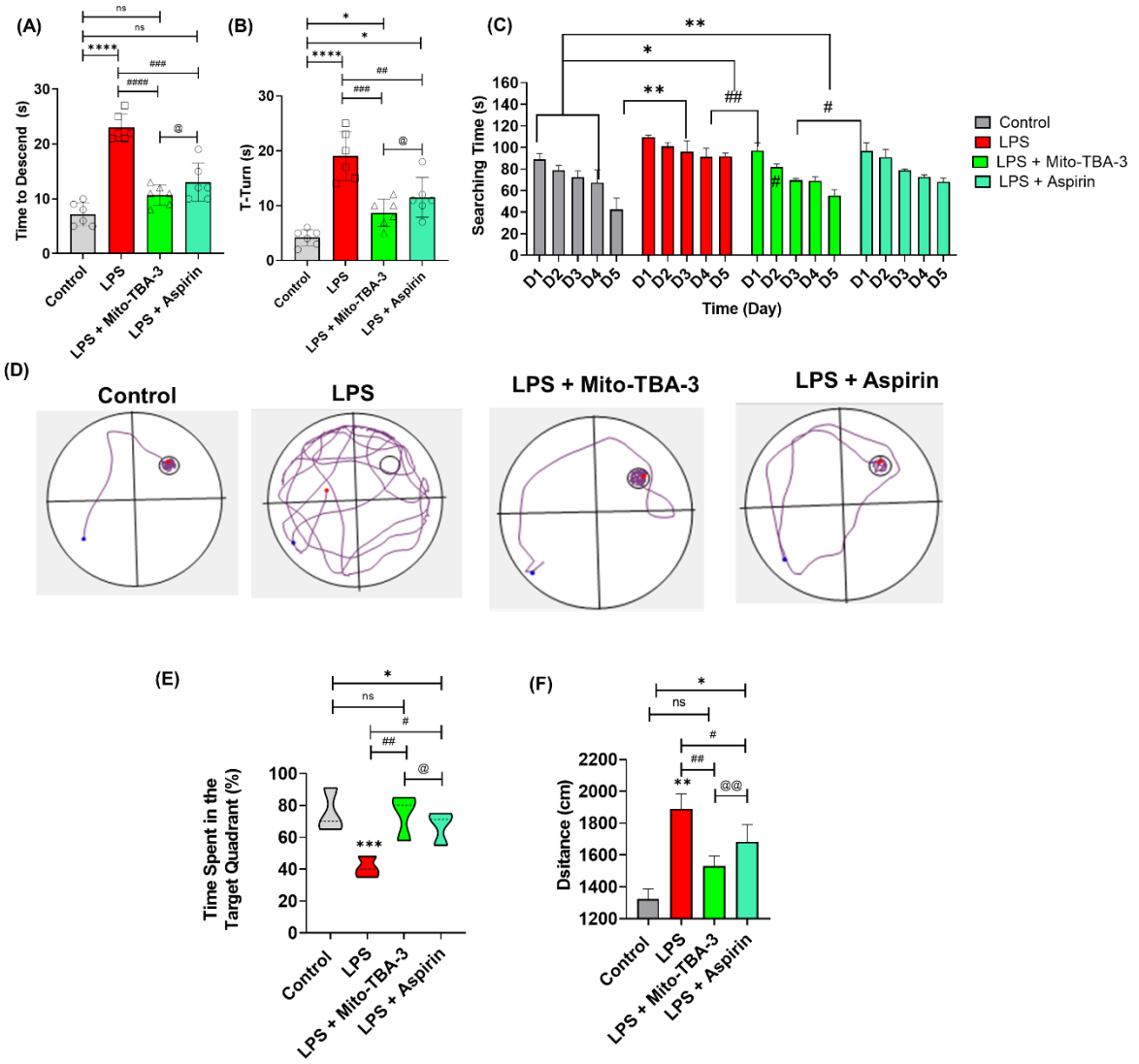


Figure 3.34 Assessment of motor coordination function by pole test. (A) Bar graph showing total time required to descent in the pole and (B) Bar graph showing time required to take the T-Turn. (C) Bar graph searching time of the platform, (D) Representative track plots of MWM in learning phase of training by different treatment groups, (E) Time spent in the target quadrant, (F) Distance to the platform. Data are represented as the mean ± s.d. from three independent experiments. Mito-TBA-3 effectively helps in restoring motor coordination as evident from the decrease in time to descent and number of T-turns. . The results are represented as the mean ± SEM. n = 6 per group from three independent experiments. Significances are marked as *P< 0.05, **P< 0.01, ***P< 0.001, **** P < 0.0001 versus the control group, $^{\#}$P<0.05, $^{\#\#}$P<0.01, $^{\#\#\#}$P<0.001, $^{\#\#\#\#}$ P < 0.0001 versus the LPS treatment group, $^{@@}$P<0.05, $^{@@}$P<0.01, $^{@@@}$P<0.001, $^{@@@@}$P < 0.0001 versus the Aspirin treatment group. Here, 'ns' is nonsignificant when compared to control. The statistical significance of all the results was calculated by using a one-way analysis of variance (ANOVA) with Tukey's post hoc test.

3.4.24 Mitigation of Compulsive and Repetitive Behavior by Mito-TBA-3: The LPS-induced rats exhibited hyperactive compulsive-like behaviour, such as digging in bedding and nibbling on inedible objects in the cage. This behaviour was markedly different from the locomotor activity. Hence, we employed the marble-burying test to

conduct a more in-depth analysis of the hyperactive behaviour that occurs after LPS administration (**Figure 3.35 A, B**).

The LPS-injected rats exhibited a notable disparity in their marble-burying behaviour. Compared with control rats, activation of anxiety-like behaviour resulted in significantly more buried marbles (**Figure 3.35 C, D**) and increased in time spent in digging, while treatment with Mito-TBA-3 resulted in significantly less buried marbles (**Figure 3.35 D**) and less time spent in digging (**Figure 3.35 E**). The findings of this study offer robust evidence in favour of a using Mito-TBA-3 as an anti-depressant.

3.4.25 Mito-TBA-3 Improves the Depression-like Behavior: The consumption of sucrose declined dramatically and reached its minimum level on successive days after the LPS challenge. In addition, administering Mito-TBA-3 as a treatment subsequent to injecting LPS resulted in a considerable increase in sucrose consumption (**Figure 3.35 F**). These results showed that Mito-TBA-3 was successful in alleviating anxiety and depression-like behaviours caused by LPS. These findings indicate a possible use of Mito-TBA-3 in those who are prone to inflammation-induced depression.

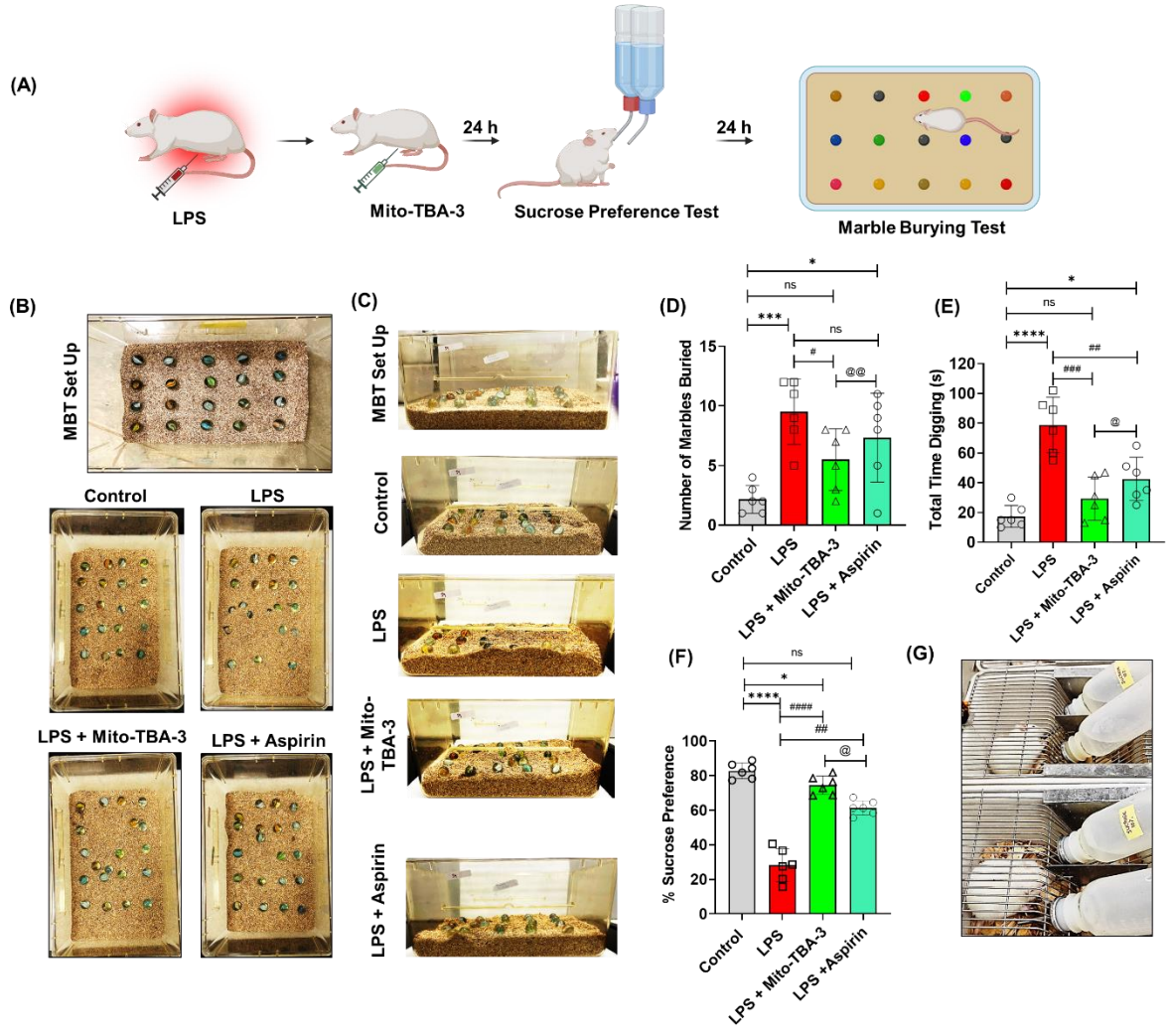


Figure 3.35 (A) Schematic illustration of the procedure followed for MBT and SPT, (B, C) Representative images of the MBT under different treatment conditions showing the repetitive compulsive behavior in LPS induced rats. Mito-TBA-3 treatment could inhibit the onset of compulsive like behavior after LPS administration as evident with the decrease in marbles buried in (D) Bar graph showing number of marbles buried, decrease in (E) total time spent in digging and increase in (F) sucrose intake, (G) Representative images of the rats set up in SPT. Data are represented as the mean ± s.d. from three independent experiments. Mito-TBA-3 effectively helps in restoring motor coordination as evident from the decrease in time to descent and number of T-turns. . The results are represented as the mean ± SEM. n = 6 per group from three independent experiments. Significances are marked as *P< 0.05, **P< 0.01, ***P< 0.001, **** P < 0.0001 versus the control group, $^{\#}$P<0.05, $^{\#\#}$P<0.01, $^{\#\#\#}$P<0.001, $^{\#\#\#\#}$ P < 0.0001 versus the LPS treatment group, $^{@@}$P<0.05, $^{@@}$P<0.01, $^{@@@}$P<0.001, $^{@@@@}$P < 0.0001 versus the Aspirin treatment group. Here, 'ns' is nonsignificant when compared to control. The statistical significance of all the results was calculated by using a one-way analysis of variance (ANOVA) with Tukey's post hoc test.

3.4.26 Inhibition of Proinflammatory Cytokines by Mito-TBA-3: The significant involvement of pro-inflammatory cytokines, such as IL-6, and TNF-α, in coordinating neuroinflammation and initiating neuronal death in several neurodegenerative illnesses has been extensively acknowledged. Thus, we examine whether Mito-TBA-3 helps reduce pro-inflammatory cytokines after LPS-induced neuroinflammation. Hence we performed ELISA to measure the expression of two major inflammatory cytokines IL-6, and TNF-α in the whole brain homogenate (**Figure 3.36 A**). As shown in **Figure 3.36 B-E** it illustrates that the levels of TNF-α and IL-6 in the brain and hippocampus homogenates of the rat stimulated with LPS were greater compared to the control group. This indicates that LPS can cause inflammation and the production of proinflammatory cytokines. However, consistent with the earlier cellular results, the expression levels of TNF-α and IL-6 were reduced after treatment with Mito-TBA-3 in both whole brain homogenate (**Figure 3.36 B, C**) and hippocampus (**Figure 3.36 D, E**), respectively. Furthermore, the ELISA results clearly indicates that Mito-TBA-3 demonstrate strong ability to inhibits the elevation of proinflammatory cytokines and hence promoting neuronal protection.

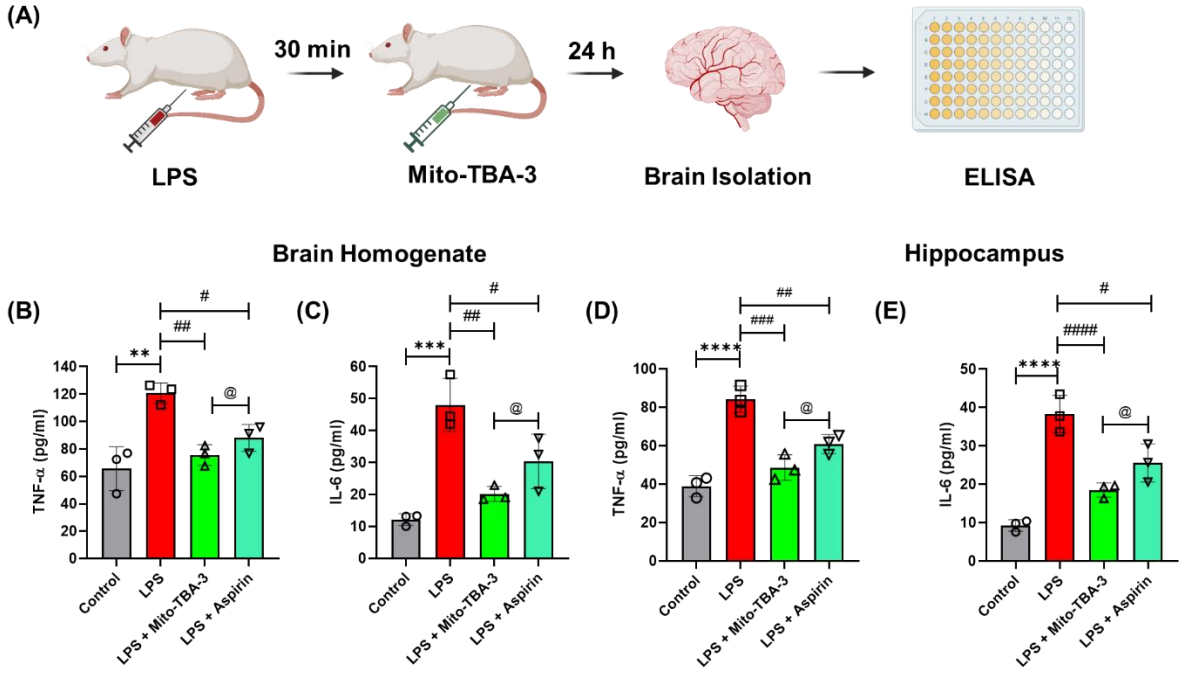


Figure 3.36 Neuroprotective effect of Mito-TBA-3 on expression of different proinflammatory cytokines in the Hippocampus and total brain homogenate of LPS induced mice model of learning and memory impairment. (A) Schematic illustration of the procedure followed for the detection of inflammatory cytokines by ELISA assay. Bar graph showing expression level of proinflammatory cytokine (B) TNF-α and (C) IL-6 total brain homogenate in LPS induced rats before and after Mito-TBA-3 and Aspirin treatment. Expression level of proinflammatory cytokine (D) TNF-α and (E) IL-6 total Hippocampus region of the brain in LPS induced rats before and after Mito-TBA-3 and Aspirin treatment.

3.4.27 Treatment with Mito-TBA-3 Effectively Reduces Neuroinflammation & Neuronal Death Following Neuroinflammation: Hematoxylin and eosin (H and E) and Nissl staining were performed to further verify the *in vivo* neuroprotective effects of Mito-TBA-3 and to investigate the pathomorphological changes observed in the hippocampus and the cortex after LPS stimulation. A thorough analysis was conducted to evaluate the shape and structural integrity of brain tissue slices after LPS administration, using H and E staining method. Distinct pink staining patterns were observed in regions abundant in proteins, such as cytoplasm, blood cells, and collagen. In contrast, areas with high concentrations of nucleic acids had a distinct pattern of blue staining. The observed variation in staining patterns can be attributed to the selective affinity of the dyes used during the staining procedure towards distinct biomolecules, hence facilitating the distinction between various cellular constituents. The use of pink staining in regions abundant in proteins and blue staining in regions abundant in nucleic acids yields significant insights into the cellular and tissue composition and organization.

In control sections, distinct and compact arrangements of cells were seen (**Figure 3.37 A**). Following LPS administration, it was observed that the experimental group, which received only saline as a therapeutic treatment, exhibited noticeable impairment in the hippocampus, as seen in **Figure 3.37 B** with a red arrow such as a considerable

reduction in cellular density, uneven distribution of cells, and the presence of cytoplasmic vacuolization. While the Mito-TBA-3 treatment demonstrates a notable change in neuron morphology compared to the saline treatment group 7 days' post-LPS administration (**Figure 3.37 C**). Moreover, the control group had a dense arrangement of cells in the CA1, CA3 and DG regions of the hippocampus, characterized by well-defined nuclei and abundant cytoplasm, as marked with green arrow (**Figure 3.37 A**). Furthermore, the control set of the group brain displayed intact parenchymal structure, devoid of any neuronal degeneration or edema. However, significant necrosis in neurons and deep staining of nuclear pyknosis were observed in the CA1, CA3 and DG regions in both the LPS group (**Figure 3.37 B**) and the LPS + Aspirin group (**Figure 3.37 D**), as indicated by the red box and black arrow respectively. Notably, the hippocampal neurons in the Mito-TBA 3 treatment group exhibited a higher density and organization of neurons compared to the other groups.

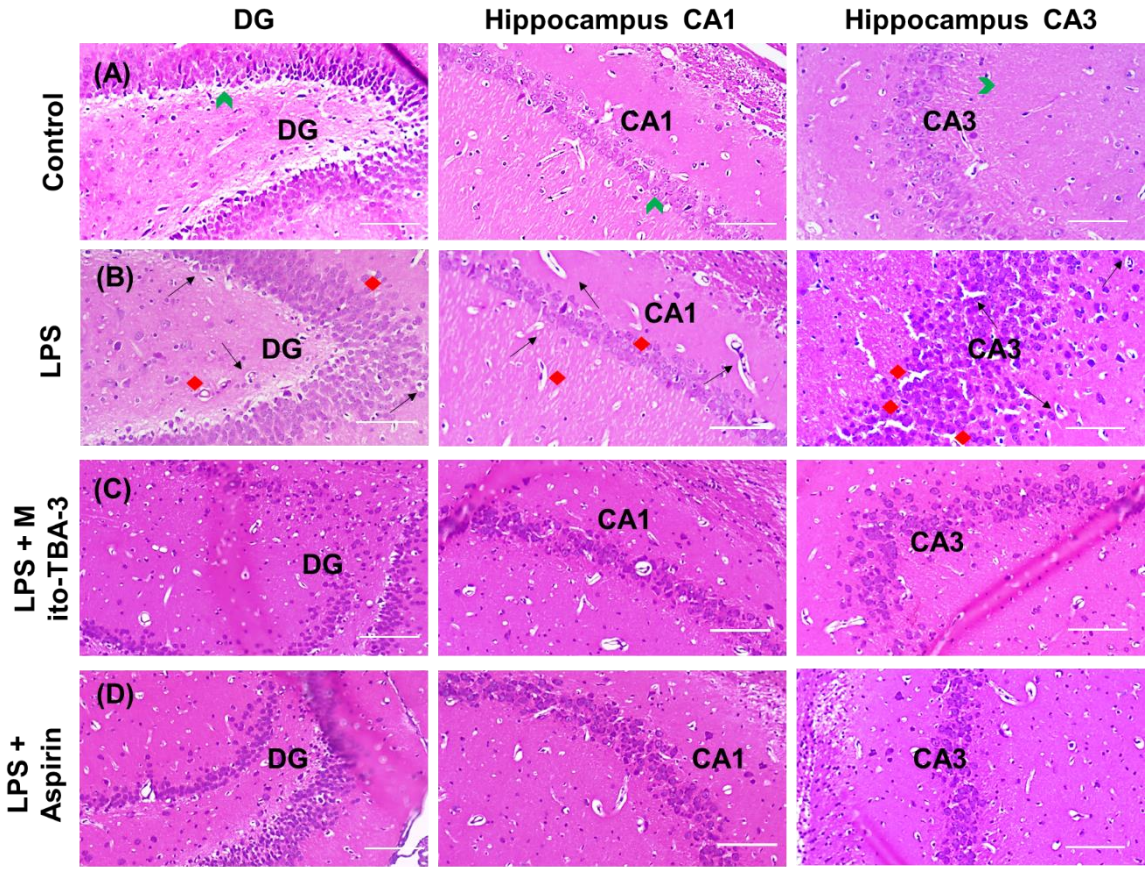


Figure 3.37 (A) Representative Hematoxylin and Eosin stained images of the DG, Hippocampus CA1 and CA3 region of the control group rat showing no karyopyknosis; dispersed nucleus shown with the black arrow and no sign of neuropil vacuolization, (B) Representative Hematoxylin and Eosin stained images of the DG, Hippocampus CA1 and CA3 region of the LPS group showing significantly higher number of neurons with necrosis, damage area, cytoplasmic shrinkage and vacuolization as shown with the red diamond (C) Representative Hematoxylin and Eosin stained images of the DG, Hippocampus CA1 and CA3 region of the Mito-TBA-3 treatment group with significantly less tissue damage and necrosis and well distribution of cells as shown with green arrow, (D) Representative Hematoxylin and Eosin stained images of the DG, Hippocampus CA1 and CA3 region of the Aspirin treatment group showing decrease in cell necrosis and shrinkage in cell body as marked with yellow arrow.

In order to get a more precise evaluation of neuronal health, we additionally investigated the extent of damage sustained by neurons using Nissl staining. The control group had a dense arrangement of cells in the CA1, CA3 and DG regions of the hippocampus, characterized by well-defined nuclei and abundant cytoplasm. However, a significant reduction in the number of intact neurons, accompanied by distorted morphology, was observed in the LPS group as compared to the control group (**Figure 3.38 A-D**). Remarkably, in the Mito-TBA 3 treatment group, there was a notable decrease in neuronal damage (**Figure 3.38 C**). These findings underscore the effectiveness of Mito-TBA 3 in mitigating neuronal damage and apoptosis, thereby attenuating the oxidative stress induced by LPS. Moreover, treatment with Mito-TBA 3 effectively reduces the occurrence of pyknotic neurons and limits the extent of necrosis in the affected area.

Overall, both Nissl and H and E staining findings highlight a notable reduction in neuronal damage and maintenance of cell structure in the group treated with Mito-TBA 3, as compared to the LPS group. Hence, these results suggest that Mito-TBA 3 have the potential to provide therapeutic advantages in neuroprotection against neuroinflammation.

3.4.28 Mito-TBA-3 Treatment Effectively Reduces Inflammation and Neuronal Death following LPS Administration: The pathological characteristics of brain neuroinflammation, such as the loss of neuronal cells, activation of reactive astrocytes, and activation of glial cells, are important factors in its pathophysiology. Neuronal apoptosis plays a crucial role in causing neurological damage after an insult. The prognosis of neuroinflammation is significantly affected by the inflammatory response that occurs after any brain damage, which is caused by the buildup of ROS. Efficiently reducing ROS levels after cerebral inflammation is crucial for minimizing subsequent brain injury. In addition, the activation of astrocytes and microglia, which are normally defensive responses in healthy tissue, can become excessively active after neuroinflammation, resulting in the release of harmful and inflammatory substances, such as reactive oxygen and nitrogen species (RONS). These mediators play a role in the development of neurodegenerative disorders. Markers such as Iba-1 in microglia and GFAP in astrocytes indicate their activation in response to severe brain inflammation. Within this particular framework, the act of restraining microglia-induced inflammation and alleviating oxidative stress are acknowledged as efficacious approaches to diminish neuronal necrosis. Hence in this virtue, the expression levels of GFAP and Iba-1 were quantified using immunohistochemistry after LPS administration to evaluate changes in inflammatory levels.

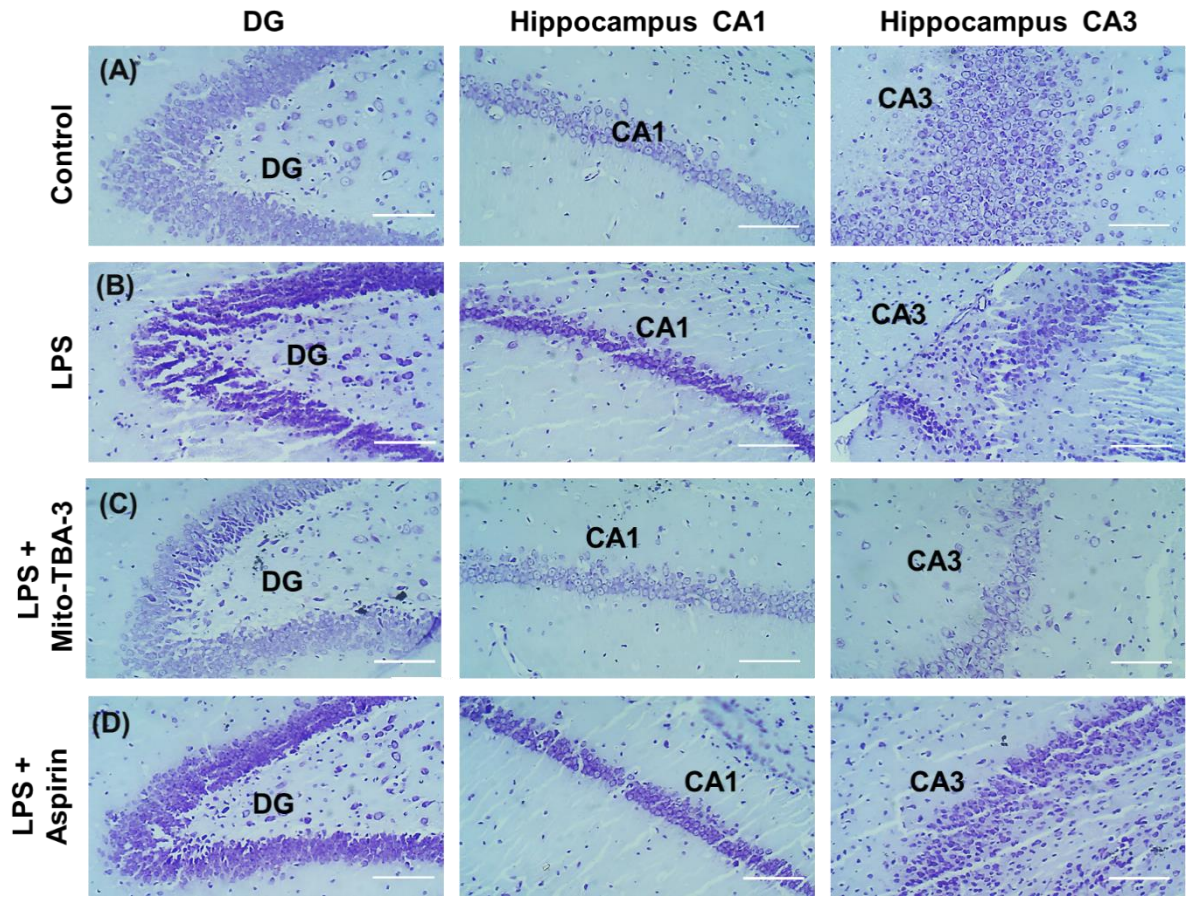


Figure 3.38 (A) Representative cresyl violet stained images of the DG, CA1 and CA3 region of the control group showing healthy neurons with no sign of karyopyknosis, hyperchromasia or neurophil vacoulation as shown with the with arrow, (B) Representative cresyl violet stained images of the DG, CA1 and CA3 region of the LPS group showing significantly high number of neurons with hyperchromasia, pyknosis, karyopyknosis and neurophil vacoulation as shown with the red arrow (C) Representative cresyl violet stained images of the DG, CA1 and CA3 region of the Mito-TBA-3 treatment group with significantly less necrotic nuclei and karyoknosis as shown with green arrow, (D) Representative cresyl violet stained images of the DG, CA1 and CA3 region of the Aspirin treatment group showing less necrotic neuronal nuclei, pyknosis and shrinkage in cell body as marked with yellow arrow.

The immunostained section of the hippocampus reveals a notable difference in the GFAP expression across all treatment conditions. The results depicted in **Figure 3.98** reveal a greater expression of GFAP-positive cells (**Figure 3.39 A-H**) and IBA1-positive cells (**Figure 3.40 A-H**) in the saline treatment group as compared to the control group in the cortex and Hippocampus region. This discovery indicates a significant stimulation of microglia and astrocytes after LPS administration **Figure 3.39 B, F** and **Figure 3.40 B, F.** Treatment with Mito-TBA-3 led to a reduction in the activation of astrocytes and microglia in both the cortex and hippocampus areas, as seen in **Figure 3.39 C, G** and **Figure 3.40 C, G,** respectively. However, the treatment with aspirin did have a protective effect. In summary, our results demonstrate that Mito-TBA-3 showed a stronger protective effect against stress-induced glia activation compared to aspirin **Figure 3.39 D, H** and **Figure 3.40 D,H**.

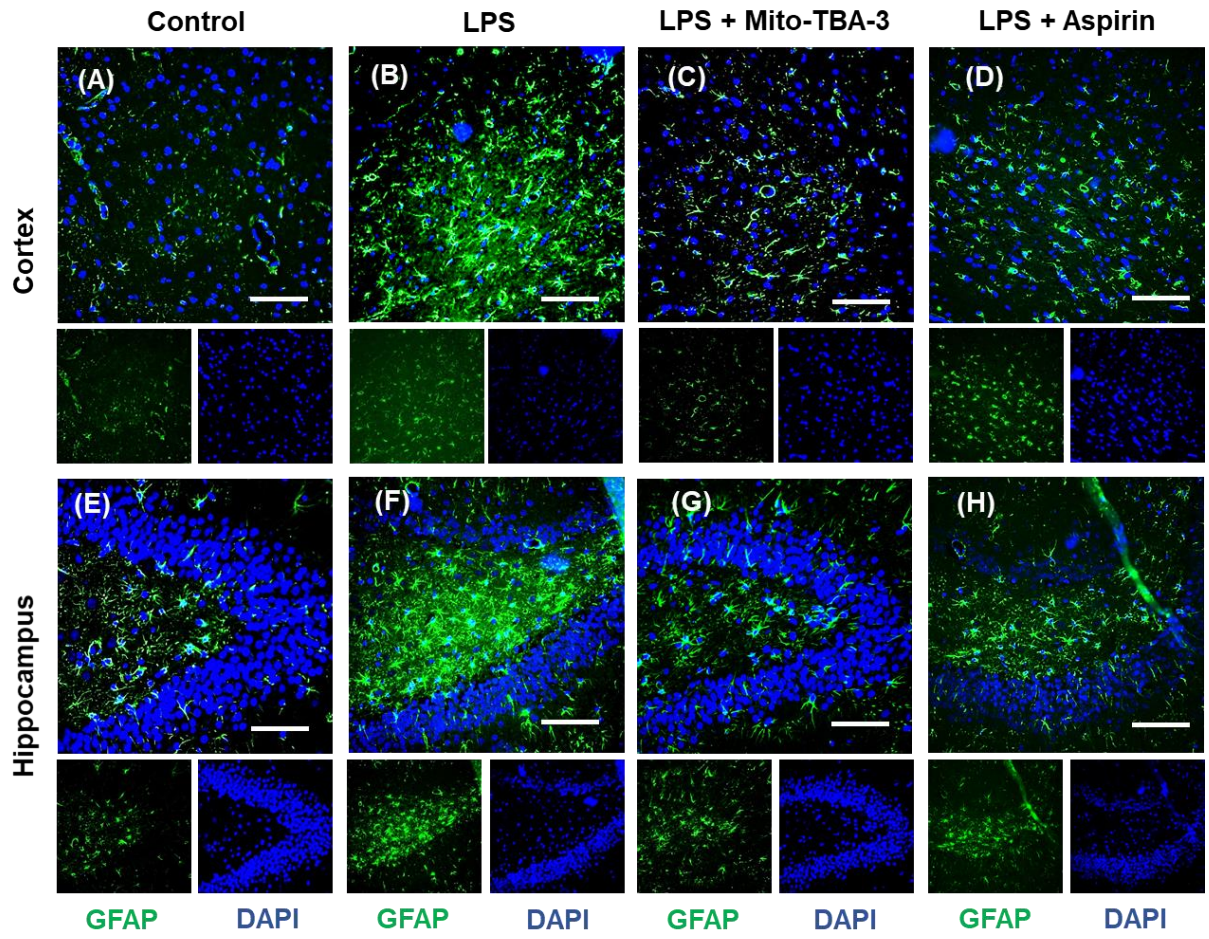


Figure 3.39 Mito-TBA-3 attenuated oxidative stress and inflammatory response in LPS induced Neuroinflammation. (A, E) Representative fluorescent microscopic images of the GFAP control group section of cortex and hippocampus region respectively, the astrocytes are not activated and less branched in the control group. (B, F) Representative fluorescent microscopic images of the LPS group section of cortex and hippocampus region respectively, astrocytes are in highly branched state due to the excessive ROS production. (C, G) Representative fluorescent microscopic images of the Mito-TBA-3 treatment group section of cortex and hippocampus region respectively, Mito-TBA-3 could able to reverse the inflammation caused due to LPS administration, as evident with less branched astrocytes and decrease in count of astrocytes. (D, H) Representative fluorescent microscopic images of the Aspirin section of cortex and hippocampus region respectively, as evident Aspirin were able to inhibit the inflammation and the astrocytes returned to their homeostatic morphology. Scale bar corresponds to 50 µm.

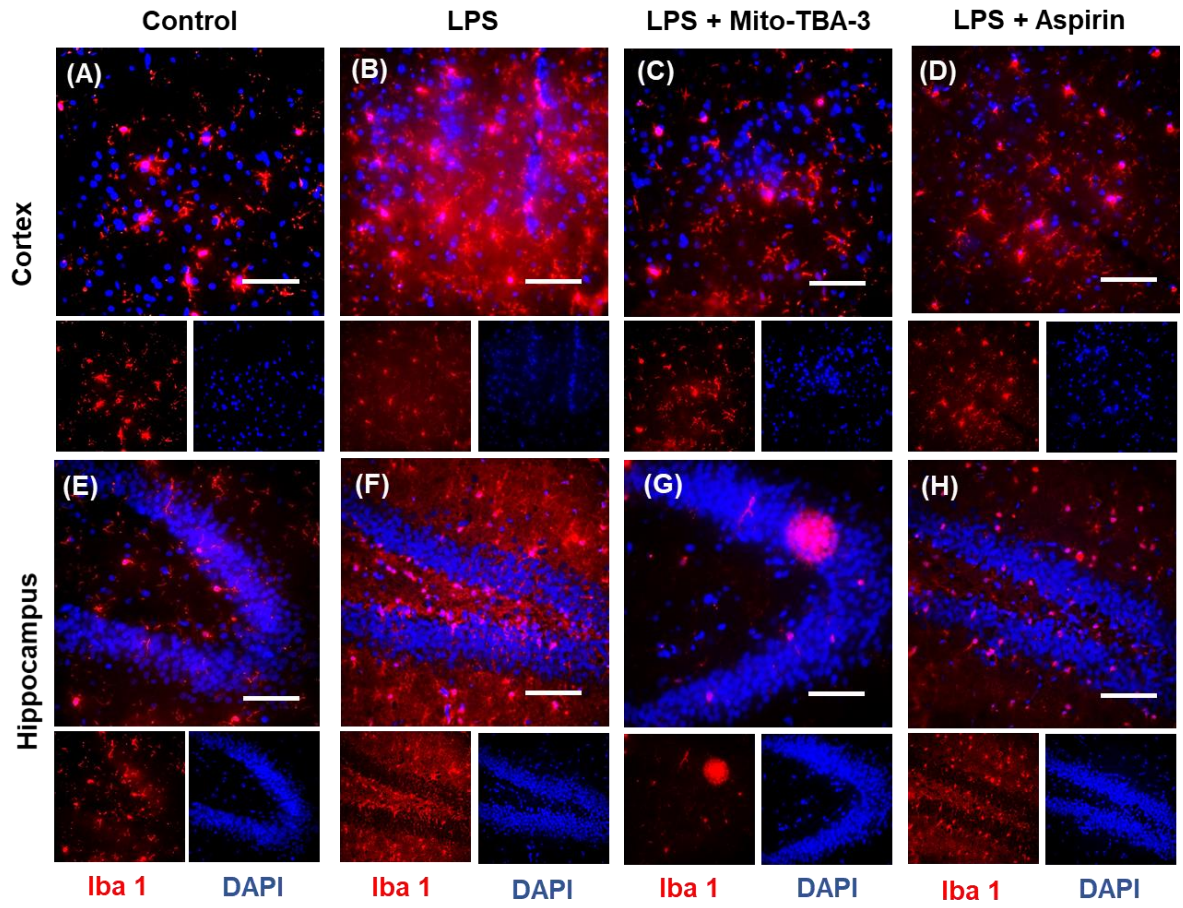


Figure 3.40 Fluorescent images of Iba1 stained cortex and Hippocampus section of Control, LPS, LPS + Mito-TBA-3 and LPS + Aspirin, Mito-TBA-3 was injected 30 minutes after LPS administration at a dose of 0.5 mg/Kg, Amoeboid Shape microglia are marked with the white arrow, healthy microglia with projections are marked with a white star. (A, E) Representative fluorescent microscopic images of the control group section of cortex and hippocampus region respectively, the microglia are in healthy state with ramified morphology and long projections, (B, F) Representative fluorescent microscopic images of the LPS group section of cortex and hippocampus region respectively, the microglia are in amoeboid shape due to high inflammation, (C, G) Representative fluorescent microscopic images of the Mito-TBA-3 treatment group section of cortex and hippocampus region respectively, Mito-TBA-3 could able to reverse the inflammation caused due to LPS administration. (D, H) Representative fluorescent microscopic images of the Aspirin section of cortex and hippocampus region respectively, as evident Aspirin were able to inhibit the inflammation and the microglia are in healthy state with ramified morphology and long projections. Scale bar corresponds to 50 µm.

The pan-neuronal marker, NeuN, was used to quantify the number of neurons in the cortex and hippocampus. **Figure 3.41 A-H** shows that there was a noticeable decrease in the number of NeuN-positive cells in the rat that was injected with LPS (**Figure 3.41 B, F**). This indicates that there was a loss of neurons following the LPS administration due to neuroinflammation. Moreover, our findings offer convincing proof that Mito-TBA-3 successfully reduced the decline in neuronal count (**Figure 3.41 C, G**). This was confirmed by measuring the number of NeuN+/DAPI+ cells in both the cortex and hippocampus of the rat that underwent LPS administration. Conversely, the group that was solely treated with Mito-TBA-3 showed a significant rise in NeuN-positive cells compared to the LPS-injected group. These findings indicated that Mito-TBA-3 had superior neuroprotective properties compared to Aspirin. To summarise, the use

of Mito-TBA we can say that it can consistently and effectively inhibit the excessive growth and enlargement of astrocytes and microglia in the brain. This helps to preserve the balance of cells and improves the inflammation of the brain caused by LPS administration.

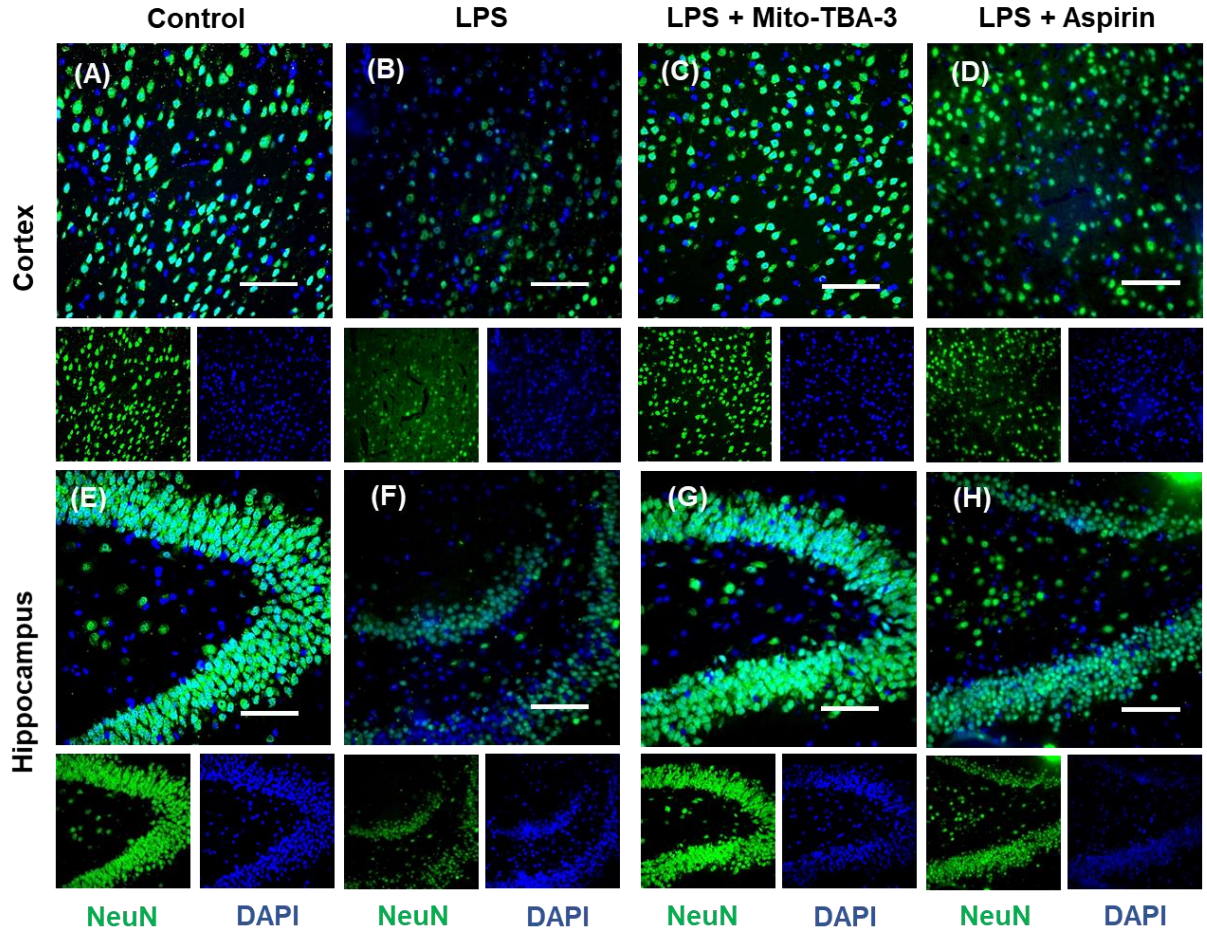


Figure 3.41 (A, E) Representative fluorescent microscopic images of the control group section of cortex and hippocampus region, respectively, the neurons are in healthy state with long neurite outgrowth. (B, F) Representative fluorescent microscopic images of the LPS group section of cortex and hippocampus region, respectively, the neurons are with degenerative neurite length due to the excessive ROS production. (C, G) Representative fluorescent microscopic images of the Mito-TBA-3 treatment group section of cortex and hippocampus region respectively, Mito-TBA-3 could able to reverse the inflammation caused due to LPS administration, as evident with retrenching of neurons and increase in neuronal cell count. (D, H) Representative fluorescent microscopic images of the Aspirin section of cortex and hippocampus region respectively, as evident Aspirin were able to inhibit the inflammation and the neurons are in healthy state with long dendrites. Scale bar corresponds to 50 µm.

Overall, our investigation finds that Mito-TBA-3 significantly inhibits the expression of reactive astrocytes and microglia, surpassing the inhibitory effects of aspirin. Therefore, Mito-TBA-3 emerges as an up-and-coming contender for neuroprotection, offering an alternate approach to managing neuroinflammation.

3.4.29 Analysis of *in vivo* Toxicity of Mito-TBA-3 on Different Body Organs To check the compatibility of Mito-TBA-3 in a preliminary study with major organs such as the heart, liver, spleen and lungs, we performed H and E staining at the end of 7

days and 14 days after treatment with different concentrations of Mito-TBA-3 (5 and 10 mg/Kg). The H and E results indicated that there were no significant differences between different organs cellular organization and morphology as compared to the control group (**Figure 3.42**), indicating that the Mito-TBA-3 does not cause any potential toxicity *in vivo.*

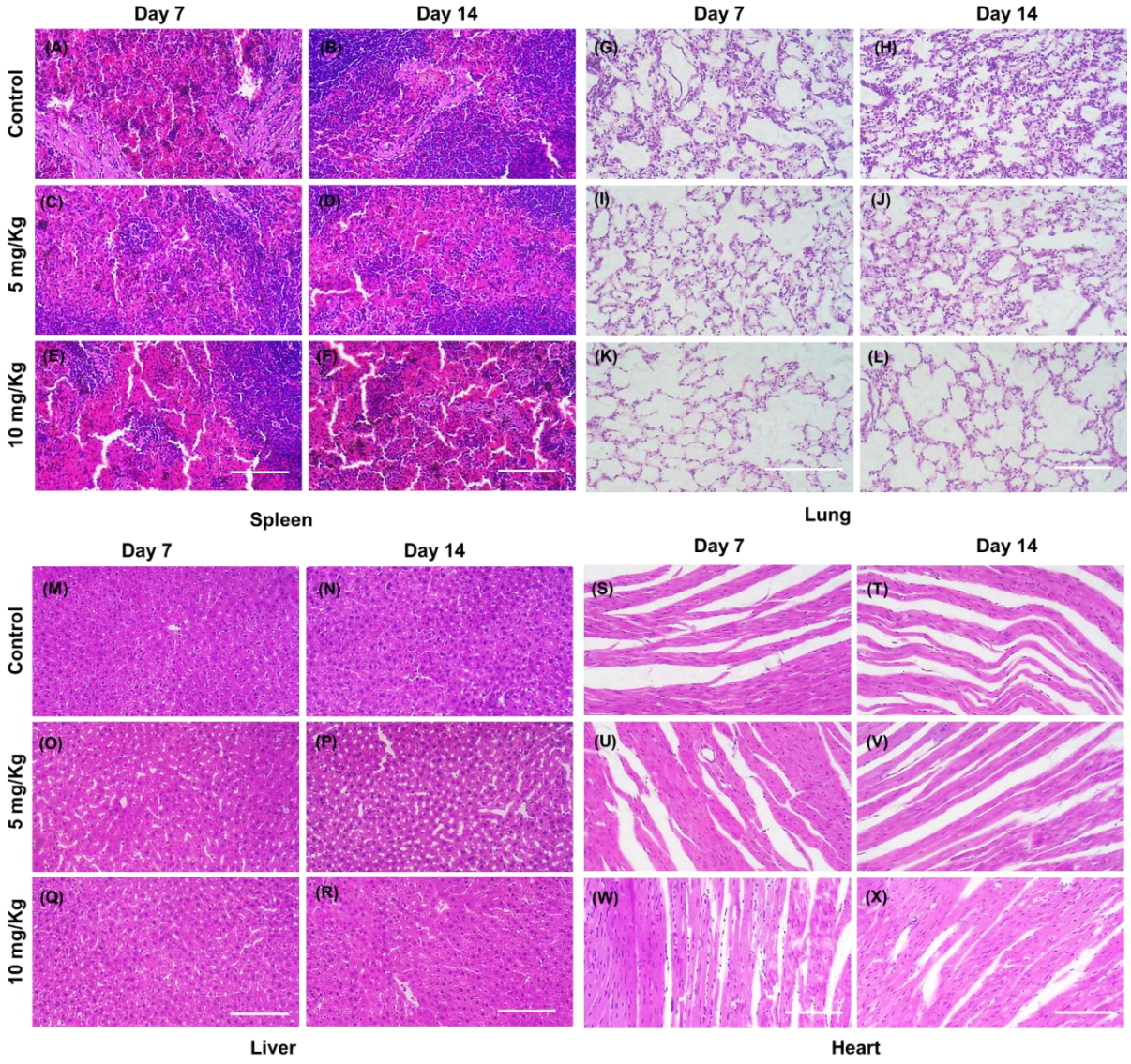


Figure 3.42 Representative images of the different organs from the different treatment groups for the evaluation of *in vivo* cytotoxicity analysis: (A-F) Shows the spleen H & E sections from control, 5 mg/Kg and 10mg/Kg of Mito-TBA-3 at Day 7 (A, C, E) and Day 14 (B, D, F) respectively, (G-L) Shows the lung H & E sections from control, 5 mg/Kg and 10mg/Kg of Mito-TBA-3 at Day 7 (G, I, K) and Day 14 (H, J, L) respectively, (M-R) Shows the liver H & E sections from control, 5 mg/Kg and 10mg/Kg of Mito-TBA-3 at Day 7 (M, O, Q) and Day 14 (N, P, R) respectively, (S-X) Shows the liver H & E sections from control, 5 mg/Kg and 10mg/Kg of Mito-TBA-3 at Day 7 (S, U, W) and Day 14 (T, V, X) respectively. Scale bar corresponds 200 µm.

3.5 CONCLUSION

In summary, we have successfully demonstrated that careful, specific structural alterations lead to potential therapeutic lead, which resulted in a notable enhancement of its ability to protect mitochondria from oxidative damage, as evident from the various biophysical results. From the structure, activity, toxicity and biophysical analysis of all compounds, compound 3c (Mito-TBA-3) has been identified as a promising candidate for the development of a high-quality drug that can be used to treat mitochondrial oxidative stress and alleviate the effects of mitochondrial and metabolic disorders caused by mitochondrial dysfunctioning. Moreover, Mito-TBA-3 does not alter mitochondria morphology polarization and showed exceptionally well antioxidant capacity against LPS and Aß induced oxidative stress in neuronal cell lines. It was found that Mito-TBA-3 attenuated LPS-induced proinflammatory response via pre-activating the TLR-4 pathway, leading to inhibition of Caspase-3 / Nuclear Factor-kappa B Pathway. *In vivo* results showed that Mito-TBA-3 have a positive therapeutic effect on LPS-induced inflammatory depression. Moreover, Mito-TBA-3 showed significant neuroprotective effects by virtue of their anti-oxidative and anti-inflammatory properties. It not only showed promising results in *in vitro* conditions but also crossed the BBB to inhibit neuroinflammation and restoring synaptic loss. Hence, Mito-TBA-3 could perhaps serve as a suitable therapeutic lead molecule for depression resulting from inflammatory infection. Therefore, our study has demonstrated the significant potential for utilising Mito-TBA-3 in the treatment of inflammatory depression and other inflammatory brain-related disorders.

3.6 REFERENCES

(1) Vakifahmetoglu-Norberg, H.; Ouchida, A. T.; Norberg, E. The Role of Mitochondria in Metabolism and Cell Death. *Biochem. Biophys. Res. Commun.* **2017**, *482* (3), 426–431.

(2) San-Millán, I. The Key Role of Mitochondrial Function in Health and Disease. *Antioxidants* **2023**, *12* (4), 782.

(3) Sies, H.; Jones, D. P. Reactive Oxygen Species (ROS) as Pleiotropic Physiological Signalling Agents. *Nat. Rev. Mol. cell Biol.* **2020**, *21* (7), 363–383.

(4) van Horssen, J.; van Schaik, P.; Witte, M. Inflammation and Mitochondrial Dysfunction: A Vicious Circle in Neurodegenerative Disorders? *Neurosci. Lett.* **2019**, *710*, 132931.

(5) Erkkinen, M. G.; Kim, M.-O.; Geschwind, M. D. Clinical Neurology and Epidemiology of the Major Neurodegenerative Diseases. *Cold Spring Harb. Perspect. Biol.* **2018**, *10* (4), a033118.

(6) Stuckler, D. Population Causes and Consequences of Leading Chronic Diseases: A Comparative Analysis of Prevailing Explanations. *Milbank Q.* **2008**, *86* (2), 273–326.

(7) Ravindranath, V.; Sundarakumar, J. S. Changing Demography and the Challenge of Dementia in India. *Nat. Rev. Neurol.* **2021**, *17* (12), 747–758.

(8) Lamptey, R. N. L.; Chaulagain, B.; Trivedi, R.; Gothwal, A.; Layek, B.; Singh, J. A Review of the Common Neurodegenerative Disorders: Current Therapeutic Approaches and the Potential Role of Nanotherapeutics. *Int. J. Mol. Sci.* **2022**, *23* (3). https://doi.org/10.3390/ijms23031851.

(9) Zhang, W.; Xiao, D.; Mao, Q.; Xia, H. Role of Neuroinflammation in Neurodegeneration Development. *Signal Transduct. Target. Ther.* **2023**, *8* (1), 267.

(10) DeTure, M. A.; Dickson, D. W. The Neuropathological Diagnosis of Alzheimer's Disease. *Mol. Neurodegener.* **2019**, *14* (1), 32.

(11) Gaugler, J.; James, B.; Johnson, T.; Reimer, J.; Solis, M.; Weuve, J.; Buckley, R. F.; Hohman, T. J. 2022 Alzheimer's Disease Facts and Figures. *Alzheimers Dement.* **2022**, *18* (4), 700–789.

(12) Olufunmilayo, E. O.; Gerke-Duncan, M. B.; Holsinger, R. M. D. Oxidative Stress and Antioxidants in Neurodegenerative Disorders. *Antioxidants* **2023**, *12* (2), 517.

(13) Tönnies, E.; Trushina, E. Oxidative Stress, Synaptic Dysfunction, and Alzheimer's Disease. *J. Alzheimer's Dis.* **2017**, *57* (4), 1105–1121.

(14) Ighodaro, O. M.; Akinloye, O. A. First Line Defence Antioxidants-Superoxide Dismutase (SOD), Catalase (CAT) and Glutathione Peroxidase (GPX): Their Fundamental Role in the Entire Antioxidant Defence Grid. *Alexandria J. Med.* **2018**, *54* (4), 287–293.

(15) Jena, A. B.; Samal, R. R.; Bhol, N. K.; Duttaroy, A. K. Cellular Red-Ox System in Health and Disease: The Latest Update. *Biomed. Pharmacother.* **2023**, *162*, 114606.

(16) Clarke, D. D. Circulation and Energy Metabolism of the Brain. *Basic Neurochem. Mol. Cell. Med. Asp.* **1999**.

(17) Lushchak, V. I.; Duszenko, M.; Gospodaryov, D. V; Garaschuk, O. Oxidative Stress and Energy Metabolism in the Brain: Midlife as a Turning Point. *Antioxidants* **2021**, *10* (11), 1715.

(18) Zheng, X.; Boyer, L.; Jin, M.; Mertens, J.; Kim, Y.; Ma, L.; Ma, L.; Hamm, M.; Gage, F. H.; Hunter, T. Metabolic Reprogramming during Neuronal Differentiation from Aerobic Glycolysis to Neuronal Oxidative Phosphorylation. *Elife* **2016**, *5*, e13374.

(19) Phaniendra, A.; Jestadi, D. B.; Periyasamy, L. Free Radicals: Properties, Sources, Targets, and Their Implication in Various Diseases. *Indian J. Clin. Biochem.* **2015**, *30* (1), 11–26. https://doi.org/10.1007/s12291-014-0446-0.

(20) Misrani, A.; Tabassum, S.; Yang, L. Mitochondrial Dysfunction and Oxidative Stress in Alzheimer's Disease. *Front. Aging Neurosci.* **2021**, *13*, 57.

(21) Amorim, R.; Cagide, F.; Tavares, L. C.; Simões, R. F.; Soares, P.; Benfeito, S.; Baldeiras, I.; Jones, J. G.; Borges, F.; Oliveira, P. J. Mitochondriotropic Antioxidant Based on Caffeic Acid AntiOxCIN4 Activates Nrf2-Dependent Antioxidant Defenses and Quality Control Mechanisms to Antagonize Oxidative Stress-Induced Cell Damage. *Free Radic. Biol. Med.* **2022**, *179*, 119–132.

(22) Kahkeshani, N.; Farzaei, F.; Fotouhi, M.; Alavi, S. S.; Bahramsoltani, R.; Naseri, R.; Momtaz, S.; Abbasabadi, Z.; Rahimi, R.; Farzaei, M. H. Pharmacological Effects of Gallic Acid in Health and Diseases: A Mechanistic Review. *Iran. J. Basic Med. Sci.* **2019**, *22* (3), 225.

(23) Taofiq, O.; González-Paramás, A. M.; Barreiro, M. F.; Ferreira, I. C. F. R. Hydroxycinnamic Acids and Their Derivatives: Cosmeceutical Significance, Challenges and Future Perspectives, a Review. *Molecules* **2017**, *22* (2), 281.

(24) Zheng, M.; Xu, C.; Ma, J.; Sun, Y.; Du, F.; Liu, H.; Lin, L.; Li, C.; Ding, J.; Chen, K. Synthesis and Antitumor Evaluation of a Novel Series of Triaminotriazine Derivatives. *Bioorg. Med. Chem.* **2007**, *15* (4), 1815–1827.

(25) Lei, T.; Graf, S.; Schöll, C.; Krätzschmar, F.; Gregori, B.; Appleson, T.; Breder, A. Asymmetric Photoaerobic Lactonization and Aza-Wacker Cyclization of Alkenes Enabled by Ternary Selenium–Sulfur Multicatalysis. *ACS Catal.* **2023**, *13* (24), 16240–16248.

(26) Moitessier, N.; Henry, C.; Maigret, B.; Chapleur, Y. Combining Pharmacophore Search, Automated Docking, and Molecular Dynamics Simulations as a Novel Strategy for Flexible Docking. Proof of Concept: Docking of Arginine– Glycine– Aspartic Acid-like Compounds into the Avβ3 Binding Site. *J. Med. Chem.* **2004**, *47* (17), 4178–4187.

(27) Teixeira, J.; Cagide, F.; Benfeito, S.; Soares, P.; Garrido, J.; Baldeiras, I.; Ribeiro, J. A.; Pereira, C. M.;

Silva, A. F.; Andrade, P. B. Development of a Mitochondriotropic Antioxidant Based on Caffeic Acid: Proof of Concept on Cellular and Mitochondrial Oxidative Stress Models. *J. Med. Chem.* **2017**, *60* (16), 7084–7098.

(28) Gupta, V.; Mahata, T.; Roy, R.; Gharai, P. K.; Jana, A.; Garg, S.; Ghosh, S. Discovery of Imidazole-Based GSK-3 β Inhibitors for Transdifferentiation of Human Mesenchymal Stem Cells to Neurons: A Potential Single-Molecule Neurotherapeutic Foresight. *Front. Mol. Neurosci.* **2022**, *15*, 1002419.

(29) Ramesh, M.; Balachandra, C.; Andhare, P.; Govindaraju, T. Rationally Designed Molecules Synergistically Modulate Multifaceted Aβ Toxicity, Microglial Activation, and Neuroinflammation. *ACS Chem. Neurosci.* **2022**, *13* (14), 2209–2221.

(30) Floegel, A.; Kim, D.-O.; Chung, S.-J.; Koo, S. I.; Chun, O. K. Comparison of ABTS/DPPH Assays to Measure Antioxidant Capacity in Popular Antioxidant-Rich US Foods. *J. food Compos. Anal.* **2011**, *24* (7), 1043–1048.

(31) Gharai, P. K.; Khan, J.; Mallesh, R.; Garg, S.; Saha, A.; Ghosh, S.; Ghosh, S. Vanillin Benzothiazole Derivative Reduces Cellular Reactive Oxygen Species and Detects Amyloid Fibrillar Aggregates in Alzheimer's Disease Brain. *ACS Chem. Neurosci.* **2023**, *14* (4), 773–786.

(32) Gharai, P. K.; Khan, J.; Pradhan, K.; Mallesh, R.; Garg, S.; Arshi, M. U.; Barman, S.; Ghosh, S. Power of Dopamine: Multifunctional Compound Assisted Conversion of the Most Risk Factor into Therapeutics of Alzheimer's Disease. *ACS Chem. Neurosci.* **2024**.

(33) Mallesh, R.; Khan, J.; Gharai, P. K.; Arshi, M. U.; Garg, S.; Gupta, S.; Ghosh, S. Hydrophobic C-Terminal Peptide Analog Aβ31–41 Protects the Neurons from Aβ-Induced Toxicity. *ACS Chem. Neurosci.* **2024**.

(34) Li, J.; Zhang, J.; Chen, Y.; Kawazoe, N.; Chen, G. TEMPO-Conjugated Gold Nanoparticles for Reactive Oxygen Species Scavenging and Regulation of Stem Cell Differentiation. *ACS Appl. Mater. Interfaces* **2017**, *9* (41), 35683–35692.

(35) Garg, S.; Jana, A.; Khan, J.; Gupta, S.; Roy, R.; Gupta, V.; Ghosh, S. Logic "AND Gate Circuit" Based Mussel Inspired Polydopamine Nanocomposite as Bioactive Antioxidant for Management of Oxidative Stress and Neurogenesis in Traumatic Brain Injury. *ACS Appl. Mater. Interfaces* **2024**.

(36) Roy, R.; Khan, J.; Pradhan, K.; Nayak, P.; Sarkar, A.; Nandi, S.; Ghosh, S.; Ram, H.; Ghosh, S. Short Peptoid Evolved from the Key Hydrophobic Stretch of Amyloid-B42 Peptide Serves as a Potent Therapeutic Lead of Alzheimer's Disease. *ACS Chem. Neurosci.* **2022**, *14* (2), 246–260.

(37) Wingett, D.; Louka, P.; Anders, C. B.; Zhang, J.; Punnoose, A. A Role of ZnO Nanoparticle Electrostatic Properties in Cancer Cell Cytotoxicity. *Nanotechnol. Sci. Appl.* **2016**, 29–45.

(38) Gerencser, A. A.; Chinopoulos, C.; Birket, M. J.; Jastroch, M.; Vitelli, C.; Nicholls, D. G.; Brand, M. D. Quantitative Measurement of Mitochondrial Membrane Potential in Cultured Cells: Calcium-induced De-and Hyperpolarization of Neuronal Mitochondria. *J. Physiol.* **2012**, *590* (12), 2845–2871.

(39) Gupta, V.; Gharai, P. K.; Kar, C.; Garg, S.; Ghosh, S. Ratiometric Fluorescent Probe Promotes Trans-Differentiation of Human Mesenchymal Stem Cells to Neurons. *ACS Chem. Neurosci.* **2024**, *15* (2), 222–229.

(40) Zhao, J.; Bi, W.; Xiao, S.; Lan, X.; Cheng, X.; Zhang, J.; Lu, D.; Wei, W.; Wang, Y.; Li, H. Neuroinflammation Induced by Lipopolysaccharide Causes Cognitive Impairment in Mice. *Sci. Rep.* **2019**, *9* (1), 5790.

(41) Seibenhener, M. L.; Wooten, M. C. Use of the Open Field Maze to Measure Locomotor and Anxiety-like Behavior in Mice. *JoVE (Journal Vis. Exp.* **2015**, No. 96, e52434.

(42) Liu, M.-Y.; Yin, C.-Y.; Zhu, L.-J.; Zhu, X.-H.; Xu, C.; Luo, C.-X.; Chen, H.; Zhu, D.-Y.; Zhou, Q.-G. Sucrose Preference Test for Measurement of Stress-Induced Anhedonia in Mice. *Nat. Protoc.* **2018**, *13* (7), 1686–1698.

(43) Zhu, T.; Wang, H.; Gu, H.; Ju, L.; Wu, X.; Pan, W.; Zhao, M.; Yang, J.; Liu, P. Melanin-like Polydopamine

Nanoparticles Mediating Anti-Inflammatory and Rescuing Synaptic Loss for Inflammatory Depression Therapy. *J. Nanobiotechnology* **2023**, *21* (1), 52.

(44) Pires, J. M.; Foresti, M. L.; Silva, C. S.; Rêgo, D. B.; Calió, M. L.; Mosini, A. C.; Nakamura, T. K. E.; Leslie, A. T. F.; Mello, L. E. Lipopolysaccharide-Induced Systemic Inflammation in the Neonatal Period Increases Microglial Density and Oxidative Stress in the Cerebellum of Adult Rats. *Front. Cell. Neurosci.* **2020**, *14*, 142.

(45) Skrzypczak-Wiercioch, A.; Sałat, K. Lipopolysaccharide-Induced Model of Neuroinflammation: Mechanisms of Action, Research Application and Future Directions for Its Use. *Molecules* **2022**, *27* (17), 5481.

(46) Vorhees, C. V; Williams, M. T. Morris Water Maze: Procedures for Assessing Spatial and Related Forms of Learning and Memory. *Nat. Protoc.* **2006**, *1* (2), 848–858.

(47) Bentea, E.; Villers, A.; Moore, C.; Funk, A. J.; O'Donovan, S. M.; Verbruggen, L.; Lara, O.; Janssen, P.; De Pauw, L.; Declerck, N. B. Corticostriatal Dysfunction and Social Interaction Deficits in Mice Lacking the Cystine/Glutamate Antiporter. *Mol. Psychiatry* **2021**, *26* (9), 4754–4769.

(48) Adak, A.; Das, G.; Khan, J.; Mukherjee, N.; Gupta, V.; Mallesh, R.; Ghosh, S. Extracellular Matrix (ECM)-Mimicking Neuroprotective Injectable Sulfo-Functionalized Peptide Hydrogel for Repairing Brain Injury. *ACS Biomater. Sci. Eng.* **2020**, *6* (4), 2287–2296.

(49) Mallesh, R.; Khan, J.; Gharai, P. K.; Ghosh, S.; Garg, S.; Arshi, M. U.; Ghosh, S. High-Affinity Fluorescent Probes for the Detection of Soluble and Insoluble Aβ Deposits in Alzheimer's Disease. *ACS Chem. Neurosci.* **2023**, *14* (8), 1459–1473.

(50) Schneider, C. A.; Rasband, W. S.; Eliceiri, K. W. NIH Image to ImageJ: 25 Years of Image Analysis. *Nat. Methods* **2012**, *9* (7), 671–675.

(51) Zielonka, J.; Joseph, J.; Sikora, A.; Hardy, M.; Ouari, O.; Vasquez-Vivar, J.; Cheng, G.; Lopez, M.; Kalyanaraman, B. Mitochondria-Targeted Triphenylphosphonium-Based Compounds: Syntheses, Mechanisms of Action, and Therapeutic and Diagnostic Applications. *Chem. Rev.* **2017**, *117* (15), 10043–10120.

(52) Jiang, Q.; Yin, J.; Chen, J.; Ma, X.; Wu, M.; Liu, G.; Yao, K.; Tan, B.; Yin, Y. Mitochondria-Targeted Antioxidants: A Step towards Disease Treatment. *Oxid. Med. Cell. Longev.* **2020**, *2020*.

(53) Xu, J.; Du, W.; Zhao, Y.; Lim, K.; Lu, L.; Zhang, C.; Li, L. Mitochondria Targeting Drugs for Neurodegenerative Diseases—Design, Mechanism and Application. *Acta Pharm. Sin. B* **2022**, *12* (6), 2778–2789.